January 2022

Fracture Initiation And Propagation In Shale Formations With Anisotropic Toughness

Nourelhouda Benouadah

FRACTURE INITIATION AND PROPAGATION IN SHALE FORMATIONS WITH ANISOTROPIC TOUGHNESS

by

Nourelhouda Benouadah

Bachelor of Applied Geosciences, Faculty of Oil and Chemistry, University of Boumerdes, Boumerdes, Algeria, 2015

Masters of Petroleum Geology, Faculty of Oil and Chemistry, University of Boumerdes, Boumerdes, Algeria, 2017

A Dissertation

Submitted to the Graduate Faculty

of the

University of North Dakota

In fulfillment of the requirements

for the degree of

Doctor of Philosophy

Grand Forks, North Dakota

August
2022

This dissertation, submitted by Nourelhouda Benouadah in partial fulfillment of the requirements for the Degree of PhD from the University of North Dakota, has been read by the Faculty Advisory Committee under whom the work has been done, and is hereby approved.

_____
Dr. Vamegh Rasouli

_____
Dr. Egor Dontsov

_____
Dr. Hui Pu

_____
Dr. Minou Rabiei

_____
Dr. Iraj Mamaghani

This dissertation is being submitted by the appointed advisory committee as having met all of the requirements of the School of Graduate Studies at the University of North Dakota and is hereby approved.

_____
Christopher Nelson
Associate Dean of the Graduate School

_____
Date

PERMISSION

Title Fracture Initiation and Propagation in Shale Formations with Anisotropic Toughness

Department Petroleum Engineering

Degree Doctor of Philosophy

In presenting this dissertation in partial fulfillment of the requirements for a graduate degree from the University of North Dakota, I agree that the library of this University shall make it freely available for inspection. I further agree that permission for extensive copying for scholarly purposes may be granted by the professor who supervised my thesis work or, in his absence, by the chairperson of the department or the dean of the Graduate School. It is understood that any copying or publication or other use of this dissertation or part thereof for financial gain shall not be allowed without my written permission. It is also understood that due recognition shall be given to me and to the University of North Dakota in any scholarly use which may be made of any material in my thesis.

Nourelhouda Benouadah
July 19th, 2022

DEDICATION

This research is lovingly dedicated to my parents Khaled Benouadah and Rabeaa Saim, my beloved sisters Lina and Ikram, my brothers Djalil and Karim, my Angels Racim and Amelia, and to Dr. Foued Badrouchi, who have been my source of inspiration. They have given me the drive and discipline to tackle any task with enthusiasm and determination. Without their love and support, this project would not have been made possible.

Nourelhouda Benouadah

ACKNOWLEDGMENTS

First and foremost, I am extremely grateful to my advisor, Prof. Vamegh Rasouli for his invaluable advice, continuous support, and patience during my PhD study. His immense knowledge and plentiful experience have encouraged me in all the time of my academic research and daily life. I wish to express my sincere appreciation to the members of my advisory committee for their guidance and support during the course of my Ph.D program at the University of North Dakota. I want to thank Dr. Egor Dontsov and ResFrac group for their continuous help and support. The financial support of the North Dakota Industrial Commission (NDIC) is highly appreciated.

ABSTRACT

Hydraulic Fracturing (HF) is the prime technology for enhanced production from shale plays. Due to their laminations at different scales, shales exhibit transverse isotropic (TI) properties. In most cases the lamination planes are nearly horizontal in shales setting with the symmetric axes being vertical, therefore, shales are referred to as TI vertical (TIV) rocks. This influences significantly the initiation and propagation of the induced fracture during fracturing operation. For instance, accurate estimation of the fracture initiation pressure (FIP) and fracture morphology is essential to ensure optimum hydraulic fracturing design in unconventional reservoirs. However, majority of studies of HF modelling in shales are based on the isotropic assumption to simplify the problem. While some recent studies demonstrate that ignoring the TI properties of shale results in a large error in estimation of stresses and consequently the design of the HF. The anisotropic toughness is a distinct feature of layered formations such as shale, which its understanding is vital especially when it comes to the estimation of hydraulic fracturing initiation pressure and morphology.

We first used analytical models to investigate the effect of the anisotropic toughness on the FIP of two fundamental fracture geometries: transverse and axial fractures. The model I stress intensity factor was used to develop the analytical models for FIP at the tip of a fracture emanating from a horizontal wellbore drilled in the direction of minimum horizontal stress (σ_h). The anisotropic toughness values parallel and perpendicular to the laminations were implemented to the estimation of the FIP of both transverse and axial fractures. These analytical models predict the FIP of different fracture lengths and variable local angles along the fracture based on the propagation direction and the fracture geometry (i.e. axial and transverse). The results of the analytical models showed that the anisotropic toughness has a noticeable effect on the FIP. The fracture initiation in anisotropic toughness was shown to have variable initiation pressure with direction and is

controlled by the local initiation angle. Consequentely, the fracture becomes more elongated in the direction of the minimum fracture toughness and contained in the direction of the maximum fracture toughness. This study shows that toughness anisotropy has a dominant effect on whether transverse or axial fracture will initiate from an open hole lateral. The fracture with lower FIP is favorable for initiation, hence, we investigated the competition between transverse and axial fractures is in a medium with anisotropic toughness. This knowledge will help engineers to optimize the design of a small notch, which will be the point of interest along the OH section to initiate and dominate other pre-existing fractures.

We then, used numerical simulations to model a number of cases of hydraulic fracturing in a medium with anisotropic toughness for variable propagation regimes. Different scenarios of radial and constant height fractures for cases of single and simultaneous propagation of multiple fractures were simulated in anisotropic toughness condition and compared to the isotropic cases. The reliability of the numerical simulator was confirmed against experimental and field data from the literature. The final step, was to simulate effect of toughness anisotropy on a field scale hydraulic fracturing model. We used the data from the Bakken Formation in the Williston Basin in North Dakota, as a field case study. The analytical results were validated using numerical simulations. Numerical simulation results showed that the overall shape of the system of fractures in case of anisotropic toughness is elongated in the direction of minimum toughness (horizontal). The results indicated that the net pressure and the fracture aperture in case of anisotropic toughness is higher compared to the isotropic case. The combined effect of stress shadow and toughness anisotropy was investigated in case of simultaneous propagation of multiple fractures. Results showed that the interaction between the fractures is high in case of toughness anisotropy. Field case hydraulic fracturing model showed to be more complex.

CONTENT

LIST OF FIGURES

List of Tables

CHAPTER 1

Characteristics of Transversely Isotropic Formations

1.1 Introduction

Shale formations belong to the class of mudrocks which are a fine-grained sedimentary rock composed of particles of less than 62.5 μm. Such a fine materials that require a high-resolution imaging to be observed has the ability to preserve the organic matter and be a potential source rocks (Mánica et al. 2019). However, the hydrocarbons generated from this type of formations remains trapped in the shale source rock. Therefore, unconventional methods are required to extract the hydrocarbons from these formations, hence they are named unconventional reservoirs. For economic production from shale plays, horizontal drilling combined with hydraulic fracturing (HF) are the key methods that are currently practiced as the main stimulation techniques in the past two decades (Daneshy 2011; Hattori et al. 2017; Li et al. 2017; Milliken and Hayman 2019). In HF, a high-pressure fluid with a predefined viscosity is injected into a low permeability formation to provide a high conductivity pathway for hydrocarbons to flow to the producing wellbore. Open hole (OH) and cased hole (CH) well completion techniques are the most commonly used methods in the oil and gas industry.

Depending on the engineering application and the completion technique, in case of OH completion, the fracture network can be developed from the pre-existing defect intersecting the

wellbore, or from a notch of a desired geometry that have been designed by engineers to be the main point of initiation and propagation (Aidagulov et al. 2015; Benouadah et al. 2021; Djabelkhir et al. 2019). However, in case of CH completion the fracture network initiates from perforation tunnels drilled around the wellbore.

Broadly speaking, different rock types exist in nature with various mechanical properties. In engineering projects, the rock mass is commonly considered as continuous, homogeneous, isotropic, and linear elastic. However, rocks always exhibit other properties such as anisotropy, heterogeneity and nonlinearity that should be taken into consideration in real projects to accurately succeed the engineering operations (Serajian and Ghassemi 2011).

Among the potential sources of unconventional reservoirs, shale plays have large volume and cover broad surfaces because of their deposition mechanism. Such rocks are characterized by the presence of an intrinsic lamination, resulting in their direction dependent behavior, which is known as anisotropy. Since the lamination in shales is in most cases in the horizontal direction with an axis of symmetry being perpendicular to it, shales are known as transversely isotropic vertical (TIV) (Britt and Schoeffler 2009) (See Figure 1.1).

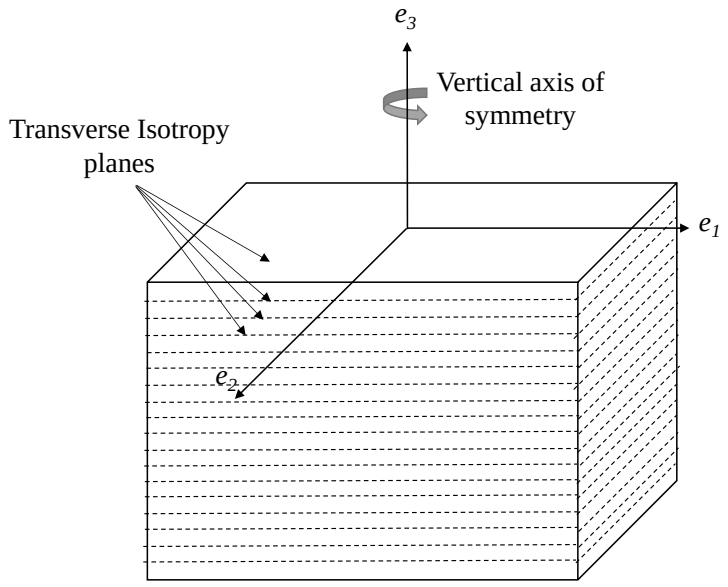

Figure 1.1: Transversely isotropic medium with vertical symmetry axis

Transverse isotropy can be a good approximation to different phenomena related to rock properties and can be seen in different parameters of the formation such as: rock elasticity, permeability, and fracture toughness. Fracture toughness is considered as one of the most important rock mechanical properties and is defined as the ability of fracture to resist the initiation of a crack. The transversely isotropic fracture toughness is a distinct feature of layered formations (Shale). Understanding the fracture toughness is vital epically when it comes to hydraulic fracturing initiation pressure, which is a key parameter for the design of hydraulic fracturing.

In previous studies, the fracture initiation pressure was estimated using the facture toughness based on isotropic assumptions. However, in anisotropic toughness conditions, estimating the pressure based on the isotropic assumption can finalize the hydraulic fracturing with suboptimal operation design.

This study focuses on understanding the HF initiation and propagation in the TIV medium. Previous literature shows that stiffness, strength, fracture toughness, and permeability are the main

properties that control anisotropy and should be considered for completion and hydraulic fracturing design (Dundar 2019; Mánica et al. 2019). The effect of various transversely isotropic parameters such as fracture toughness and young's modulus on the fracture initiation pressure and geometry of an induced fracture is studied using analytical models and numerical simulations. We performed analysis on the effect of various parameters on efficient hydraulic fracturing design in transversely isotropic medium.

In the following sections, the objectives and the methodology used in this study will be presented along as with the significance of the work. Finally, the structure of the thesis content will be outlined.

1.2 Objectives

As explained above, understanding the impact of anisotropy on HF initiation and propagation is of significant importance. Therefore, the overall goal of this study is to investigate the impact of TIV medium properties on fracture initiation and propagation. The detailed objectives of this work can be summarized as follows:

1. Comprehensive review of existing literature on the impact of the TIV medium on fracture initiation and propagation. This includes analytical models, lab experimental studies, numerical simulations and field observations.
2. Under what conditions will axial and transverse fractures be created in TIV medium? In addition, what is the impact of the anisotropic parameters such as fracture toughness on initiation pressure and the competition between axial and transverse fractures?
3. Determine the impact of the in-situ field stresses on the type of fractures developed (axial versus transverse) around the wellbore in a TIV medium.

4. The applications and limitations of analytical models in estimation of HF initiation pressure in TIV medium will be discussed.
5. Capabilities and unique features of simulations for HF modelling and studying the effect of anisotropy on fracture initiation and propagation. ResFrac software, which is a numerical simulator equipped with anisotropic features, will be implemented in this study to investigate the effect of anisotropic parameters on HF initiation and geometry after propagation.
6. Assess the impact of the degree of TIV fracture toughness on the net pressure of radial and constant height fracture geometries along with the final fracture morphology and compare it to the isotropic fracture toughness.
7. Understand fracture morphology of single and multiple hydraulic fractures in TIV medium for different propagation regimes and different fracture geometries.
8. The combined effect of stress shadow and TIV fracture toughness on the morphology of multiple hydraulic fractures will be discussed.
9. Conduct numerical simulations using published lab and field data of the Bakken Formation as a real field example of hydraulic fracturing in a medium with anisotropic toughness.
10. Recommend notch geometry and orientation in lateral wellbore with existing natural fractures to dominate fracture initiation in desired spot for a suitable hydraulic fracturing design in Shale Formations.

1.3 Methodology

The methodology that will be used to achieve the above objectives comprises of data inventory, analytical solutions, and numerical simulations. These are briefly explained below.

1. In order to perform calibrated numerical simulations, we collect sets of lab data from the literature. Similarly, field scale data will be gathered for the same purpose. The simulations will be based on data from Bakken formation.
2. Numerical simulations will be run using ResFrac software to estimate fracture net pressure in TIV medium and in presence of fractures with different geometries. Sensitivity analysis of toughness anisotropy on single and multiple fractures will be done for different propagation regimes.
3. Different analytical models will be introduced to predict the fracture initiation in a borehole with a crack emanating from its edge in a transversely isotropic (TIV) formation. The impact of fracture toughness on the fracture initiation and propagation behavior will be studied.
4. Analytical models based on the anisotropic assumption will be used to determine the effect of TIV fracture toughness on the FIP and the competition between axial versus transverse fractures and the impact of the fracture length.
5. The results of analytical models and numerical simulations will be compared to draw some practical applications in terms of determining the best parameters for an optimum HF operation in a medium with TIV toughness.

1.4 Significance

The results of this research study will present multifold novelties including the following:

1. This research project helps to address the gaps between analytical solutions and numerical simulations and elaborate potential solutions.

2. New analytical models to predict the fracture initiation pressure in a medium with anisotropic toughness.

3. This study is dedicated to give a better understanding of hydraulic fracturing in anisotropic medium and presents numerical modelling of real fracking in anisotropic formations, which in turn will help to solve many engineering challenges such as notch design, perforation clusters placement, proppant screen-out and transport, and HF design by offering an effective solution for better shale gas extraction in the future.

4. The use of ResFrac software which is a coupled hydraulic fracturing and reservoir simulator, with its unique features implemented in this study is one of the first attempt to study the impact of toughness anisotropy on fracture propagation and its morphology for single and multiple hydraulic fractures.

5. The project provides better understanding and predictive capabilities for the complex interactions between the fractures in a medium with anisotropic toughness for different propagation regimes. Which is an important prerequisite for improved and optimized reservoir

6. Practical recommendations and suggestions that are proposed in this study can improve the operation of HF in TIV medium, which in turn can be of significant financial benefits for the companies.

1.5 Thesis Structure

This thesis consists of five chapters.

Chapter 1 provides the background to the project and a very brief explanation of the isotropic and anisotropic medium characteristics, emphasizing the concept of TIV. It also contains the objectives of this study, the methodology used and the significance of this research.

In **Chapter 2** a brief review of the literature regarding the HF in TIV medium methods will be presented. In addition, a summary of past studies related to the lab work, numerical simulations

and analytical models to estimate initiation pressure of HF in TIV medium with a notch and the fracture geometry evolvement will be given.

Chapter 3 presents a brief overview of the background and theory of the simulation used in this study and the features and modelling using ResFrac software. Constitutive formulation and model setup are also summarized and presented in this chapter.

Chapter 4 comprises the analytical models that study the impact of the parameters in TIV fracture toughness on HF initiation pressure and stress intensity factor. These models integrate the impact of different parameters including two fracture geometries (axial and transverse) with different fracture sizes, fracture toughness anisotropy ratio and the local initiation angle on the fracture initiation and propagation pressures. Also, the impact of TIV fracture toughness on the competition between transverse and axial fractures will be modelled and discussed. The range of applications and limitations of these models will be discussed.

Chapter 5 presents the results of the numerical simulations. The simulations consider the impact of TIV fracture toughness on the net pressure of HF emanating from a horizontal wellbore in TIV medium. Simulations for single radial and constant height fractures are conducted for different scenarios of TIV fracture toughness degrees. Multiple hydraulic fracture propagation is also simulated for the same fracture geometries in different propagation regimes and for different spacing between the fractures. Therefore, the combined effect of TIV fracture toughness and stress shadow is discussed in this chapter. The data from Bakken Formation is used as a field example to simulate the effect of TIV fracture toughness on multiple hydraulic fracturing behavior. In addition, in this Chapter, the results of the impact of TIV fracture toughness on the pressure are compared with the results of the analytical models presented in the preceding Chapter and conclusions are made.

In **Chapter 6** a summary of the findings from this study will be presented along with some recommendations and future studies that can be carried out.

CHAPTER 2

Review of Literature

2.1 Introduction

In the previous Chapter, the differences between isotropic and anisotropic medium were briefly discussed and the concept of TIV was explained. The existence of fractures in the rock mass may play a beneficial or a detrimental role depending on the engineering operation. During drilling operation, these fractures often intersect the wellbore wall causing circulation loss. They take in drilling fluid and prevent its return to the surface, which may damage the reservoir and can cause engineers to lose control of the well. Therefor significant economic consequences may happened (Ma et al. 2019). On the other hand, in HF, the intersection of the induced fracture with the natural fractures enhances production of hydrocarbons. This stimulation technique is used to increase the productivity from rocks with low permeability. Therefore, the knowledge of the fracture mechanics is key in the design and operation of oil and gas related projects such as wellbore stability and hydraulic fracturing. Shale plays are the most common hydraulically fractured reservoirs. These formations are characterized by their lateral expansion; therefore, horizontal drilling is combined with HF technique to increase the well production. Transverse isotropy is one of the important characteristics of shales due to their layering nature. Simplifying the anisotropic characteristic of shales to an isotropic problem has shown to result in large error in estimation of

the design parameters (Amadei 1983; Khan et al. 2012; Suarez-Rivera et al. 2006; Valliappan et al. 2019). Therefore, it is necessary to apply the TIV formulations in simulations of shale formations and HF design.

In this Chapter, we present a brief overview of the past research and studies on the impact of the anisotropy on HF initiation and propagation in shale formations with TIV characteristic. We classify these studies into analytical models, numerical simulations, experimental studies and field practices.

2.2 Analytical Models

While the maturity in the field of fracture mechanics is increasing, the analytical and theoretical models are still limited due to the complexity of the problem such as material anisotropy, heterogeneity, and hydro-mechanical coupling. However, in HF simulations, it is necessary to take into account the impact of rock anisotropy on the fracture behavior (Martemyanov et al. 2017; Savitski et al. 2013). Therefore, efforts have been made to investigate the challenging problem of fracture behavior in anisotropic medium and understand the rock anisotropy and the theory of stress measurements. However, further studies are needed to investigate different aspects of the problem.

Berry and Fairhurst (1966) and Berry (1968) presented the solution that enables the consideration of the impact of rock anisotropy and analytical expressions of stress determination in anisotropic rocks.

Amadei (1983) reported that for problems involving anisotropic formations, over 50% of errors on in situ stress measurements can be resulted from the assumption that the rock is isotropic.

Thomsen (1986) proposed some anisotropy parameters from simple method of mathematical equations that describes the transversely isotropic medium with vertical axis of symmetry (TIV).

Later on, a new approach proposed by Nadri et al. (2012) for the estimation of Thomson anisotropy parameters on arbitrary geometry of TI shale samples.

Moukhtari et al. (2020a) further investigated the governed dimensionless parameters including Thomsen parameters to investigate the fracture growth perpendicular to the isotropy plane in TI medium. Moreover, a numerical quantification of the HF growth led to the development of the exact near-tip elastic modulus expression as a function of the fracture propagation direction in TI medium.

Khan et al. (2012) used field data from the largest shale gas play in Canada (Horn River Basin), which exhibited a strong anisotropy of Young's modulus varying from 1.2 to 3.5, to evaluate the importance of taking into account the effect of the mechanical anisotropy. They considered the anisotropic effect on horizontal stresses given by Amadei et al. (1987) and Pan and Amadei (1995) to illustrate the stress computation and fracture design. The results, as shown in Figure 2.1, indicate that the mechanical anisotropy strongly influences the fracture geometry and breakdown pressure.

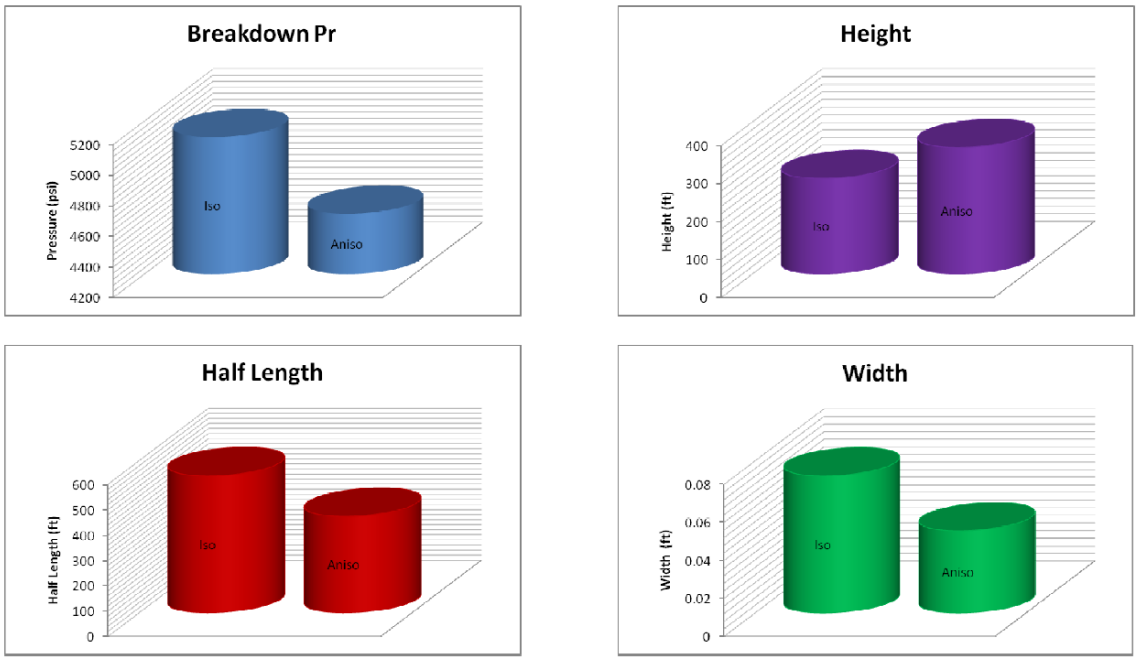

Figure 2.1: Breakdown pressure and fracture geometry in isotropic versus anisotropic formations (After Khan et al. 2012)

The vertical and horizontal far field stresses are expressed respectively as following (Khan et al. 2012):

$$\sigma_v = g\int_0^z \rho_b(z)dz \tag{2.1}$$

$$\sigma_h = K_0(\sigma_v - \alpha P_p) + \alpha P_p + \sigma_{Tectonic} \tag{2.2}$$

where

ρ_b : bulk density

g : acceleration due to gravity

z : vertical depth

α : Biot's poro-elastic coefficient

P_p : pore pressure

The effect of anisotropy does not affect the vertical stress. However, the anisotropy can affect the horizontal stresses and the effect is expressed in the modified parameter K_0 proposed by Amadei et al. (1987) and Pan and Amadei (1995), where K_0 for isotropic and transversely isotropic material with horizontal plane of isotropy are, respectively:

$$K_0 = \frac{\nu}{1-\nu} \tag{2.3}$$

$$(K_0)_{aniso} = \frac{E_h}{E_v}\frac{\nu_v}{1-\nu_h} \tag{2.4}$$

where ν is Poisson's ratio for isotropic material, E_h and E_v are the horizontal and vertical Young's modulus, and ν_h and ν_v are Poisson's ratio in the horizontal and vertical directions, respectively, for anisotropic material.

The anisotropic minimum horizontal stress is expressed as following:

$$\sigma_{h\_aniso} = \frac{E_h}{E_v}\frac{\nu_v}{1-\nu_h}(\sigma_v - \alpha P_p) + \alpha P_p + \sigma_{Tectonic} \tag{2.5}$$

This expression shows that an increase of the anisotropic ratio E_h/E_v, leads to an increase in the minimum horizontal stress which in turn affects the prediction of fracture barriers and containment. Li et al. (2017) used this relationship to predict the fracture initiation pressure in anisotropic formations. The results of this study showed that an increase in the anisotropic ratio E_h/E_v leads to an increase in the fracture initiation pressure of both transverse and axial fractures. On the other hand, the equations for the isotropic and anisotropic tangential hoop stresses around a borehole wall of fluid pressure P_b are, respectively (Jaeger 1979; Khan et al. 2012; Suarez-Rivera et al. 2006):

$$\sigma'_{\theta} = (\sigma'_H + \sigma'_h) - 2(\sigma'_H - \sigma'_h)\cos 2\theta - (P_b - \alpha P_p) \tag{2.6}$$

$$\sigma'_{\theta\_aniso} = a(\theta, g_1, g_2)\sigma'_H + b(\theta, h_1, h_2)\sigma'_h + c(\theta, g_1, g_2)\Delta P_b \tag{2.7}$$

where

$$\Delta P_b = P_b - \alpha P_p \tag{2.8}$$

and a, b and c are material anisotropic parameters in terms of functions of the angular orientation along the wellbore, and they are written as following (Jaeger 1979; Suarez-Rivera et al. 2006):

$$a(\theta, g_1, g_2) = (1+g_1)(1+g_2)\times(1+g_1+g_2-g_1g_2-2\cos 2\theta)/(1+g_1^2-2g_1\cos 2\theta) \\ /(1+g_2^2-2g_2\cos 2\theta) \tag{2.9}$$

$$b(\theta, h_1, h_2) = (1+h_1)(1+h_2)\times(1+h_1+h_2-h_1h_2-2\cos 2\theta)/(1+h_1^2-2h_1\cos 2\theta) \\ /(1+h_2^2-2h_2\cos 2\theta) \tag{2.10}$$

$$c(\theta, g_1, g_2) = -(1+(g_1+g_2)^2-3g_1^2g_2^2-2(g_1+g_2)(1-g_1g_2)\cos 2\theta-2g_1g_2\cos 4\theta)/(1+g_1^2-2g_1\cos 2\theta) \\ /(1+g_2^2-2g_2\cos 2\theta) \tag{2.11}$$

where g_1, g_2, h_1 and h_2 are the coefficient of hoop stress and are calculated as:

$$g_1 = \frac{\sqrt{a_{1a}}-1}{\sqrt{a_{1a}}+1} \tag{2.12}$$

$$g_2 = \frac{\sqrt{a_{2a}}-1}{\sqrt{a_{2a}}+1} \tag{2.13}$$

$$h_1 = \frac{\sqrt{a_{1b}}-1}{\sqrt{a_{1b}}+1} \tag{2.14}$$

$$h_2 = \frac{\sqrt{a_{2b}}-1}{\sqrt{a_{2b}}+1} \tag{2.15}$$

Where in above equations:

$$a_{2a} = \frac{A_1 \pm \sqrt{A_1^2 - 4B_1}}{2} \tag{2.16}$$

$$a_{1a} = \frac{B_1}{a_{2a}} \tag{2.17}$$

$$a_{2b} = \frac{A_2 \pm \sqrt{A_2^2 - 4B_2}}{2} \tag{2.18}$$

$$a_{1b} = \frac{B_2}{a_{2b}} \tag{2.19}$$

A_1 and B_1 represent the coefficients in the orientation parallel to E_h, and A_2 and B_2 are the coefficients in the orientation parallel to E_v, and are expressed as:

$$A_1 = \frac{E_v}{G_{vh}} - 2\nu_{vh} \tag{2.20}$$

$$B_1 = \frac{E_v}{E_h} \tag{2.21}$$

$$A_2 = \frac{E_h}{G_{vh}} - 2\nu_{vh}\frac{E_h}{E_v} \tag{2.22}$$

$$B_2 = \frac{E_h}{E_v} \tag{2.23}$$

E_h is the Young's modulus parallel to the plane of isotropy, E_v is the Young's modulus normal to the plane of isotropy, ν_{vh} is Poisson's ratio measured on a vertical direction to the bedding, and G_{vh} is the shear modulus which can be calculated as:

$$G_{vh} = \frac{E_{45}}{2(1+\nu_{45})} \tag{2.24}$$

Here, E_{45} and ν_{45} are the apparent Young's modulus and Poisson's ratio measured on samples cut on 45° to the bedding.

These parameters were used by Suarez-Rivera et al. (2006) in order to evaluate the effect of the anisotropic parameters on the stress concentration around the wellbore. The results showed that the higher the elastic anisotropy is, the more difficult to initiate a transverse HF in a horizontal wellbore.

Within the context of this research, these analytical models are used to demonstrate the effect of different anisotropic parameters in shales on the HF initiation and propagation.

With regard to investigating the effect of toughness anisotropy on the hydraulic fracture, Bessmertnykh and Dontsov (2018) developed a simple model for an elliptical hydraulic fracture. They demonstrated that in the toughness dominated propagation the aspect ratio of a fracture scales as the ratio of vertical to horizontal toughness squared. That is if the vertical toughness is twice the horizontal toughness, then this would result in the aspect ratio of the ellipse being four. On the other hand, when viscosity dominates, then the fracture becomes radially symmetric. Zia et al. (2018) studied the impact of fracture toughness anisotropy on the propagation of a planar 3D hydraulic fracture perpendicular to the isotropy plane. They confirmed earlier observations for the fracture aspect ratio and analyzed the transition from viscosity to toughness dominated regime and the effect of different toughness anisotropy functions. The latter demonstrated how the final hydraulic fracture shape is governed by the variation of fracture toughness with propagation direction. Assuming that the fracture toughness K_c is a function of the local propagation direction, they used the following expression to determine the direction dependent fracture toughness:

$$K_c(\alpha) = K_{c,1} + (K_{c,3} - K_{c,1}) f(\alpha) \tag{2.25}$$

where

α : local propagation direction angle

$K_{c,1}$: fracture toughness in the horizontal direction $(\alpha = 0)$

$K_{c,3}$: fracture toughness in the vertical direction $(\alpha = \pi/2)$

$f(\alpha)$: function describing the toughness variation with the propagation direction

They also defined the scaled transition time t_{mk} from viscosity to toughness dominated regime with respect to the horizontal $(t_{mk,1})$ and vertical $(t_{mk,3})$ directions. They found that the ratio of these transition time-scales is inversely proportional to the anisotropic ratio of fracture toughness to the power nine as expressed it in the form of:

$$\frac{t_{mk,1}}{t_{mk,3}} = \left(\frac{K_{c,3}}{K_{c,1}} \right)^9 . \tag{2.26}$$

This equation shows that a small anisotropic ratio of fracture toughness ($K_{c,3}/K_{c,1}$) leads to a very large transition time between viscosity and toughness dominated propagation regime which will affect the final hydraulic fracture geometry. Hence, toughness anisotropy needs to be carefully integrated into the equations that are used to predict the geometry of HF. In addition, they proposed the direction dependence toughness for an elliptical fracture to remain elliptical:

$$K_C = K_{C,3} \times \left(sin^2 \beta + \frac{1}{\gamma^2} cos^2 \beta \right)^{1/4} \tag{2.27}$$

where the elliptical parameter β is defined as:

$$\beta = arctan\left(\frac{1}{\gamma^2} tan(\alpha) \right). \tag{2.28}$$

In this equation, γ is the aspect ratio and is related to the directional fracture toughness as:

$$\gamma = \frac{a}{b} = \left(\frac{K_{c,3}}{K_{c,1}} \right)^2 , \tag{2.29}$$

where *a* and *b* are, respectively, the length of the major and minor axes of the ellipse.

Dontsov (2019) further investigated the planar hydraulic fracture driven by a power-law fluid in a homogeneous rock formation with anisotropic fracture toughness. Results confirmed the effect of toughness anisotropy on the aspect ratio as well as provided approximate solutions and their bounds for the transition regimes. All the above studies indicate that there are cases in which toughness anisotropy is significant and therefore needs to be considered in design of HF in shales.

In chapter 4 we elaborate more on these models and use them to study the effect of rock anisotropy on the fracture initiation pressure and fracture morphology. The results will be compared to the numerical simulations of the TIV models in chapter 5.

2.3 Numerical Simulations

Numerous numerical models have been developed to model and design HF in shale rocks. However, due to the anisotropy of the shale including the existence of natural fractures that create complex medium, the HF modelling is challenging.

Hattori et al. (2017) presented an overview of HF in shale formations where they introduced the most recent researches on the shale anisotropy. In this work, they described some useful numerical methods that can be used to simulate real fracking problems. They presented different methods such as the cohesive methods (**Figure 2.2**), multiscale models, discrete numerical methods such as boundary element method (BEM), extended finite element method (X-FEM), meshless methods, discrete element method (DEM), and peri-dynamics numerical method. These methods are useful

as a first estimation of fracking model with some limitations associated with each model. In addition, they do not fully consider the complexity of the shale reservoirs, such as the multiscale characteristics of the shale fracturing and the complex fracture network that can develop after the propagation of the crack. Therefore, these concerns deserve considerable attention in the future work.

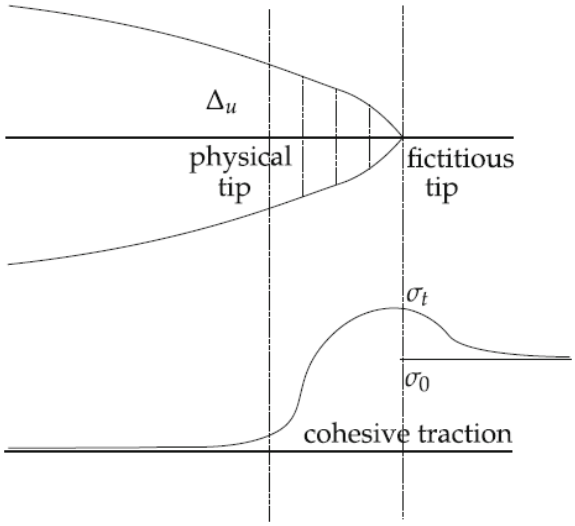

Figure 2.2: Cohesive crack (after Hattori et al. 2017)

Xia and Zeng (2019) investigated the impact of bedding inclination on the hydraulic fracture initiation and propagation using numerical model developed for TI rocks. The bonded particle element method combined with smooth joints models were applied to build the TI numerical model. Figure 2.3 shows that the bedding plane orientation has a great impact on the HF propagation direction. The results showed that the existence of bedding induces the HF to propagate along the bedding planes and the fracture breakdown pressure may be different for different bedding inclination angles.

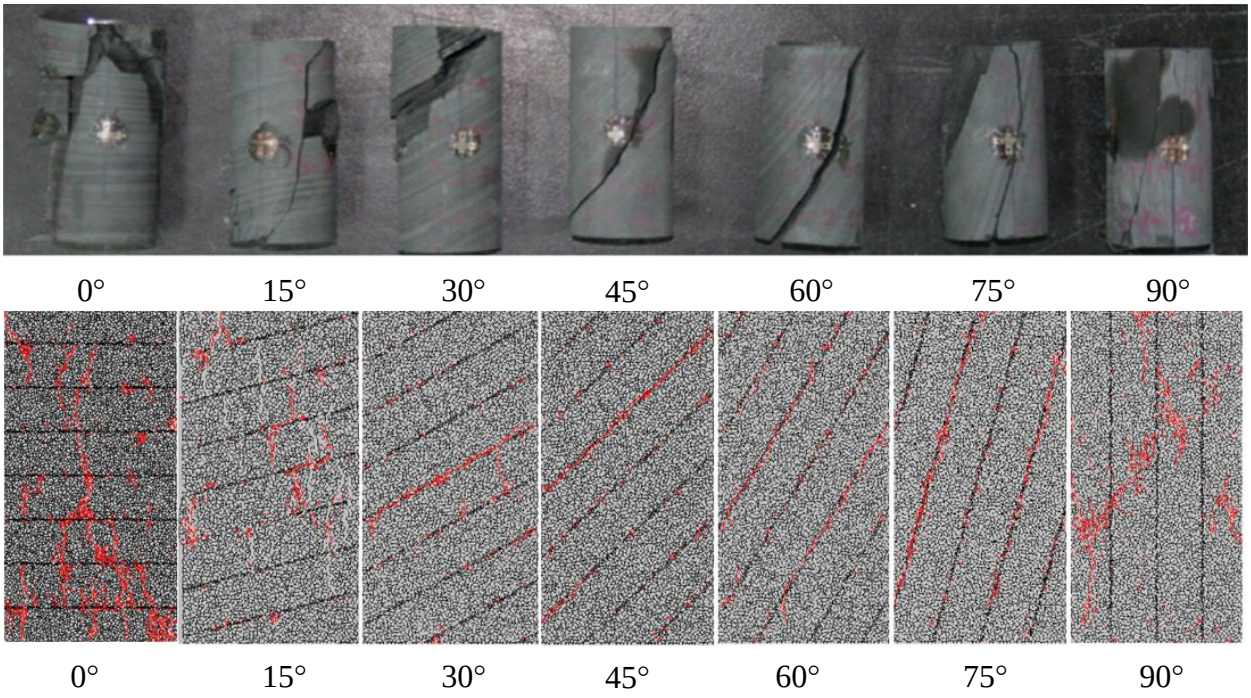

Figure 2.3: Failure patterns of different inclination specimen: a) experimental results, b) numerical simulation results: the red color is the micro-crack, the black color is the bedding plane (after Xia and Zeng 2019)

Valliappan et al. (2019) used a 2-D numerical model, based on extended finite element method (XFEM) as shown in **Figure 2.4** , to investigate the impact on hydraulic fractures propagation due to various parameters that incorporate the effect of anisotropy (ultimate tensile strength, Young's modulus, permeability and grain orientation). In addition, the impact of the degree of anisotropy and the initial fracture geometry on the fracture behavior have been investigated for anisotropic material. Figure 2.5 depicts the model geometry they used. The initial vertical crack to model the hydraulic fracture growth is placed in the bottom of the model and the influence of each anisotropic parameter on the HF is investigated.

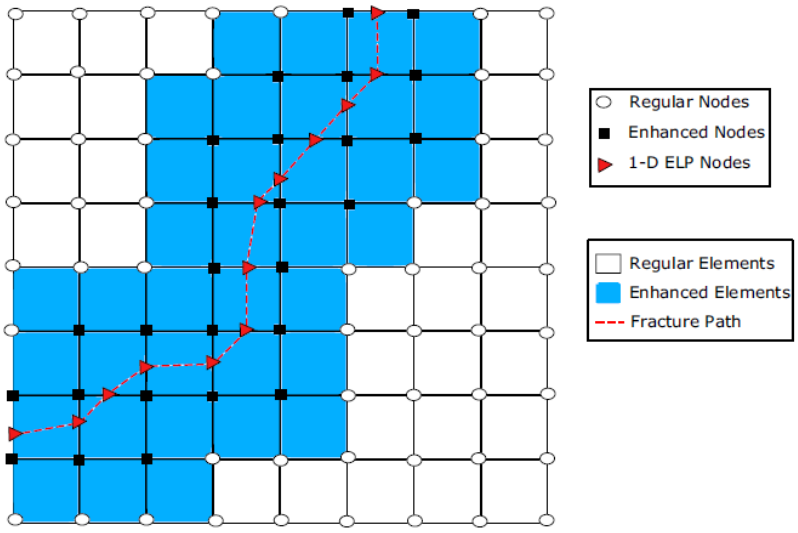

Figure 2.4: Discretization in XFEM (after Valliappan et al. 2019)

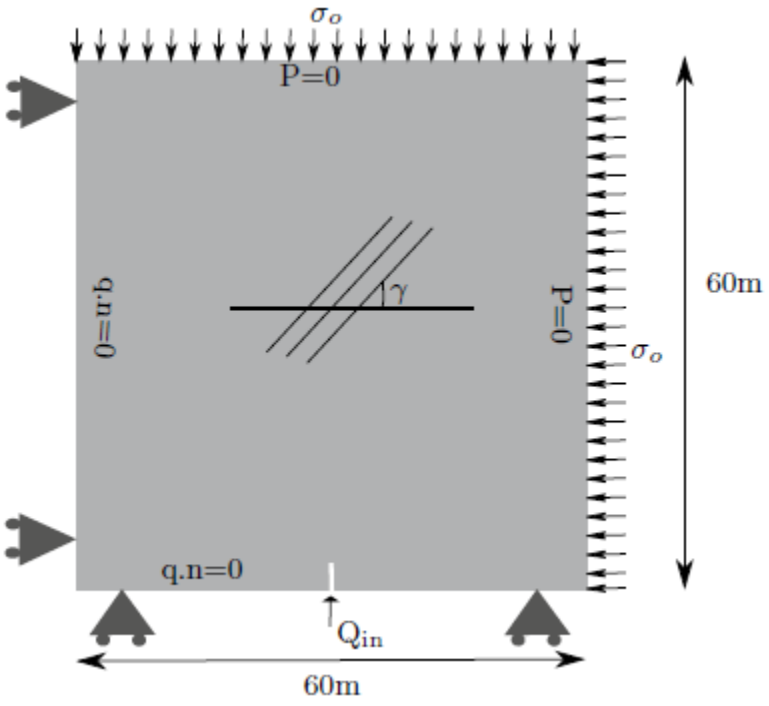

Figure 2.5: Geometry and boundary conditions of the hydraulic fracture problem (Valliappan et al. 2019)

The results of the fracture geometry as a function of increasing the anisotropic ratio of the Young's modulus, as depicted in **Figure 2.6**, show that the impact of the Young's modulus in the parallel direction ($E_{//}$) has a greater effect on fracture propagation than the Young's modulus in the

direction vertical to the plane of isotropy ($E_{\perp}$). For the case where the anisotropy is caused by increasing $E_{//}$, the fracture grows significantly; however, in the case of increasing the anisotropy by decreasing $E_{\perp}$, smaller fracture is observed.

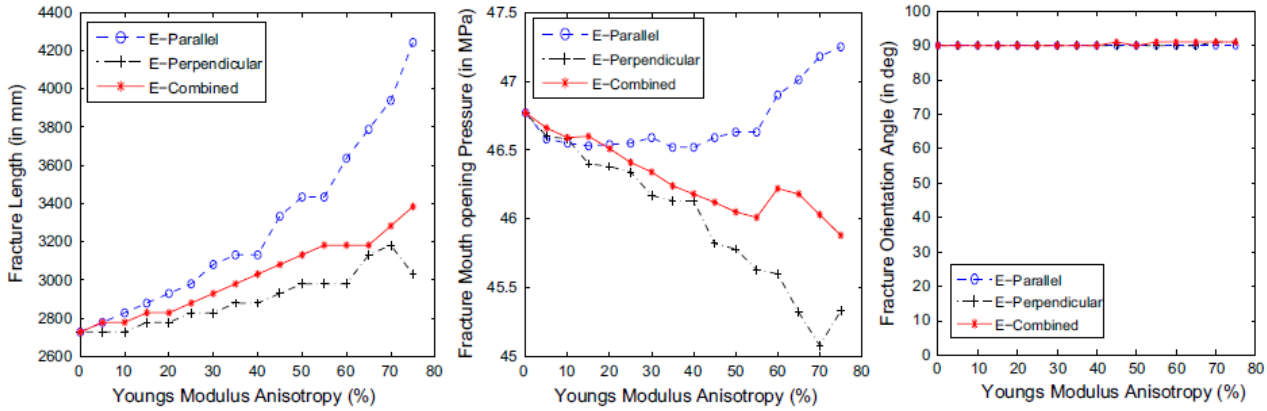

Figure 2.6: Fracture variation with Young's modulus anisotropy (Valliappan et al. 2019)

The results of simulating the impact of anisotropy due to Tensile strength on the HF propagation are shown in Figure 2.7. The authors concluded that the fracture tends to propagate in the direction perpendicular to the minimum ultimate tensile strength ($T_{ult-\perp}$).

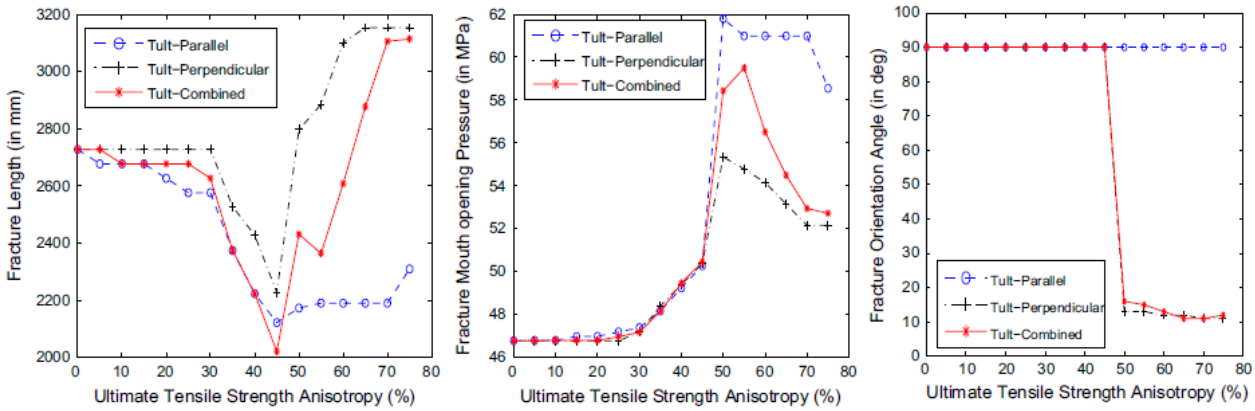

Figure 2.7: Fracture geometry variation with ultimate tensile strength anisotropy (Valliappan et al. 2019)

In addition, in their attempt to investigate the effect of the grain orientation, Valliappan et al. (2019) conducted a series of numerical simulations on HF propagation at different grain orientations. The results presented in Figure 2.8 show that the HF tends to deviate along the grain direction.

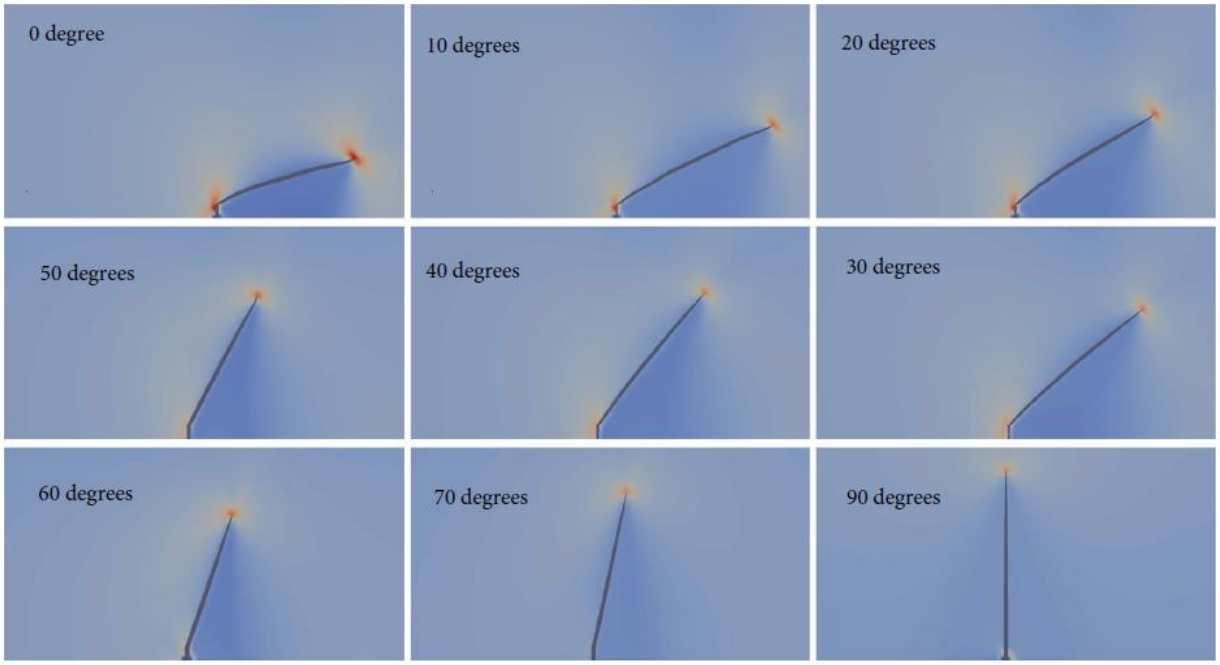

Figure 2.8: Propagation of an initial vertical fracture with different grain orientation angles for a material anisotropy of 55% (Valliappan et al. 2019)

Moukhtari et al. (2020a) studied the effect of material anisotropy on the fracture geometry deviation from radial shape. The exact expression for near-tip as a function of the propagation direction was derived and extended to TI problem. Then a numerical solver was used and verified from toughness dominated elliptical HF solution in TI medium. The quantitative growth of the HF was estimated numerically using a finite discretization coupled with near-tip solution for a steadily moving HF in TI medium. Figure 2.9 shows the evolution of fracture width for a transition from viscosity to toughness dominated regime, where the elongation in toughness-dominated regime is much higher than in viscosity-dominated regime. The elongation in the two orthogonal directions

of the anisotropic material as a function of the transition time-scales gives the form of toughness anisotropy in the toughness regime. These results confirm that the toughness anisotropy is clearly of first importance as it affects the final fracture shape and positively influences the vertical containment of HF propagation.

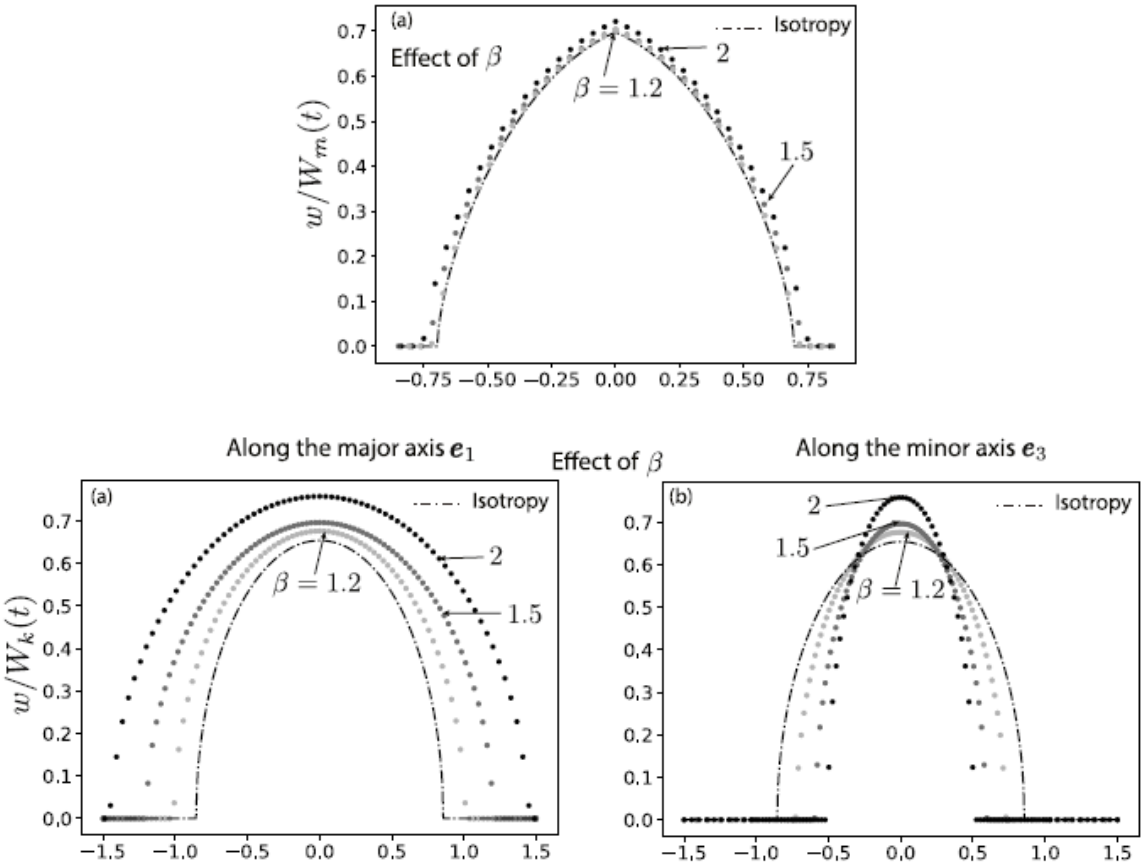

Figure 2.9: Fracture width evolution along the major and minor axes for anisotropic elasticity β = (1.2, 1.5, and 2) for viscosity dominated regime (Top) and toughness dominated regime (bottom) (Moukhtari et al. 2020)

Simultaneous propagation of multiple closely spaced hydraulic fractures in anisotropic fracture toughness and the sensitivity of the results to fracture propagation regimes was investigated by (Dontsov and Suarez-Rivera 2020). While it was seen that the fracture morphology strongly varies with the propagation regime, the fracture toughness anisotropy also dramatically affected the hydraulic fracture behavior. Figure 2.10 shows the results of the simultaneous propagation of 10

hydraulic fractures with spacing of 6.1 m in anisotropic fracture toughness and different scenarios of propagation regimes in the parametric space.

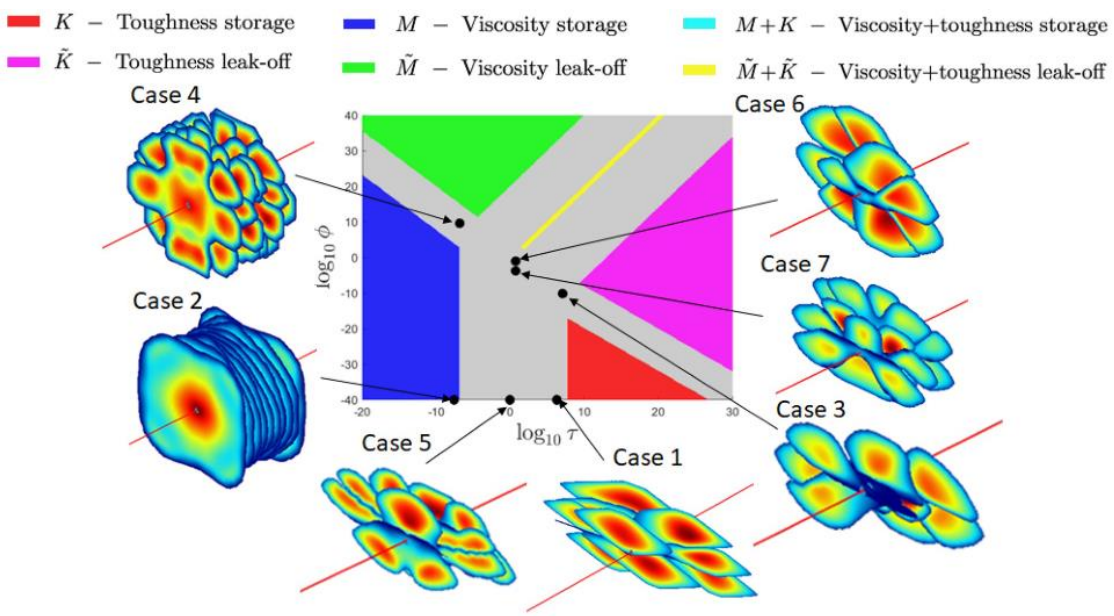

Figure 2.10: Simultaneous propagation of 10 fractures in different propagation regimes shown as black circles in the parametric space with anisotropic fracture toughness

In this study, a fully coupled 3D physics-based hydraulic fracturing and reservoir simulator is used to investigate the impact of TIV on the HF initiation and fracture morphology. The formulation and the advantages of these methods will be presented in Chapter 3. We will simulate the effect of different anisotropic parameters on the HF initiation and the final shape after propagation. The results of the numerical simulations will be presented in Chapter 5 and compared to the analytical models presented in Chapter 4.

2.4 Experimental Studies

A series of large uniaxial and true tri-axial HF experiments have been conducted in order to investigate the effect of the bedding plane on HF propagation behavior in the vertical plane of

laminated shale formation as shown in Figure 2.11 (Tan et al. 2017). The results of these experiments (Figure 2.12) showed that when encountering a bedding plane or natural fractures, the complex fracture network derive from the initial HF.

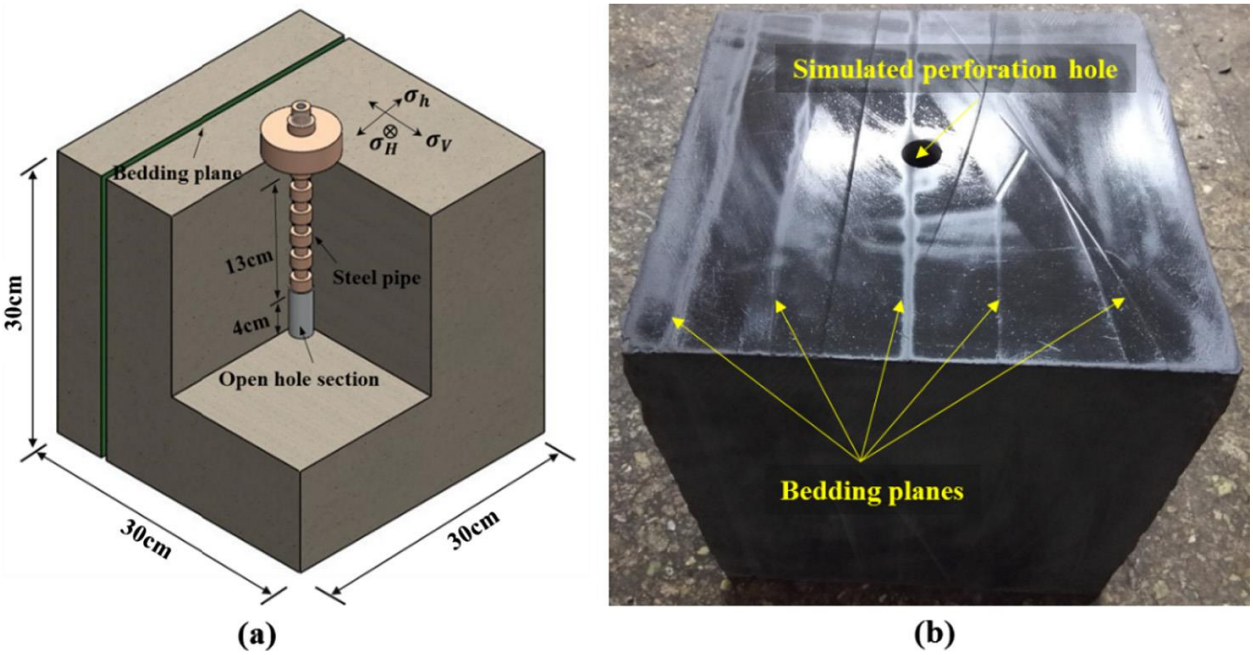

Figure 2.11: Illustration of testing specimen: (a) schematic diagram and (b) real fracturing specimen (Tan et al. 2017)

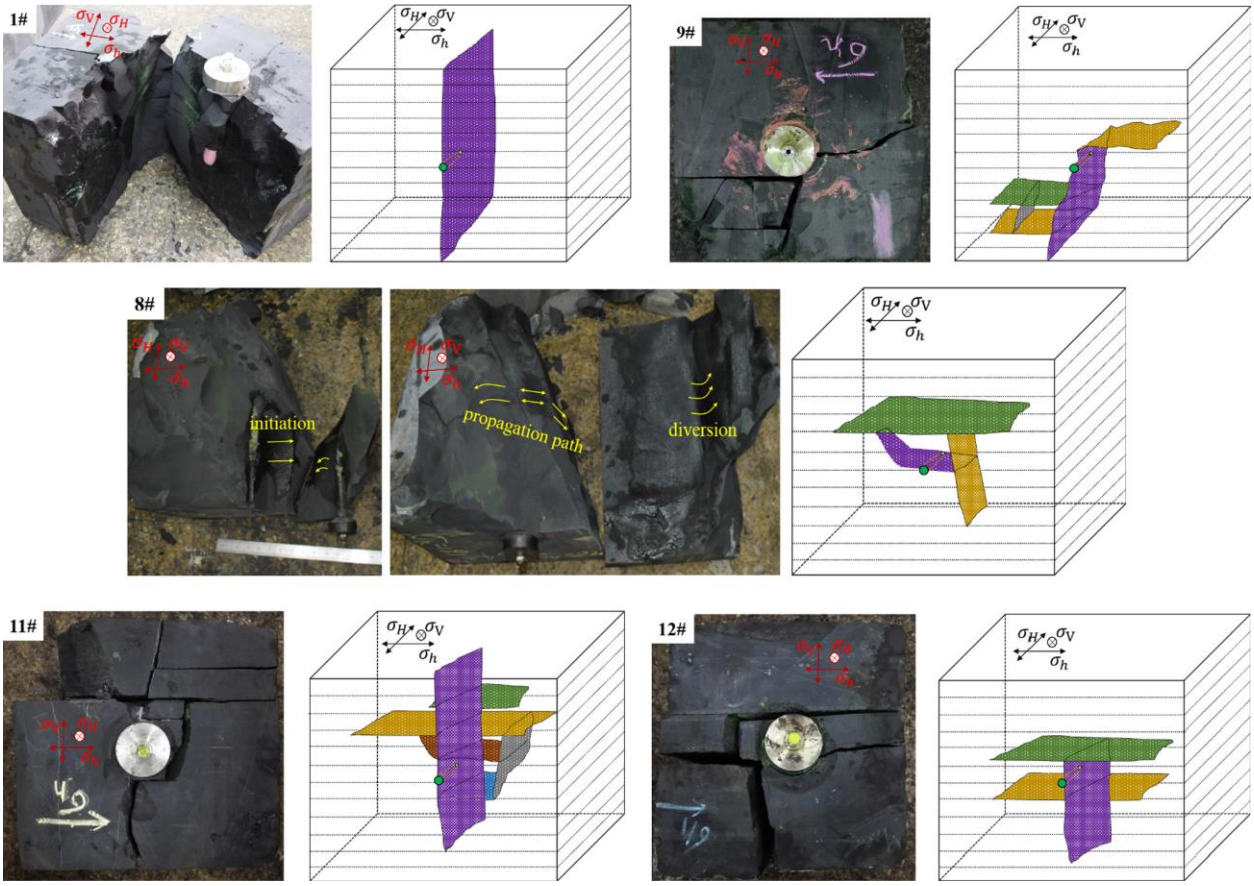

Figure 2.12: Hydraulic fracture geometries of some representative specimens (Tan et al. 2017)

Suarez-Rivera et al. (2013) conducted HF tests on large blocks from tight shale outcrops to investigate the fracture complexity and containment in shale. Figure 2.13 shows the results of a large-block experiment of HF in a horizontal wellbore drilled in the direction of the minimum horizontal stress parallel to the bedding and the initial fracture is oriented vertical to the bedding plane. The results show a development of a secondary fractures deviated from the initial fracture following the direction parallel to the bedding plane, whereas the initial fracture continue propagating vertical to the bedding. This fracture network form a “fish bone” geometry.

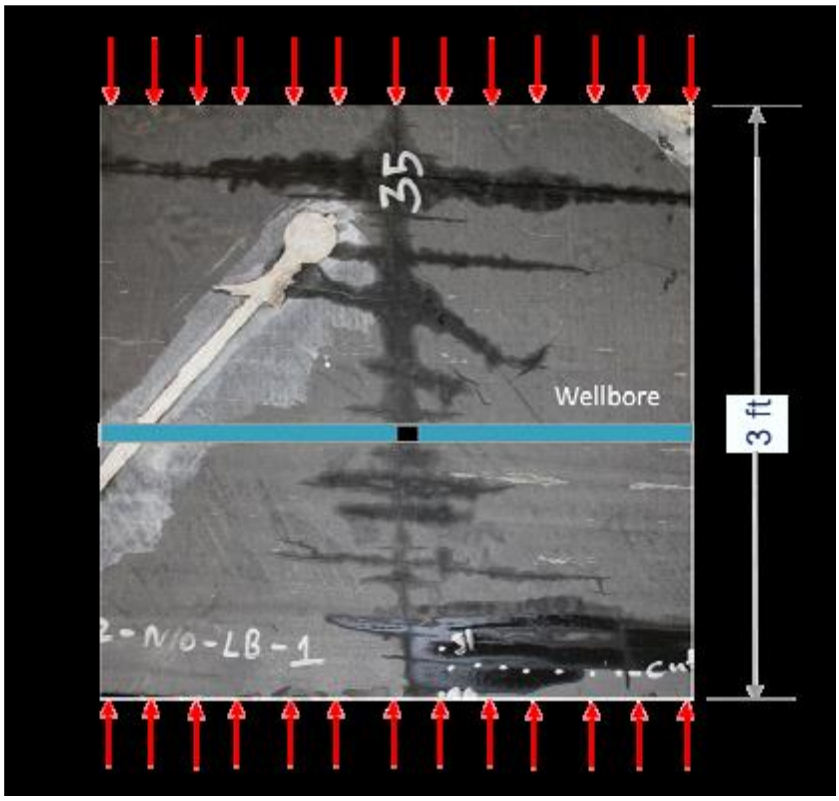

Figure 2.13: Hydraulic fracture propagation in large-scale tight shale outcrop (Suarez-Rivera et al. 2013)

In an attempt to characterize the shale fracture toughness anisotropy, Chandler et al. (2016) conducted a series of experiments in order to investigate the effect of weak interfaces (bedding plane) on fracture toughness measurements on shale samples and the HF propagation behavior. Tests have been conducted on the three principle crack orientations with respect to the bedding plane as shown in Figure 2.14. Low values of fracture toughness are recorded when the crack planes is parallel to the bedding; however, in case where vertical crack propagating normal to the bedding, higher fracture toughness values are observed and the crack tends to deviate toward the direction parallel to the bedding.

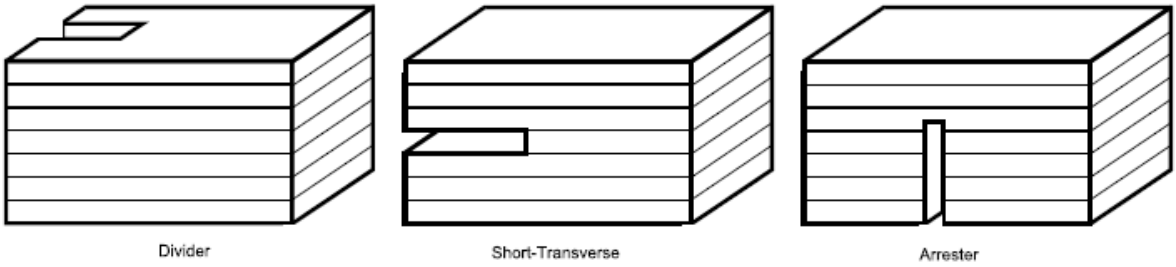

Figure 2.14: The three principal crack-plane orientations relative to bedding planes: Divider, Short Transverse, and Arrester (after Chandler et al. 2016)

While in this study we do not perform any lab experiments, we use the published lab data to simulate them numerically and compare the results with the physical observations in the lab to calibrate the numerical models. Such results are presented in Chapter 5.

2.5 Field Practices

Different methods can be used to assist in evaluating and monitoring the HF operations at field scale. For example, the sonic scanner may be used to determine the near wellbore stress anisotropy, radioactive tracer logs to evaluate the fracture height, and historical production data including the bottomhole pressure and near-wellbore pressures losses, and resistivity and acoustic imaging (Li et al. 2015). These methods are able to help understanding the fracturing process, evaluating the dominant HF azimuth and its geometry. However, unlike lab experiments, the field studies cannot be completely controlled and repeated. This difficulty is due to the difference of geologic conditions rock properties as well as in-situ stresses that are different in each field. Also, except the micro-seismic data, there is no other direct method to observe the fracture geometry, and micro-seismic is not acquired in many cases during a fracking job. For this reason, not many field observations concerning the impact of the material anisotropy on HF are reported.

In an attempt to demonstrate the existence of significant near wellbore complexity, both during stimulation and production, Ugueto et al. (2019) combines Distributed Acoustics Sensing DAS,

Distributed Temperature Sensing DTS and downhole pressure gauge data as a diagnostic tools to characterize the near wellbore region of an unconventional reservoir. The dimensions of longitudinal and transverse components in horizontal wellbores were quantified using the diagnostics presented. The results showed that near wellbore tortuosity is better quantified using DAS and downhole pressure gauges. They also highlight the risk of stress shadow and gave recommendations for a better frac placement.

Khan et al. (2012) used field data from a well in the Horn River Basin (HRB) to demonstrate the impact of mechanical anisotropy on fracture design. The anisotropic Young's modulus and Poisson's ratios were computed from Sonic Scanner logs and calibrated using core data, and mini-frac data was used to calibrate the stresses as shown in Figure 2.15. Near wellbore stress conditions control, the HF initiation and propagation and the shape of the HF geometry. Therefore, the anisotropy of the mechanical properties can lead in a wrong estimation of stresses, which in turn affects HF evaluation. In their study, they concluded that it is important to consider the anisotropic parameters in the estimation of the HF design since the isotropic approach underestimates the fracture height and overestimates the fracture width and half-length. This misestimation of the fracture geometry can lead to several problems in proppant design, proppant transportation and even early screen-out.

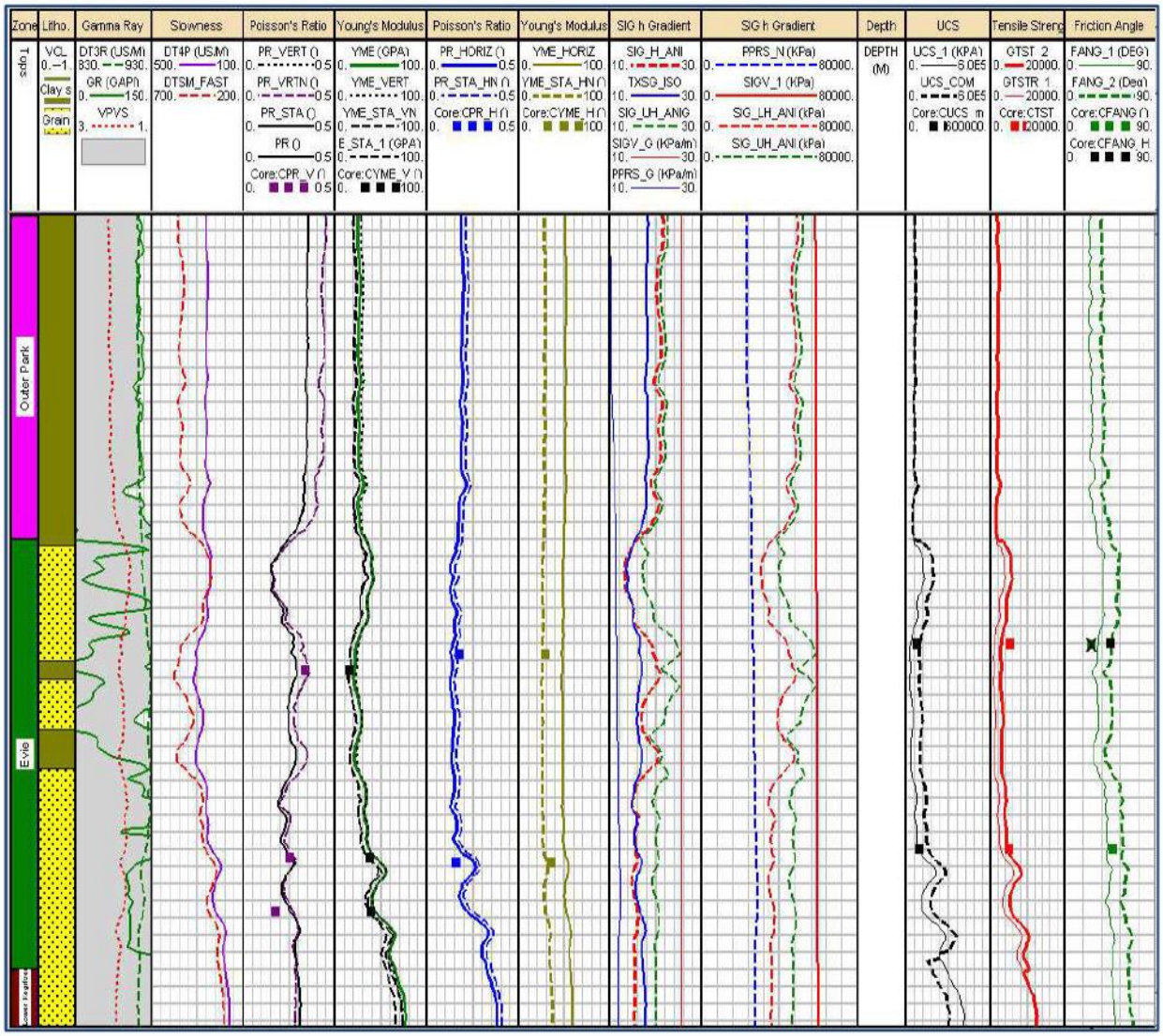

Figure 2.15: Calibrated 1D Mechanical Earth Model of Well A (Khan et al. 2012)

Warpinski and Teufel (1987) conducted a field study to investigate the influence of geologic discontinuities on HF propagation from mine-back observations at shallow depth. In their attempt to study the effect of bedding planes on the fracture propagation, as shown in Figure 2.16, they observed that HF was terminated at the bedding plane with a short propagating fracture length.

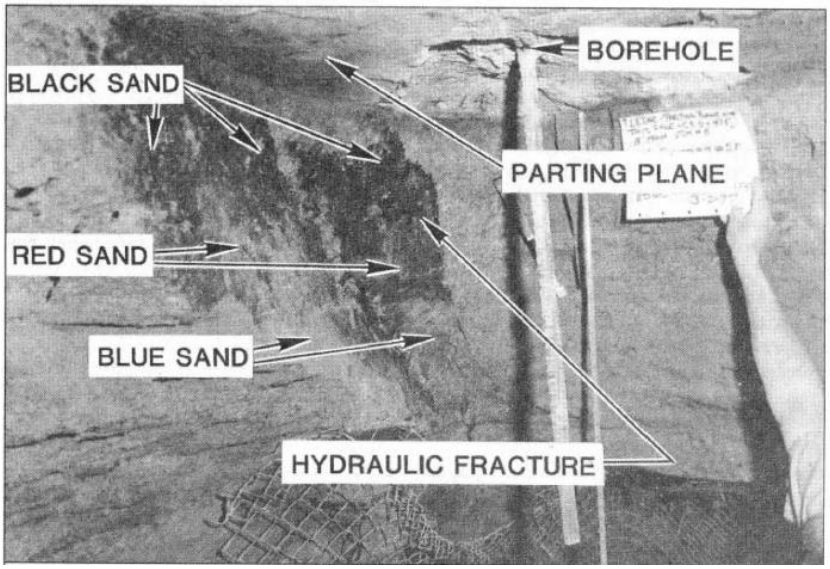

Figure 2.16: Photograph of fracture terminating near parting plane (Warpinski and Teufel, 1987)

Ketter et al. (2008), in their field study, used 256 horizontal wells in order to evaluate the causes of near-wellbore problems encountered in the Barnett Shale, concerning the inefficient fracture initiation pressure which led to proppant placement and stimulation issues. In their work, image logs were used to examine the stress anisotropy around the wellbore. In high stress area, the pressure to initiate a fracture was seen to be 50% higher than in low stress area. The high and low stress anisotropy in a horizontal section drilled in the direction of the minimum horizontal stress are presented in Figure 2.17 and Figure 2.18. Only transverse fractures were observed in high horizontal stress anisotropy where longer and narrower fracture fairways generated as shown in Figure 2.17. However, in low horizontal stress anisotropy, both longitudinal and transverse fractures were observed along the horizontal section of the wellbore. Shorter fracture lengths and wider fracture fairways are expected for this type of stress environment as shown in Figure 2.18. Qualifying the high and low stress anisotropy along the wellbore using image logs allows locating and placing the perforation cluster in suitable areas for better fracture initiation.

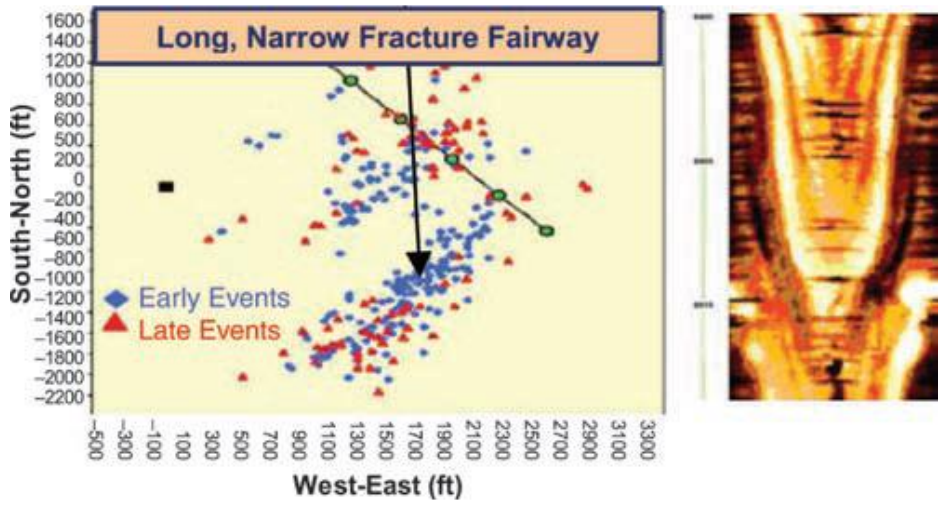

Figure 2.17: Microseismic events (left) and resistivity image (right) for case of high stress anisotropy (Ketter et al. 2008)

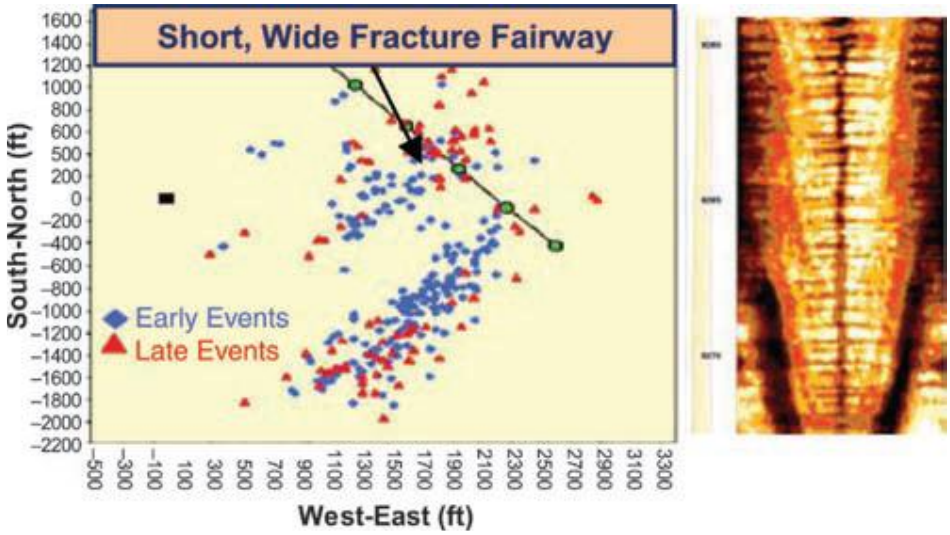

Figure 2.18: Microseismic events (left) and resistivity image (right) case of low stress anisotropy (Ketter et al. 2008)

In this study, we use the data from the Bakken formations in North Dakota as a field case example for simulation purposes.

2.6 Summary

A summary of different analytical models, numerical simulations, experimental testing, and some field scale practices to investigate the HF modelling in TI medium was presented in this Chapter.

The focus was to understand the impact of the material anisotropy due to different parameters on the HF initiation, propagation and the final geometry. The outcome of these studies revealed the importance of taking in to consideration the rock anisotropy in rock engineering projects such as well stability, HF design, proppant design and well stimulation. Different methods can be used to evaluate the material anisotropy and its effect on the fracture initiation pressure and final fracture geometry. The stress anisotropy is one of the parameters that affect the placement of the perforation clusters. The results of these researches show the importance of integrating the anisotropy as part of the HF design and how this may help to control the initiation of the HF in terms of location and pressure. In addition, it can help to prevent the proppant screen-out effect, high frictional pressure losses near wellbore and facilitate the proppant placing. Shale stimulation is of great importance and require further studies, especially in multi-stage HF in horizontal wellbores. In our research, we will further investigate this topic using some analytical models and 3D numerical simulations that are presented in the following Chapters. In the next chapter, an overview of ResFrac, the numerical simulator that will be used in this study to model the HF in TIV medium will be presented with the description of the formulation.

CHAPTER 3

Introduction to ResFrac Simulator

3.1 Introduction

In this Chapter, a brief overview of ResFrac, which is a fully coupled 3D physics-based hydraulic fracturing and reservoir simulator designed by *ResFrac Corporation* is presented (McClure et al. 2018). In addition, a summary of the governing formulation will be given. The anisotropic module in the ResFrac will be applied in Chapter 5 for simulation of single and multiple hydraulic fracturing in TIV medium in this study, as one of the first attempt for such applications.

3.2 The Overall Formulation of ResFrac

ResFrac is a fully coupled 3D physics-based hydraulic fracturing and reservoir simulator, developed by *ResFrac Corporation*. An Adaptive implicit method (AIM) is used in this simulator, with implicit/explicit solution scheme separately for different properties to optimize the simulator performance. The fluid flow and poroelastic stress changes are fully coupled using finite volume method, while the boundary element method is used to capture stress interaction between fracture elements. The simulator is a mesh based code where the matrix, wellbore and fracture are meshed separately (see Figure 3.1). ResFrac uses a rectilinear grid for matrix elements leading to a rectangular and conforming blocks. Cuboids are used to mesh matrix elements, wells are meshed

as line segments, and the fractures are meshed with rectangles having displacement discontinuity. The 1D subgrid method is used to estimate the fluid exchange between fracture and matrix elements, which preserves accuracy, even for coarse non-conforming meshes (McClure et al. 2018).

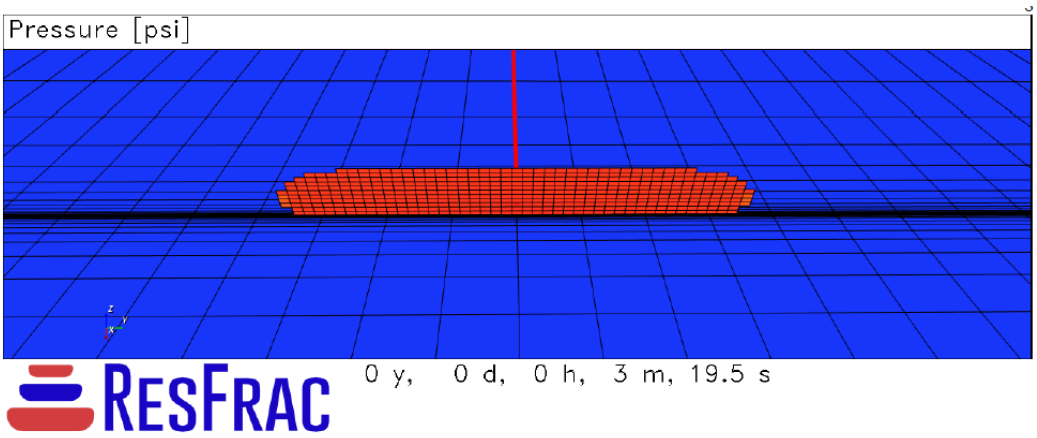

Figure 3.1: Example of ResFrac simulation mesh (McClure et al. 2018)

ResFrac adopts the finite volume method. For every element, the mass balance for different type of fluid component: molar, energy, proppant, water solutes are solved in each time step. Wellbore elements have an additional momentum balance equation for flow rate calculation. Matrix and fracture elements, each have mechanical deformation related formulation that consider stress shadow effect of fracture opening and stress change due to pressure change in the matrix (McClure et al. 2018).

3.2.1 Fluid Flow

For a component *c*, the molar flow rate from matrix element *i* to *j* is given by Darcy's law (Aziz and Settari 1979) :

$$q_{c,ij} = T_{ij} \sum_{p=1}^{p=3} \frac{z_{c,p,ij} k_{rp,ij} \rho_{M,p,ij}}{\mu_{p,ij}} \left(\Phi_{p,i} - \Phi_{p,j} \right), \tag{3.1}$$

where:

T_{ij} : parameter includes element geometric effect to average the permeability (Karimi-Fard, Durlofsky, and Aziz 2004):

p : is the phase,

$z_{c,p,ij}$: is the flowing molar fraction,

$k_{rp,ij}$: is the relative permeability that cannot exceed 1. Calculated based on power law brooks-Corey method as:

$$k_{rp} = k_{rp,multiplier} \left(\frac{s_p - s_{pr}}{1 - s_{pr}} \right)^{np}, \tag{3.2}$$

$\rho_{M,p,ij}$: is the flowing molar density,

$\mu_{p,ij}$: is viscosity,

Φ_p : is the fluid potential of each phase.

The volumetric fluid flow rate per element volume between the matrix element and the collocated fracture element is controlled by a shape factor a and the matrix element permeability k_m and is calculated as following (Zimmerman et al. 1993):

$$Q_d = \frac{-ak_m}{\mu} \left(P_f - P_m \right), \tag{3.3}$$

Where

P_f : pressure in the fracture element,

P_m : pressure in the matrix element.

a. fluid flow through the fracture

For the fluid flow through the fracture, the code consider Darcy and non-Darcy flow, Newtonian and non-Newtonian fluid, multiphase flow. In the following, the expressions for calculating fracture aperture are described, and followed by the calculation of the flow rate through the fracture.

In case of fluid pressure inside the fracture P_f is less than the normal stress acting on the fracture σ_n, the fracture is defined as mechanically closed and the aperture is expressed as:

$$E_{(\sigma_n > P_f)} = E_{res} + \frac{1 - C_{pr,c}}{1 - C_{pr}} \left[E_{cr} + E_b \right], \tag{3.4}$$

where,

E_{res} : is the irreducible aperture at very high effective normal stress.

E_{cr} : represent the contribution of unpropped fracture roughness to the aperture (Barton, Bandis, and Bakhtar 1985)(Willis-Richards, Watanabe, and Takahashi 1996) calculated as:

$$E_{cr} = E_0 (1 - \gamma_b) \left(\frac{1}{1 + \frac{9(\sigma_n - P_f)}{\sigma_{n,ref}}} \right), \tag{3.5}$$

where $\sigma_{n,ref}$ is the effective normal stress at E_{cr} reaches 10% of its maximum value. E_0 is the aperture part that is filled with proppant.

E_b : is the contribution of propped fracture to aperture, and calculated as:

$$E_b = \left(E_0\gamma_b + E_{pr}\right)exp\left(-C_{b,\phi}\left(\sigma_n - P_f\right)\right), \tag{3.6}$$

where:

γ_b : is the fraction of the fracture "roughness" part of E_0, and calculated as: $\gamma_b = min\left(1.0, \frac{C_{pr,c}}{C_{p,max}}\right)$

C_{pr} : is the volume fraction of proppant.

$C_{pr,max}$: the maximum possible proppant volume fraction in a packed bed.

$C_{pr,c}$: is the effective volume fraction of proppant at closure.

E_{pr} : the constant propped aperture where the fluid is drained from the element until closure.

In case of a mechanically open fracture, when the fracture walls have come out of contact because fluid pressure P_f exceeds the normal stress σ_n, the aperture is calculated as:

$$E_{(\sigma_n = P_f)} = E_0 + E_{res} + E_{pr} + E_{open}, \tag{3.7}$$

The aperture is calculated with keeping E_0, E_{res}, and E_{pr} constant within each timestep and adding E_{open} as an unknown in the system of equations.

The volumetric flow rate q_p of phase p, is expressed in a form of weighted average γ_f of the volumetric flow rate of fluid/proppant slurry in an open fracture $q_{p,o}$ and flow rate that is similar to a value of pure fluid passing through a closed fracture $q_{p,c}$. q_p and γ_f are defined as:

$$\gamma_f = \frac{E_{open}}{0.1\left(E_0 + E_{pr} + E_{res}\right) + E_{open}}, \tag{3.8}$$

$$q_p = \gamma_f q_{p,o} + \left(1 - \gamma_f\right) q_{p,c}, \tag{3.9}$$

If $E_{open} = 0$, $\gamma_f = 0$, and then $q_p = q_{p,c}$. If E_{open} is large, $\gamma_f = 1$, and then $q_p = q_{p,o}$.

$q_{p,c}$ and $q_{p,o}$ are weighted equally if $\gamma_f = 0.5$. This happens when $E_{open} = 0.1\left(E_0 + E_{pr} + E_{res}\right)$.

b. fluid flow in the wellbore

In case of fluid flow in the wellbore, the governed equation for momentum balance is expressed as following (Hasan and Kabir 2002):

$$\frac{d\left(\bar{\rho} v\right)}{dt} - \frac{dP}{dz} - v\frac{d\left(\bar{\rho} v\right)}{dz} + g\,sin\left(\theta_w\right)\bar{\rho} + \frac{f v^2 \bar{\rho}}{D} = 0, \tag{3.10}$$

Where:

$\bar{\rho}$: the average density in the element including all fluid phases and proppant,

D: wellbore diameter,

v: superficial velocity,

f: the fanning friction factor,

g: the gravitational constant,

θ_w: the angle from vertical.

For the perforation pressure drop between the wellbore elements and the fracture elements, the following equation by (Cramer 1987) is used:

$$\Delta P_{pf} = \frac{0.808 Q^2 \bar{\rho}}{C_{pf}^2 N_{pf}^2 D_{pf}^4}, \tag{3.11}$$

where

Q: total volumetric flow rate,

N_{pf}: the number of perforations in cluster,

D_{pf}: the diameter of the perforations,

C_{pf}: the coefficient of discharge.

Thermal transport and proppant transport in the fracture and wellbore are also implemented in the simulator

3.2.2 Fracture Initiation and Propagation

ResFrac models the fracture propagation using linear elastic fracture mechanics where the fractures are assumed to propagate in a linear way (McClure et al. 2018). The fracture is mechanically initiated when the fluid pressure at the initiation point must exceed the locally calculated minimum horizontal stress. This happen only if the fluid pressure is high enough and thus the fracture toughness has an impact on the fracture initiation. When the stress intensity factor K_I reaches the fracture toughness K_{IC} ($K_I / K_{IC} = 1$), the fracture tip extends.

In ResFrac, the fracture toughness can be direction dependent values, different in the vertical and horizontal directions. In addition, it can be scaled with fracture size and modelled as following (Delaney et al. 1986; Scholz 2010):

$$K_{IC} = K_{IC,init}\left(1 + K_{IC,fac}\sqrt{L_{eff}}\right), \tag{3.12}$$

where,

$K_{IC,init}$: the initial fracture toughness,

$K_{IC,fac}$: scaling parameter,

L_{eff} : the fracture length-scale.

3.2.2 Limited Entry Condition

In multiple hydraulic fracturing, the fracture design optimization is mainly related to cluster spacing, well spacing, and limited-entry condition. One main consideration in multiple hydraulic fracturing is the stress shadow effect between fractures, which tends to localize the flow into a small number of fractures in the stage. Therefore, the limited entry method is of great interest, to allow equal distribution of fluid to the fractures (McClure et al. 2020).

3.3 Model Setup

In this section, the primary parameters to set up a HF model in ResFrac are presented. ResFrac can model HF propagation and rock deformation in naturally fractured reservoirs in three dimensions (3D). Multiple boreholes and injection points can be simulated in different formation types. The model can have any number of fractures and can consist of any number of segmented boreholes with one or multiple clusters (i.e., fluid injection points). The code also allows injections from open-hole and cased-hole completion segments. Figure 3.2 highlights the typical elements in ResFrac used to simulate a HF model.

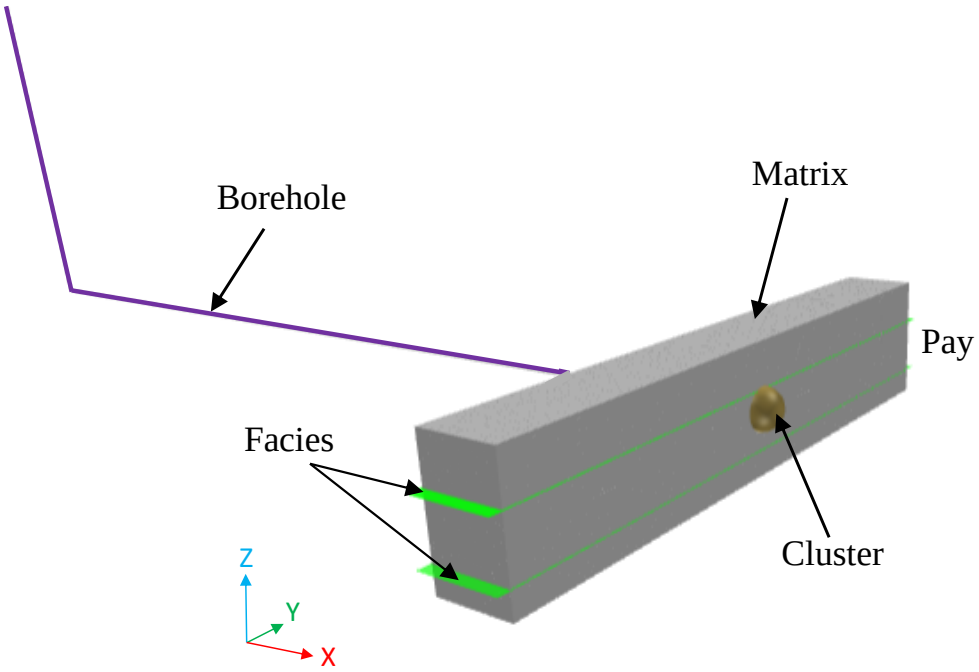

Figure 3.2: Sketch plot of a HF model in ResFrac

The matrix mesh geometry, size and location should be carefully specified to be large enough so that the fractures will never reach the edges, which are "no flow" boundary conditions. The matrix region can be specified to focus only on the region of interest (few stages as shown in Figure 3.2) or the entire length of lateral sometimes.

The data of the HF model properties can be input with both metric and field units. Formation properties of different geologic unites (Facies) are specified by the user within depth intervals. These properties include permeability, porosity, fracture toughness, Young's modulus, the in-situ stresses and the orientation of the minimum stress, initial fluid saturation, and other parameters. In ResFrac, the anisotropy of intact rock elasticity, fracture toughness, and permeability are defined separately. Therefore, the user can employ different anisotropic functions for the intact rock's Young's modulus, permeability, and for the fracture toughness. Figure 3.3 shows an example of

facies list panel with an example of TIV fracture toughness and Young's modulus input for the target layer.


GEOLOGICAL UNITS (FACIES LIST)

	Name	K1c horizontal [MPa-m^(1/2)]	K1c vertical [MPa-m^(1/2)]	Horizontal Young's modulus [MPa]	Vert over horiz modulus
1	Pay	1	3	30000	0.5

New Row Resize Table

Figure 3.3: Facies list panel with example of anisotropic fracture toughness and Young's modulus input

Well location and geometry along as with the inner diameter, are specified with a series of vertices all the way to the surface as shown in Figure 3.4. However, as mentioned previously, only the zone of interest should be comprised within the matrix region.

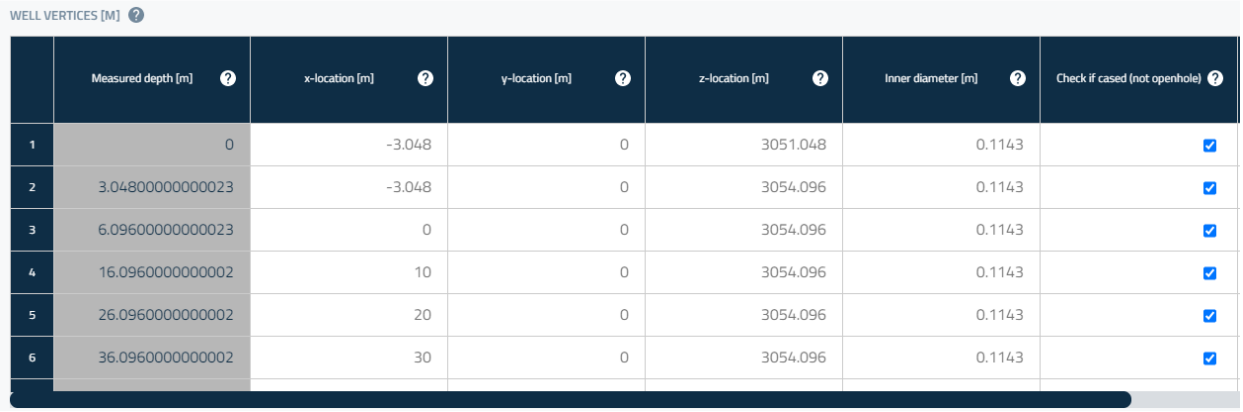
WELL VERTICES [M]

	Measured depth [m]	x-location [m]	y-location [m]	z-location [m]	Inner diameter [m]	Check if cased (not openhole)
1	0	-3.048	0	3051.048	0.1143	☑
2	3.04800000000023	-3.048	0	3054.096	0.1143	☑
3	6.09600000000023	0	0	3054.096	0.1143	☑
4	16.0960000000002	10	0	3054.096	0.1143	☑
5	26.0960000000002	20	0	3054.096	0.1143	☑
6	36.0960000000002	30	0	3054.096	0.1143	☑

Figure 3.4: Well vertices panel

Next, the stages location and perforation cluster design can be specified. The user can define the distance between perforation clusters, stage number, perforation diameter, and the relative number of perforations of each cluster as shown in Figure 3.5. Fluid injection design can be defined from the fluid model option and water solutes panel, where the user can define the fluid type and fluid viscosity.

PERFORATION CLUSTERS

	Measured depth [m]	x-location [m]	y-location [m]	z-location [m]	Stage number	Number of perforations	Perforation diameter [m]
1	7.00000000000045	0.904000000000222	0	3054.096	1	12	0.0127
2	17.0000000000005	10.9040000000003	0	3054.096	1	12	0.0127
3	27.0000000000005	20.9040000000003	0	3054.096	1	12	0.0127
4	37.0000000000005	30.9040000000003	0	3054.096	1	12	0.0127
5	47.0000000000005	40.9040000000003	0	3054.096	1	12	0.0127

Figure 3.5: Perforation clusters panel

The last step is the injection schedule, here, the type of the injection fluid along as with the injection rate and the time of injection are defined from the well control panel. At this step, the user can also do the proppant design by selecting the proppant type and concentration as shown in Figure 3.6. In addition to injection sequence, the user can do the production design by specifying the production type, start production time, duration, maximum production rate, and minimum production pressure. In this study, we are not interested on the production design.

INJECTION SEQUENCE BOUNDARY CONDITION CONTROL RECORDS

	Start time [Hours]	Duration [Hours]	Stage	Fluid type	Slurry injection rate [m^3/s]	Proppant type	Proppant mass per volume [kg/m^3]
1	0	1	All stages	PureWater	0.1	None	0

Figure 3.6: Injection sequence panel

Several secondary and advanced options, that the user is not familiar with, can be defined in Resfrac simulations. These parameters is set to default values while the user can use the help button to get more information on these parameters.

After completing all these steps, the HF model is ready to be executed and the user need only to hit the Run simulation button to submit and run the simulation.

3.4 Summary

In this Chapter a summary of ResFrac formulation for both isotropic and anisotropic media simulation was introduced along with different features of ResFrac which uses numerical hydro-mechanical coupling scheme. In addition, the steps for setup and running the HF model were presented. ResFrac is able to simulate the effect of different anisotropic parameters for HF initiation and propagation. Such applications will be presented in Chapter 5. In the next Chapter, the analytical models to investigate the HF initiation in anisotropic medium will be presented. The effect of TIV fracture toughness along with the effect of initial fracture geometry and size on the fracture initiation pressure will be investigated and compared with the numerical simulations of Chapter 5. The evaluation of the competition between axial and transverse fractures in a medium that exhibit TIV fracture toughness will be presented.

CHAPTER 4

Analytical Models

4.1 Introduction

As stated in the previous Chapters, the presence of laminations resulted in the TIV nature of shale formations that makes the HF modeling in such formations more complicated than in isotropic medium. The challenge, however, is that material anisotropy due to different parameters can control the HF initiation, propagation and the fracture geometry. Therefore, it is important to integrate the anisotropy as part of the HF design.

In this Chapter, first, a brief review of the fracture pressure estimation from the tensile stress singularity at the tip of a fracture emanating from a hole in an infinite elastic medium given by Nilson and Proffer (1984a). This is based on the assumption of isotropic medium. The impact of transversely isotropic fracture toughness studied by Bessmertnykh and Dontsov (2018) and Zia et al. (2018) will be presented, which calculates the transversely isotropic fracture toughness based on the directional fracture toughness. This direction dependent fracture toughness will be implemented to estimate the fracture initiation pressure for both transverse and axial fractures; and the influence of it on the FIP will be the main focus of this study.

The analytical models proposed by Khan et al. (2012) and Suarez-Rivera et al. (2006) which integrate the anisotropy of Young's modulus effect on horizontal stresses given by Amadei et al.

(1987), Pan and Amadei (1995) and Jaeger (1979) to illustrate the stress computation and fracture design will be briefly discussed and implemented to the estimation of the fracture initiation pressure. In these analytical models, we will use typical parameters of Bakken Shale Formation.

4.2 Fracture Initiation Pressure Models

Here, we consider a pre-existing fracture with a given length emanating from a horizontal wellbore. Two fracture geometries are considered in this study, axial and transverse fracture Figure 4.1. Assuming that the crack of a specific length propagates under the hypotheses of linear elastic fracture mechanics (LEFM), we use the mode I stress intensity factor to estimate the magnitude for initiation pressure of each fracture geometry. According to Nilson and Proffer (1984a), the strength of the tensile stress singularity at the tip of a fracture emanating from a hole in an infinite elastic medium can be calculated as shown in equation (4.1):

$$K_I = \frac{2}{\sqrt{\pi}}\sqrt{L}\int_0^L (P_f - \sigma) f\left(\frac{x}{L}, \frac{L}{a}\right)\frac{dx}{\sqrt{L^2 - x^2}} \tag{4.1}$$

In this equation:

K_I is the mode I stress intensity factor,

L is the length of the fracture,

a is the radius of the hole,

x is the position variable along the fracture,

$P_f(x)$ is the internal pressure within the fracture,

$\sigma(x)$ is external confining stress acting normal to the fracture plane,

$P_f(x) - \sigma(x)$ is the net pressure.

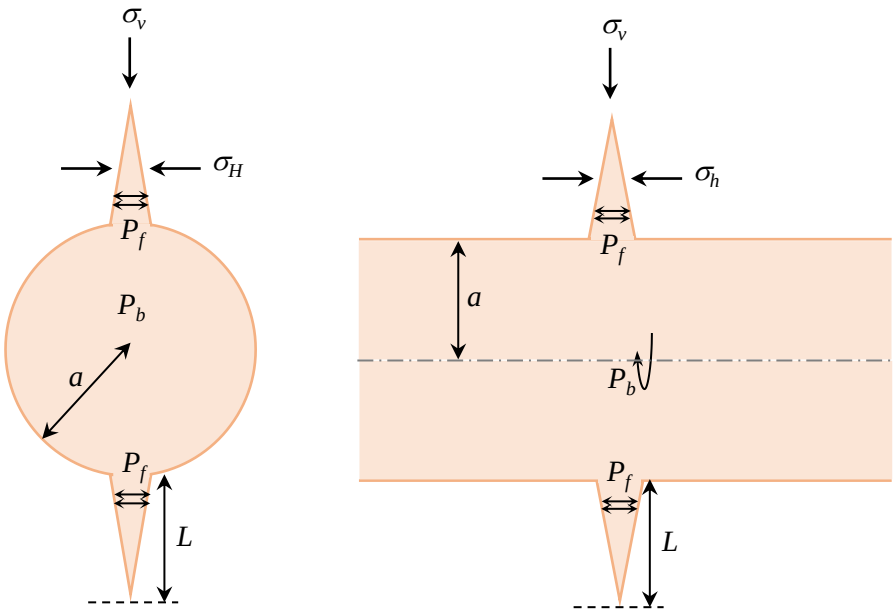

Figure 4.1: Axial (left) and transverse fracture (right) emanating from a horizontal wellbore drilled along σ_h

The input data used in this study, tabulated in Table 4. 1, correspond to typical parameters of Bakken Shale Formation.

Table 4. 1 Bakken Shale Formation mechanical properties and in-situ stresses (Schmidt et al. 2011)

Property	Value	Unit
Density, ρ	2650	kg/m^3
Young's Modulus, E	30	GPa
Uniaxial Compressive Strength, UCS	50	MPa
Tensile Strength, T_o	5	MPa
Toughness, $K_{IC\text{-}isotropic}$ $K_{C,1}$, $K_{C,2}$	1	Mpa.m^0.5
Friction Angle, ϕ	30	degree
Poisson's Ratio, v	0.25	-
Porosity, $\emptyset$	2	%
Permeability, K	1e-5	Darcy
Minimum Horizontal Stress, σ_h	54.8	MPa
Maximum Horizontal Stress, σ_H	61.6	MPa
Vertical Stress, σ_v	68.4	MPa
Fluid Viscosity, μ	0.002	Pa.s
Flow Rate, Q	0.08	m^3/s
Borehole Radius, a	0.11	m

Figure 4.2 represents the cross section of a horizontal wellbore with radius a drilled along the direction of σ_h, with an axial fracture of length "L" edging at the wellbore. Here, in addition to the wellbore pressure (P_b) and the average pressure in the crack (P_f), we include the pore pressure (P_p) effect, due to the fluid pressure inside the pores, or also known as the reservoir pressure. Pressurization rate can be formulated as dimensionless parameter (f_p):

$$f_p = \frac{P_f - P_p}{P_b - P_p} \tag{4.2}$$

The internal fracture pressure $P_f(x)$ in equation (4.1) depends on the pressurization rate. In case of slow pressurization, where there is enough time for the fluid pressure to equilibrate inside the crack, the internal crack pressure is equal to the wellbore pressure $P_f = P_b$, and f_p=1. However, in

case of fast pressurization, the fluid pressure cannot diffuse into the crack, hence the internal pressure is equal to the pore pressure $P_f = P_p$ and f_p=0. The discussions presented in this section are for the slow pressurization rate. In the case of fast pressurization limit, the fracture initiation pressure is infinite for the case of transverse fracture and it is higher than slow pressurization limit (up to a factor of two) for axial fracture as noted by Detournay and Carbonell (1997a).

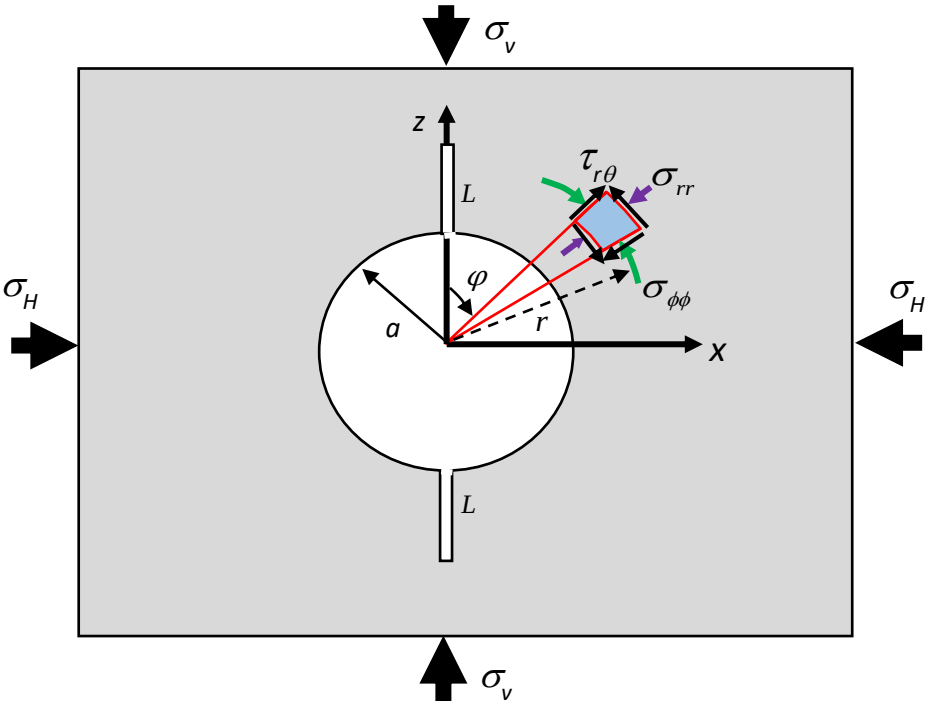

Figure 4.2: Fracture mechanics model for crack growth in a pressurized circular borehole (Djabelkhir 2020)

Assuming normal faulting stress regime ($\sigma_v > \sigma_H > \sigma_h$), as shown in Figure 4.2 the two far field stresses acting on the wellbore wall are σ_v and σ_H. If axial (longitudinal) fractures develop around the wellbore in this case, it will be along σ_v direction where $\varphi = 0°$ (perpendicular to the least tangential stress, $\sigma_{\theta\theta}$, i.e. on the top and bottom of the wellbore, along z direction).

For a homogeneous and isotropic elastic rock, the induced stresses can be estimated from Kirsch's equations (Kirsch 1898):

$$\sigma_{rr} = \frac{1}{2}(\sigma_v + \sigma_H)\left(1 - \frac{a^2}{r^2}\right) + \frac{1}{2}(\sigma_v - \sigma_H)\left(1 - \frac{4a^2}{r^2} + \frac{3a^4}{r^4}\right)cos\,2\varphi + \frac{a^2}{r^2}P_b \tag{4.3}$$

$$\sigma_{\theta\theta} = \frac{1}{2}(\sigma_v + \sigma_H)\left(1 + \frac{a^2}{r^2}\right) - \frac{1}{2}(\sigma_v - \sigma_H)\left(1 + \frac{3a^4}{r^4}\right)cos\,2\varphi - \frac{a^2}{r^2}P_b \tag{4.4}$$

$$\sigma_{yy} = \sigma_h - 2\nu(\sigma_v - \sigma_H)\frac{a^2}{r^2}cos\,2\varphi \tag{4.5}$$

$$\sigma_{r\theta} = \frac{1}{2}(\sigma_v - \sigma_H)\left(1 + \frac{2a^2}{r^2} - \frac{3a^4}{r^4}\right)sin\,2\varphi \tag{4.6}$$

Similarly, in the case of strike-slip stress regime, if axial (longitudinal) fractures develop around the wellbore, it will be along σ_H direction where $\varphi = 90°$ (perpendicular to the least tangential stress,σ_{qq} i.e. on the sides of the wellbore along *x* direction).

In both cases of normal and strike-slip stress regimes, the transverse fractures develop orthogonal to the wellbore axis, perpendicular to the *y* direction or direction normal to σ_h. Therefore, the external confining stress $\sigma(x)$ in equation (4.1) for axial and transverse fractures are respectively:

$$\sigma(x) = \sigma_{\theta\theta} = \frac{1}{2}(\sigma_v + \sigma_H)\left(1 + \frac{a^2}{r^2}\right) - \frac{1}{2}(\sigma_v - \sigma_H)\left(1 + \frac{3a^4}{r^4}\right)cos\,2\varphi - \frac{a^2}{r^2}P_b \tag{4.7}$$

$$\sigma(x) = \sigma_h \tag{4.8}$$

The configuration or weight function *f* in equation (4.1) is dependent on geometry of the problem and can be expressed as a combined effect of radial divergence (f_{rad}) and stress free (uniformly pressurized) notch surface (f_{notch}):

$$f = f_{rad}\,f_{notch} = \left(\frac{x/L + a/L}{1 + a/L}\right)^n \left[1 + 0.3\left(1 - \frac{x}{L}\right)\left(\frac{1}{1 + L/a}\right)^{2m}\right] \tag{4.9}$$

In this study, for a cylindrical cavity, which is the geometry of the borehole, *m*=2. However, for spherical cavity, *m*=3. In planar problem, corresponding to an axial fracture in the case of a

horizontal wellbore (see Figure 4.1 (left)), *n*=0, whereas *n*=1 in case of axisymmetric problems, corresponding to transverse fracture shown in Figure 4.1 (right). This means that equation (4.9) can be written for axial and transverse fractures, respectively, as followings:

$$f = \left[1 + 0.3\left(1 - \frac{x}{L}\right)\left(\frac{1}{1 + L/a}\right)^4\right] \tag{4.10}$$

$$f = \left(\frac{x/L + a/L}{1 + a/L}\right)\left[1 + 0.3\left(1 - \frac{x}{L}\right)\left(\frac{1}{1 + L/a}\right)^4\right] \tag{4.11}$$

The pressure required to initiate a crack of length L at the wellbore with a fracture toughness K_{Ic} is the minimum wellbore pressure that fulfils the condition $K_I/K_{Ic} = 1$ i.e. when the mode I intensity factor be equal to the fracture toughness. In the case of TIV medium is when the mode I intensity factor be equal to the direction dependent fracture toughness K_c i.e. ($K_I/K_c = 1$).

We used the characteristic pressure defined by Abbas et al. (2013) as $P^* = \sqrt{32/\pi}K_{IC}/\sqrt{a}$ to scale the stresses, and the pressure while the fracture toughness is scaled by $K_{IC-isotropic}$. In the following $\Pi = P_f / P^*$.

Figure 4.3 shows the results of the scaled initiation pressure for different fracture sizes of both transverse and axial fractures in isotropic medium and normal stress regime, which will be compared later to different anisotropic scenarios. From Figure 4.3 it is seen that as the notch length increases, the initiation pressure reduces and ultimately it converges to the scaled far field stresses. The curves corresponding to the transverse and axial fractures cross for approximately *L/a* = 0.15. This means that for transverse and axial cracks of the same lengths, and larger than this ratio, the transverse fracture will be more likely to initiate.

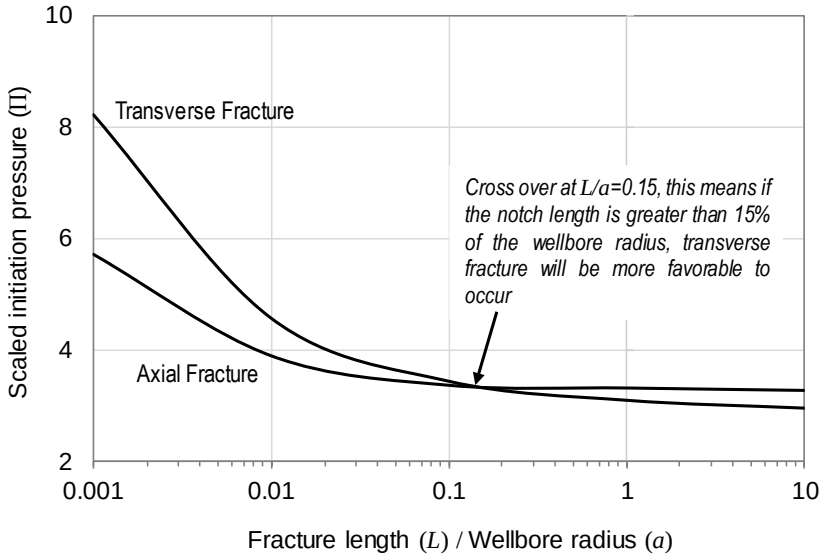

Figure 4.3: Fracture initiation pressures for transverse and axial fractures in isotropic medium

4.3 TIV due to Toughness

We consider the problem shown in Figure 4.4 for a medium with TIV toughness. The toughness, thus, is dependent to the angle α between the local fracture front propagation direction and the axis $\overrightarrow{e_1}$ in case of transverse fracture and the axis $\overrightarrow{e_2}$ in case of axial fracture. As it is seen, the properties $K_{C,1}$ and $K_{C,2}$ are within the plane of isotropy defined by $(\overrightarrow{e_1}, \overrightarrow{e_2})$ and thus $K_{C,1} = K_{C,2}$. However, $K_{C,3}$ is along the axes $\overrightarrow{e_3}$ that is vertical to the plane of isotropy.

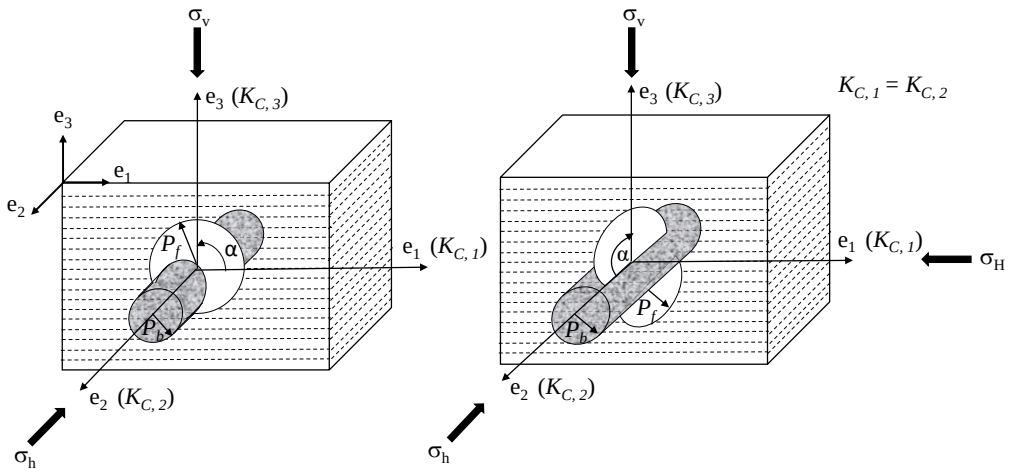

Figure 4.4 Transverse and axial fractures emanating from a horizontal wellbore in a medium with TIV toughness

According to Zia et al. (2018), assuming that the toughness K_C is a function of the local propagation direction α (see Figure 4.4), the direction dependent toughness is defined by the following expression:

$$K_C(\alpha) = K_{C,1} + (K_{C,3} - K_{C,1}) f(\alpha) \tag{4.12}$$

where

α: local propagation direction angle at the fracture front

$K_{C,1}$: fracture toughness in the horizontal direction $(\alpha = 0)$

$K_{C,3}$: fracture toughness in the vertical direction $(\alpha = \pi/2)$

$f(\alpha)$: function describing the toughness variation with the propagation direction

Then, they proposed the direction dependent fracture toughness for a fracture to remain elliptical as:

$$K_C = K_{C,3} \times \left(sin^2 \beta + \frac{1}{\gamma^2} cos^2 \beta \right)^{1/4} \tag{4.13}$$

where the elliptical parameter β is defined as:

$$\beta = arctan\left(\frac{1}{\gamma^2} tan(\alpha)\right) \tag{4.14}$$

In this equation, γ is the aspect ratio that is related to the directional fracture toughness $K_{C,1}$ and $K_{C,3}$ as (Bessmertnykh and Dontsov 2018):

$$\gamma = \frac{c}{b} = \left(\frac{K_{C,3}}{K_{C,1}}\right)^2 \tag{4.15}$$

where *c* is the length of the major axis along the direction of $\overrightarrow{e_1}$ and *b* is the minor axis along the direction of $\overrightarrow{e_3}$. Accordingly, in the case of toughness dominated regime, for toughness ratio $K_{C,3}/K_{C,1} = 2$, the fracture aspect ratio is *c*/*b* = 4.

In the following, we investigate the impact of the toughness anisotropy ratio $K_{C,3}/K_{C,1}$ and the local direction angle α on the direction dependent toughness K_C using Eq. (4.13) and Eq. (4.14). We assume that $K_{C,3} > K_{C,1}$, $K_{C,2}$ and $K_{C,1} = K_{C,2} = K_{IC-isotropic}$, and we vary $K_{C,3}$.

Figure 4.5 shows the direction dependent toughness K_C as a function of the ratio $K_{C,3}/K_{C,1}$ for different angles α. The results indicate that as the toughness ratio $K_{C,3}/K_{C,1}$ increases the direction dependent toughness K_C increases in all the fracture front local angles ($\alpha = \pi/6$, $\pi/4$, $\pi/3$, and $\pi/2$), except in case of the direction $\alpha = 0$, here the direction dependent toughness $K_C = K_{C,1}$. Because $\alpha = 0$ corresponds to the direction of $K_{C,1}$ and in this study we keep $K_{C,1}$ constant and we vary only $K_{C,3}$, hence, no matter what is the ratio of anisotropy $K_{C,3}/K_{C,1}$, the direction dependent toughness K_C corresponds to the toughness in that direction $K_{C,1}$.

It is seen that as the local angle moves from $\alpha = 0$ (in the direction of the minimum toughness $K_{C,1}$) to $\alpha = \pi/2$ (in the direction of the maximum toughness $K_{C,3}$), the TI toughness K_C increases. This means that the fracture is more resistant to the initiation in the local angle $\alpha = \pi/2$

corresponding to the direction of the maximum toughness $K_{C,3}$, however, this resistance of the fracture is reduced progressively when moving toward the minimum toughness $K_{C,1}$ corresponding to the local angle $\alpha = 0$. Consequently, the toughness at the fracture front in case of TIV formations is variable with the local angle α and with the degree of anisotropy $K_{C,3}/K_{C,1}$.

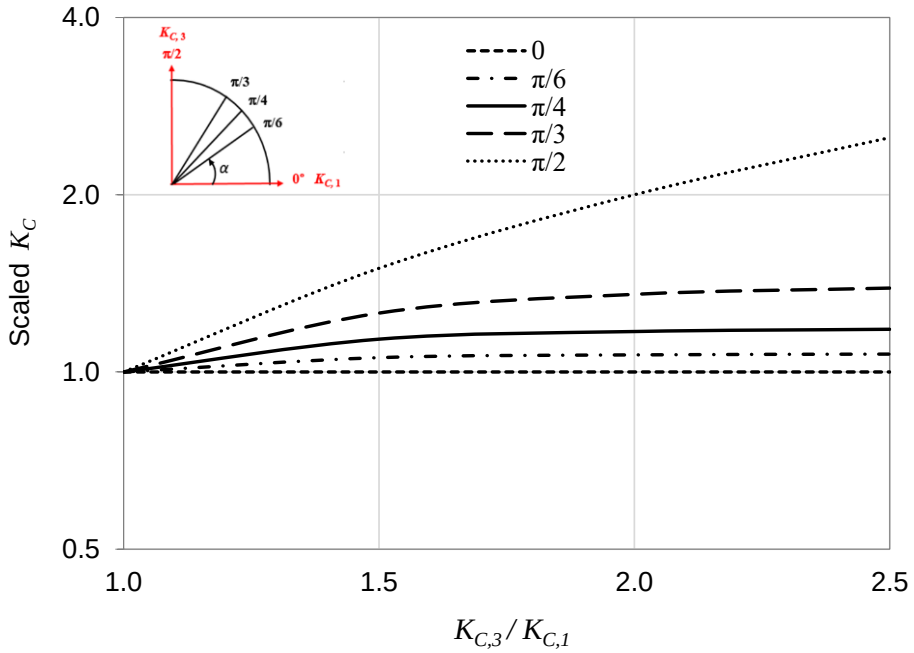

Figure 4.5: Scaled direction dependent fracture toughness (K_C) versus the anisotropic ratio $K_{C,3}/K_{C,1}$ for different angles (α)

4.4 Effect of TIV Toughness on FIP

Considering the problem shown in Figure 4.4, in this Section, the FIP is estimated by implementing the direction dependent toughness K_C to the calculation of initiation pressure in Eq. (4.1) for transverse and axial fractures with different lengths. The effect of the parameters of the direction dependent toughness including the ratio $K_{C,3}/K_{C,1}$ and the local direction angle α on the FIP is investigated. To evaluate this effect, we assume that $K_{C,3} > K_{C,1}$, $K_{C,2}$ and $K_{C,1} = K_{C,2} = K_{IC-isotropic}$, and vary $K_{C,3}$. Since we are interested in investigating the effect of the toughness anisotropy, we consider the normal stress regime for all our analysis in this work.

First, in order to verify our analytical model, we compare the initiation pressure calculated for the isotropic toughness in Figure 4.3 with the initiation pressure estimated for TI toughness used in this study, where we set the anisotropy ratio to 1 ($K_{C,3}/K_{C,1}=1$). The results of the scaled FIP (Π) using the isotropic approach versus the anisotropic approach with $K_{C,3}/K_{C,1}=1$ is presented in Figure 4.6. It is seen that the results of both approaches for isotropic toughness are in good agreement.

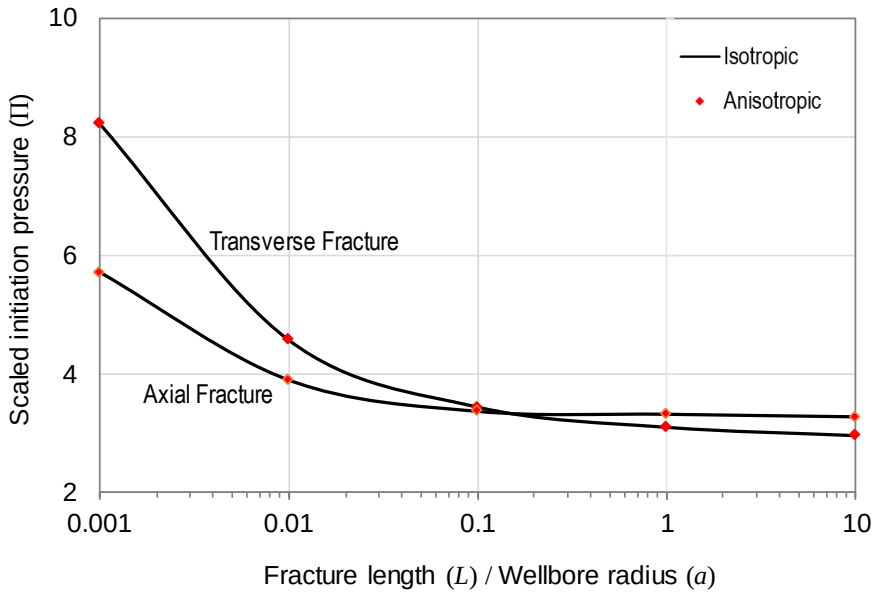

Figure 4.6: FIP predicted from isotropic and anisotropic model with $K_{C,3}/K_{C,1}$ = 1

After the model verification, we investigated the effect of the TI toughness $K_{C,3}/K_{C,1}$ and the angle α on the FIP. In order to do so, we estimated the FIP at the local angles ($\alpha=0$, $\pi/6$, $\pi/4$, $\pi/3$, and $\pi/2$) for different fracture sizes of both transverse and axial fractures with varying the toughness anisotropy $K_{C,3}/K_{C,1}$. The results of scaled FIP (Π) for transverse and axial fractures are presented respectively in Figure 4.7 and Figure 4.8, which show that as the ratio $K_{C,3}/K_{C,1}$ increases from 1 to 3, the estimated FIP of both axial and transverse fractures increases. Higher

values of the FIP are seen for small fracture lengths compared to the large fractures. The FIP also increases with the local angle α, as it is seen that the FIP estimated at $\alpha = 0$ is increasing progressively when moving toward the direction of $\alpha = \pi/2$. Also, with increasing $K_{C,3}/K_{C,1}$ higher FIP contrast is seen in case of $\alpha = \pi/2$ compared to the other angles $\alpha = 0$, $\pi/6$, $\pi/4$, $\pi/3$. In case of anisotropic ratio $K_{C,3}/K_{C,1} = 3$, the FIP of transverse fracture with length $L/a = 0.001$ estimated at the angle $\alpha = \pi/2$ is approximately 2.5 times higher than FIP estimated for isotropic toughness.

In term of competition between transverse and axial fractures, the transverse fracture of small lengths shows higher FIP values compared to the axial fracture of the same lengths. However, for higher fracture lengths: $L/a = 1$ and $L/a = 10$, the FIP values of axial fracture become higher than those of the transverse fracture. This can prove that the cross over point happened somewhere between $L/a = 0.1$ and $L/a = 1$ as it is mentioned previously and shown in Figure 4.6. The effect of the TIV toughness on the competition between axial and transverse fractures will be studied in details in the following section.

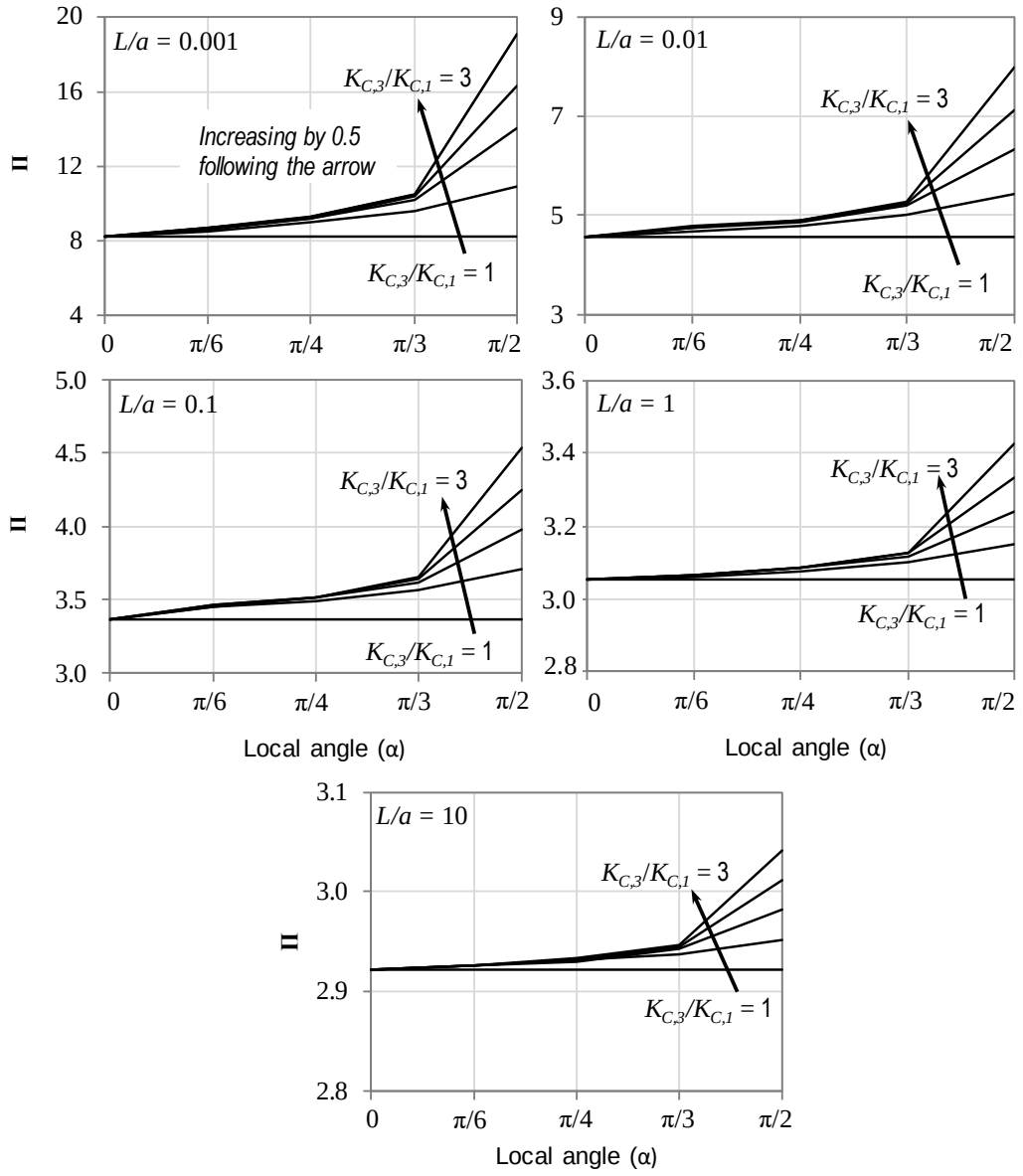

Figure 4.7: FIP (Π) of transverse fracture versus the local initiation angle $\alpha = \pi/4$, for variable anisotropic ratio $K_{C,3}/K_{C,1}$ and for different fracture lengths (a) $L/a = 0.001$, (b) $L/a = 0.01$, (c) $L/a = 0.1$, (d) $L/a = 1$, (e) $L/a = 10$

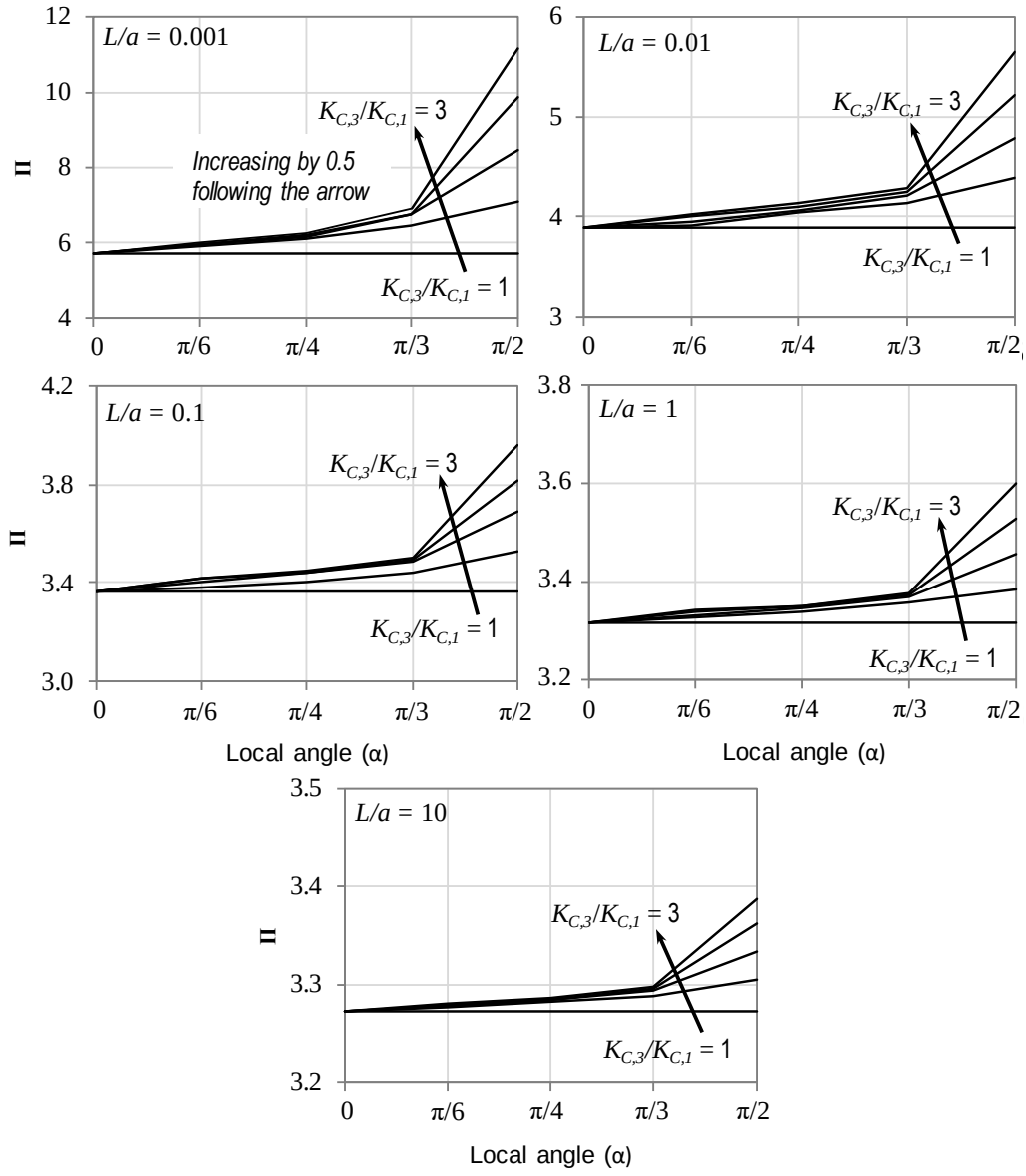

Figure 4.8: FIP (Π) of axial fracture versus the local initiation angle $\alpha = \pi/4$, for variable anisotropic ratio $K_{C,3}/K_{C,1}$ and for different fracture lengths. (a) L/a = 0.001, (b) L/a = 0.01, (c) L/a = 0.1, (d) L/a = 1, (e) L/a = 10

To evaluate the effect of the TI toughness on the FIP of different lengths in details, we fixed the ratio of anisotropy to $K_{C,3}/K_{C,1} = 2$ and estimated the FIP for different fracture sizes of both transverse and axial fractures with varying the local initiation direction ($\alpha = 0, \pi/6, \pi/4, \pi/3$, and $\pi/2$). Figure 4.9 and Figure 4.10 show the FIP of transverse and axial fractures with variable fracture length and variable local angle (α), in anisotropic toughness with $K_{C,3}/K_{C,1}$ =2. It is seen

that for both fracture geometries, as the fracture length increases, the effect of anisotropy on the fracture initiation decreases. The FIP increases gradually at the fracture front from the angle $\alpha = 0$ to $\alpha = \pi/2$. In addition, higher FIP contrast is seen for small fracture lengths, with moving from $\alpha = 0$ to $\alpha = \pi/2$, compared to the larger fractures; and for transverse fracture compared to axial fracture as seen from Figure 4.10. This can be explained by the fact that with moving far from the wellbore, stress field effect is dominant. In particular, for slow pressurization rate, the FIP of large transverse fractures ultimately converge toward the minimum horizontal stress σ_h. However, for large axial fractures the FIP asymptote toward the stress estimated using Haimson-Fairhust (*H-F*) criteria for the case of slow pressurization: $\frac{1}{2}(3\sigma_H - \sigma_v + T_0)$, as shown in Figure 4.10.

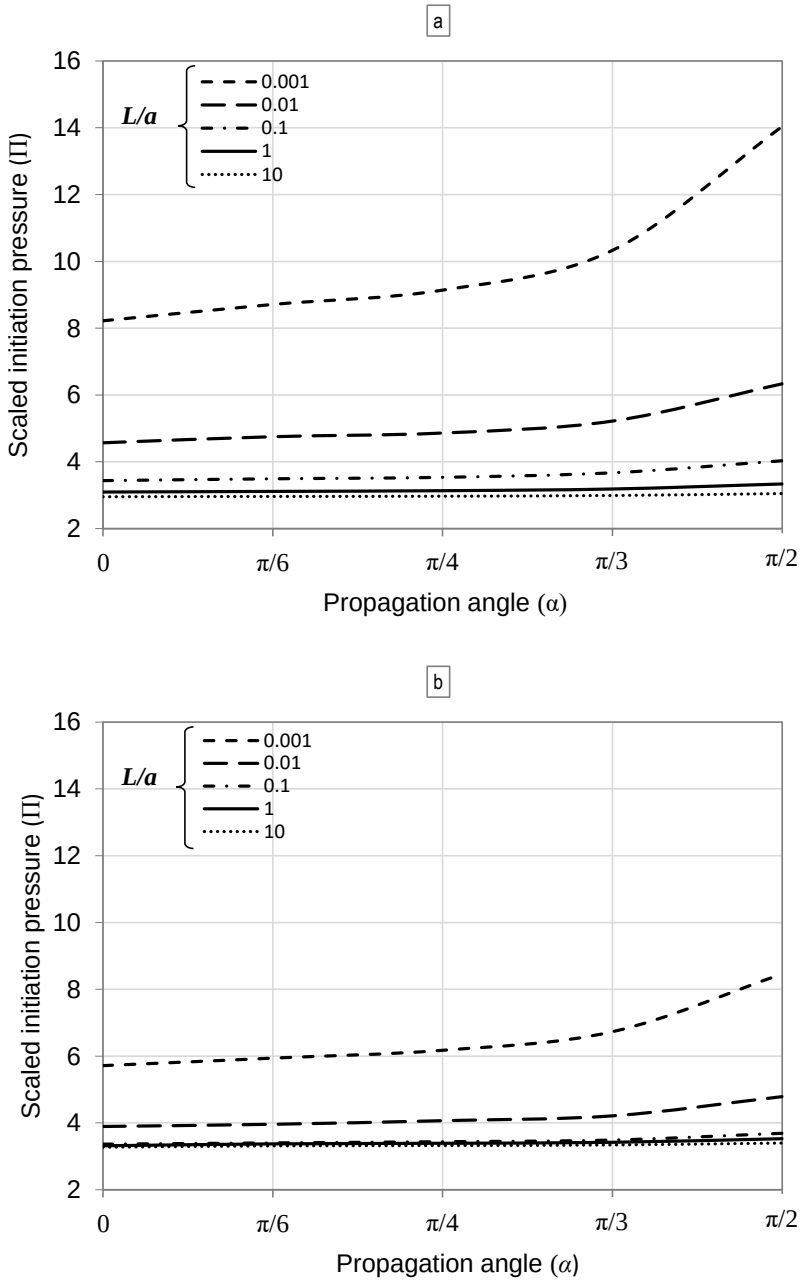

Figure 4.9: Scaled FIP (Π) of transverse (a) and axial (b) fractures as function of local initiation direction angle (α) for variable fracture length, with $K_{C,3}/K_{C,1}$ =2

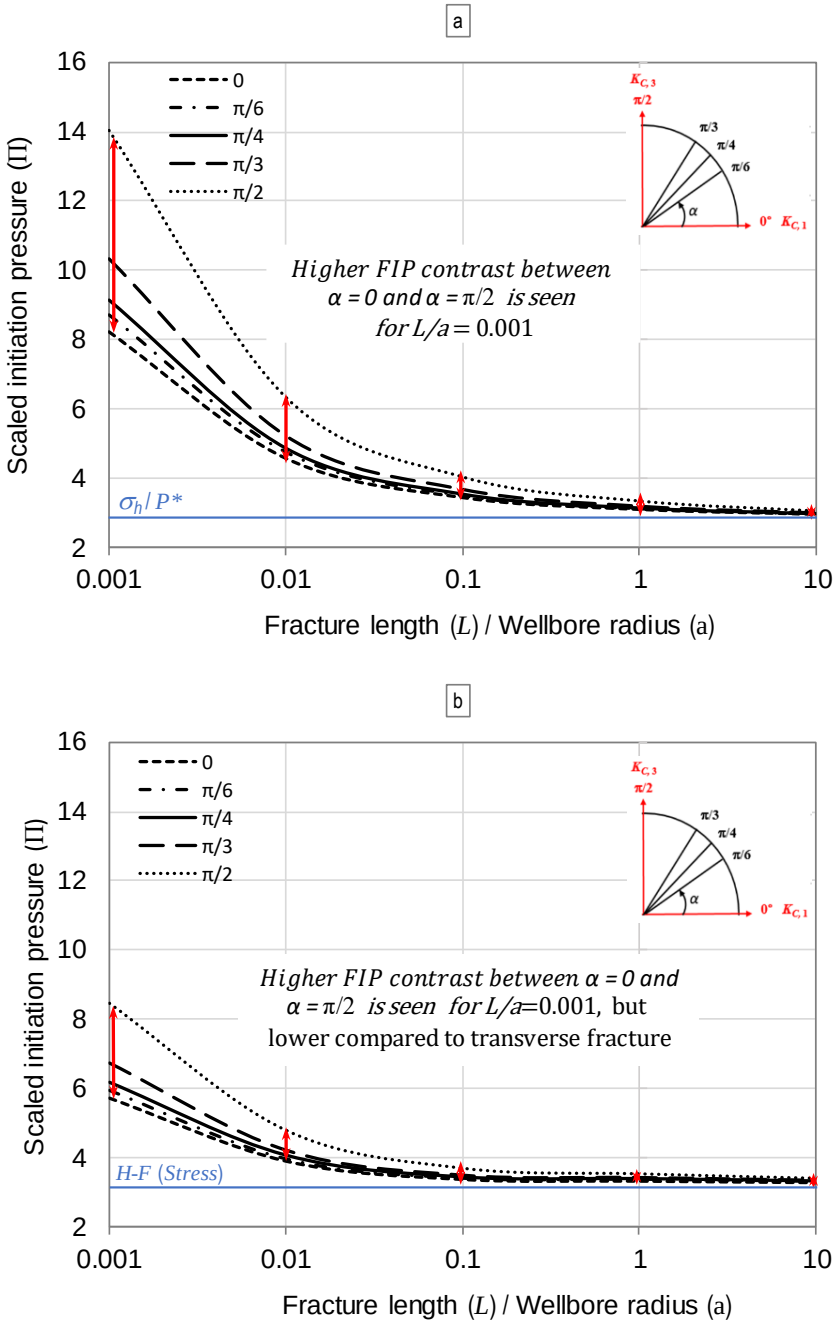

Figure 4.10: Scaled FIP (Π) of transverse (a) and axial (b) fractures as function of fracture size for different local initiation direction angle (α), with $K_{C,3}/K_{C,1}$ =2

The FIP profile for different sizes of transverse and axial fractures with anisotropic toughness is displayed in Figure 4.11. In this figure A, B, C, D, and E correspond respectively to the FIP profile of the normalized fracture lengths: $L/a = 0.001$, $L/a = 0.01$, $L/a = 0.1$, $L/a = 1$ and $L/a = 10$. It is seen that for all fracture lengths of both transverse and axial fractures, the FIP is different for different local angles α. In particular, the FIP is lower in the direction $\alpha = 0$ and $\alpha = \pi$, which correspond to the direction of minimum toughness $K_{C,1}$.While it increases gradually when moving toward the direction of maximum toughness $K_{C,3}$ $(\alpha = \pi/2)$. For instance, the FIP of transverse fracture with length $L/a = 0.01$ in the direction $\alpha = \pi/2$ and $\alpha = 0$ is respectively: $\Pi_{(\alpha=\pi/2)} = 14.08$ and $\Pi_{(\alpha=0)} = 8.22$. Consequently, in case of $K_{C,3}/K_{C,1} = 2$, the FIP in the direction of the maximum toughness $K_{C,3}$ $(\alpha = \pi/2)$ is approximately 71% higher than the FIP in the direction $\alpha = 0$ of the minimum fracture toughness $K_{C,1}$ $(\alpha = 0)$.

Accordingly, the initiation pressure of the fracture is variable with direction and depends on the local direction angle α at the fracture front. While it is easier to initiate the fracture in case of $\alpha = 0$ because of the low resistance of the fracture in this direction, it is getting gradually harder to initiate it when moving toward the direction of high resistance $\alpha = \pi/2$. This can affect the fracture shape and make it more elongated in the direction of minimum fracture toughness $K_{C,1}$, as it was noticed that the fracture can initiate and propagate in the direction of minimum resistance earlier than in other directions.

The fracture is pressurized until it reaches a state where the stress intensity factor is equal to the fracture toughness $K_I/K_C = 1$ at the direction of minimum fracture toughness that correspond to the diraction $\alpha = 0$, but this pressure still not enough to initiate the fracture in the other directions. So, the fracture initiates only in the direction of $\alpha = 0$ while the pressure keeps increasing inside

the fracture until it reaches the state where $K_I/K_C = 1$ for all angles of the fracture. This pressure corresponds to the maximum pressure which is in the direction of maximum toughness at the angle $\alpha = \pi/2$. Therefore, the fracture become more elongated in the direction of minimum toughness corresponding to $\alpha = 0$ and contained gradually when moving toward the direction of the maximum toughness $\alpha = \pi/2$.

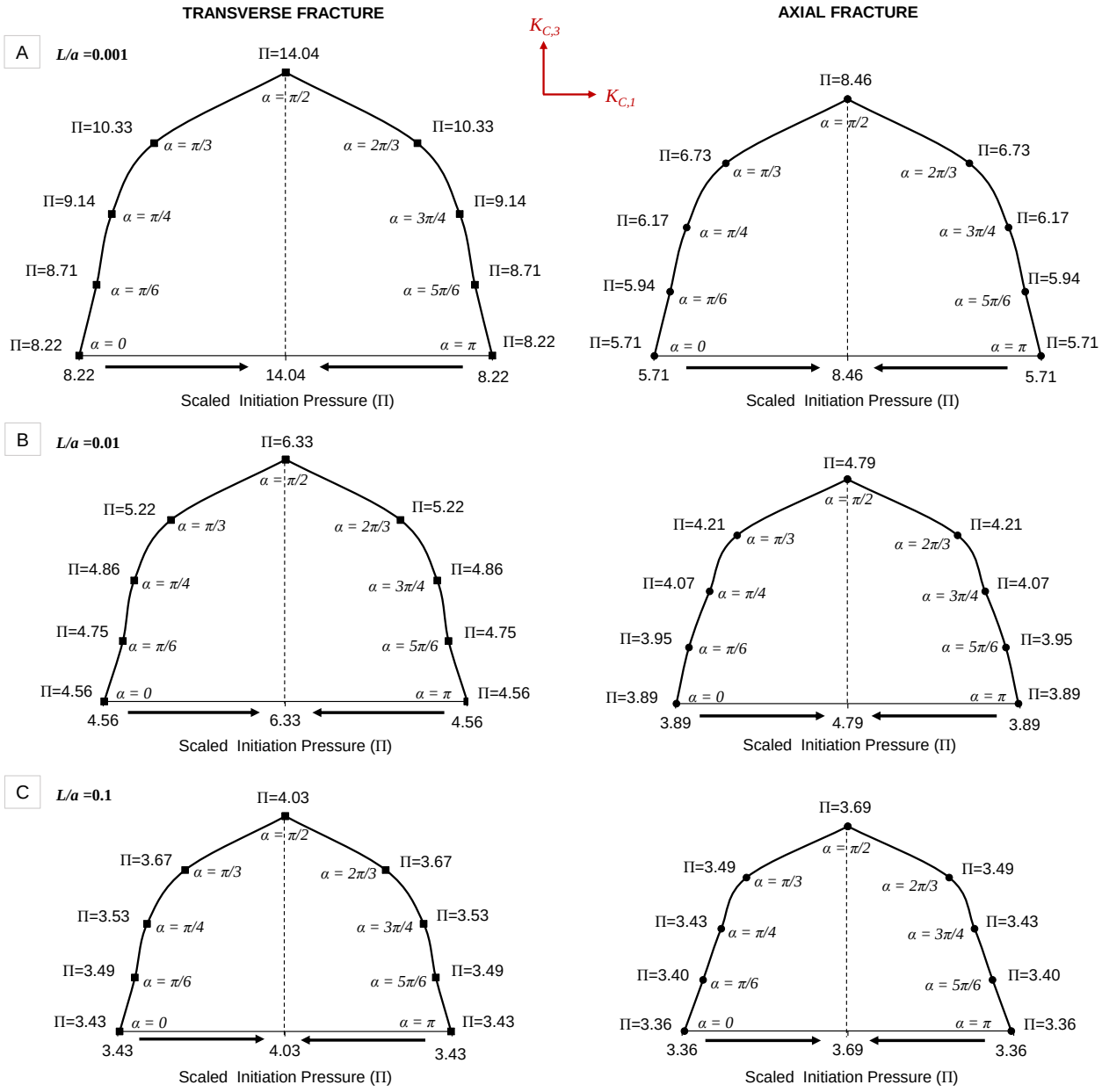

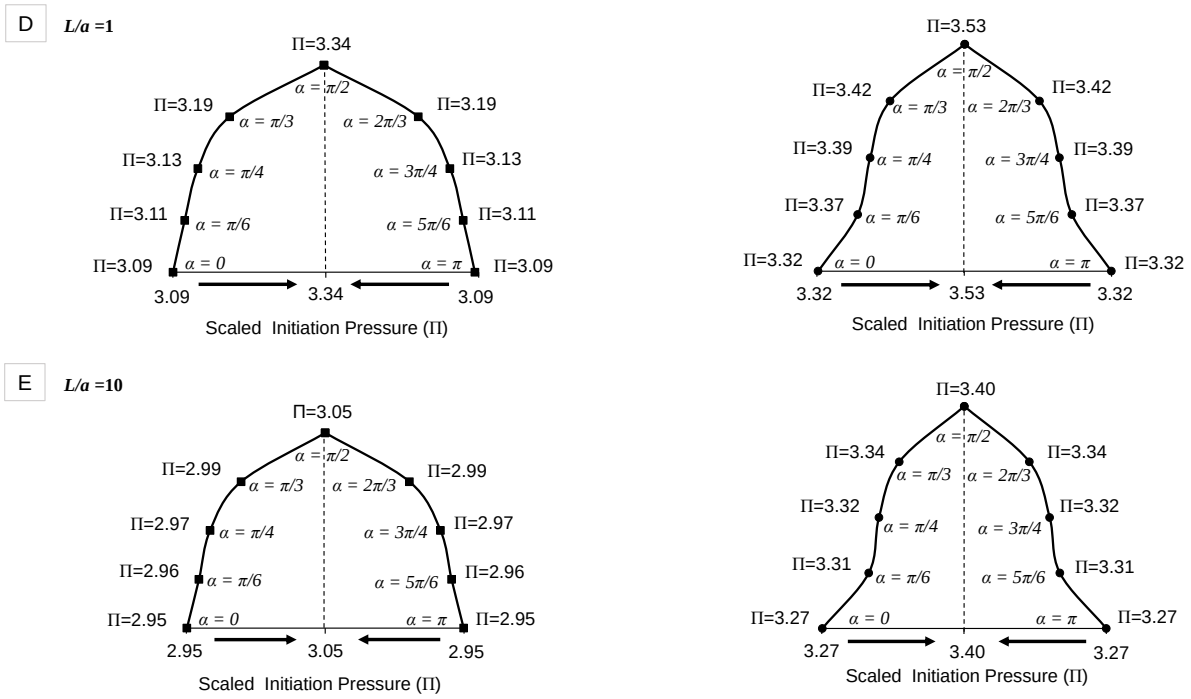

Figure 4.11: Scaled FIP (Π) of transverse (left) and axial (right) fractures at different local initiation direction (α), with $K_{C,3}/K_{C,1}$ =2 for fracture lengths, A: L/a = 0.001, B: L/a = 0.01, C: L/a = 0.1, D: L/a = 1, E: L/a = 10. The scaled FIP (Π) increases following the arrows

4.5 Effect of TIV Toughness on the Competition between Transverse and Axial Fractures

In order to investigate the effect of toughness anisotropy on the competition between transverse and axial fractures, we plotted the FIP of transverse versus axial fractures of same length as function of local initiation direction (α) in case of anisotropic medium with $K_{C,3}/K_{C,1} = 2$. It is to be mentioned that the fracture with the lowest FIP is the most favourable one for initiation.

Figure 4.12, shows that higher values of FIP (Π) are seen for transverse fracture of small lengths: $L/a = 0.001$, $L/a = 0.01$, and $L/a = 0.1$, presented in (a), (b), and (c) compared to axial fractures of same lengths at same angles. However, for large fractures: $L/a = 1$ and $L/a = 10$ displayed in (d) and (e) higher FIP is seen for axial fractures. It is to be noted that at length $L/a =$

0.1, the curves for axial and transverse fractures converge toward each other's and right after that the transition happened and lower pressure is seen for axial fracture.

This means that for small fracture lengths less than a critical length, axial fractures are always favourable to initiate because they have lower FIP compared to transverse fractures of same lengths, however, transverse fractures are easier to initiate in case of larger fractures higher than the critical length. This critical length is the transition length from axial to transverse is shown as the cross over point in Figure 4.13 and it depends on the field stress anisotropy and stress regime as proven by Benouadah et al. (2021) and toughness anisotropy as will be discussed next in this section.

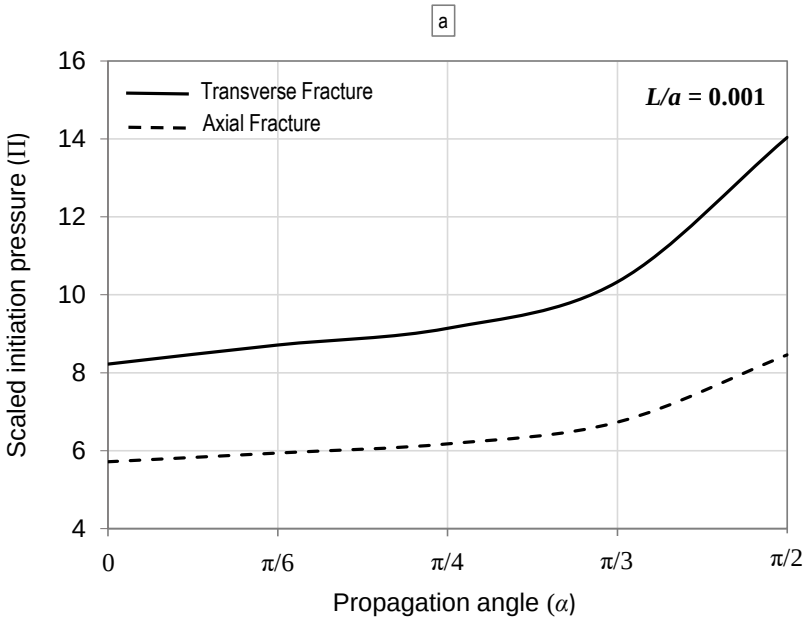
a
Transverse Fracture
Axial Fracture
L/a = 0.001
Scaled initiation pressure (Π)
16
14
12
10
8
6
4
0
π/6
π/4
π/3
π/2
Propagation angle (α)

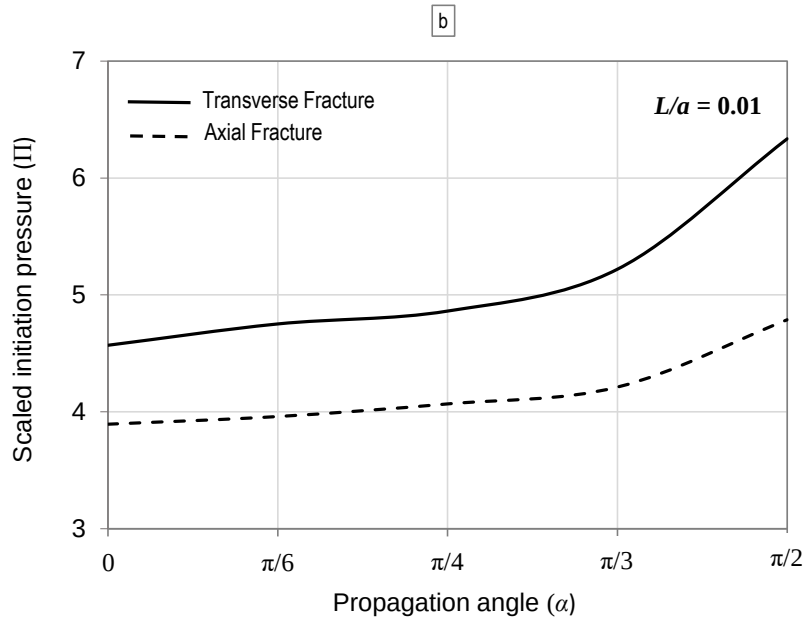
b
Transverse Fracture
Axial Fracture
L/a = 0.01
Scaled initiation pressure (Π)
7
6
5
4
3
0
π/6
π/4
π/3
π/2
Propagation angle (α)

c

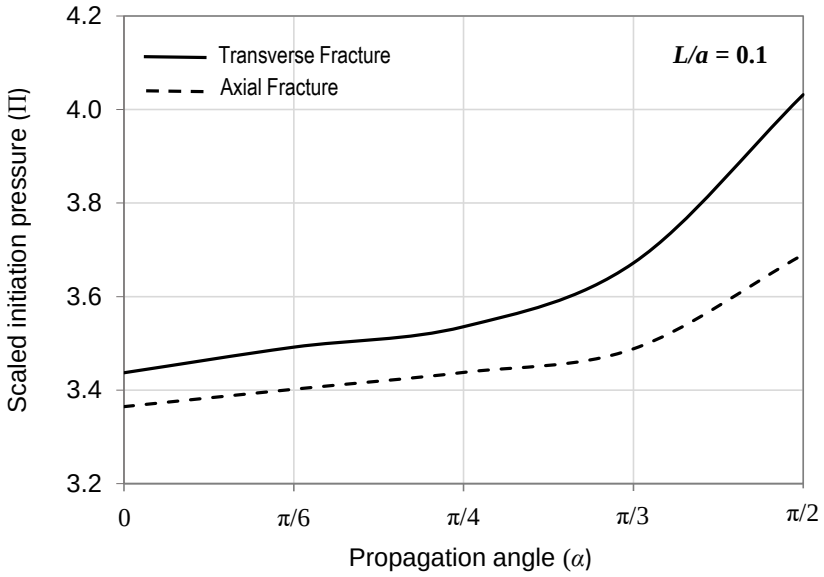
Transverse Fracture
Axial Fracture
L/a = 0.1
Scaled initiation pressure (Π)
4.2
4.0
3.8
3.6
3.4
3.2
0
π/6
π/4
π/3
π/2
Propagation angle (α)

d

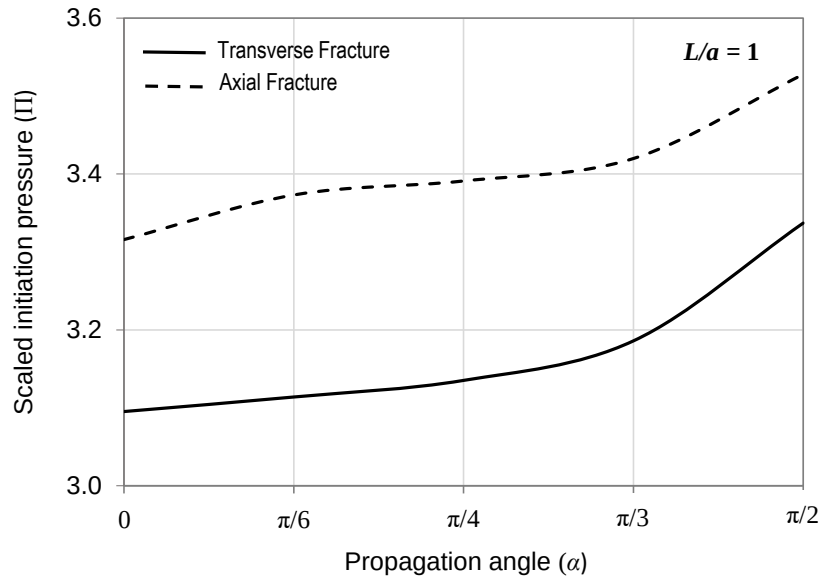
Transverse Fracture
Axial Fracture
L/a = 1
Scaled initiation pressure (Π)
3.6
3.4
3.2
3.0
0
π/6
π/4
π/3
π/2
Propagation angle (α)

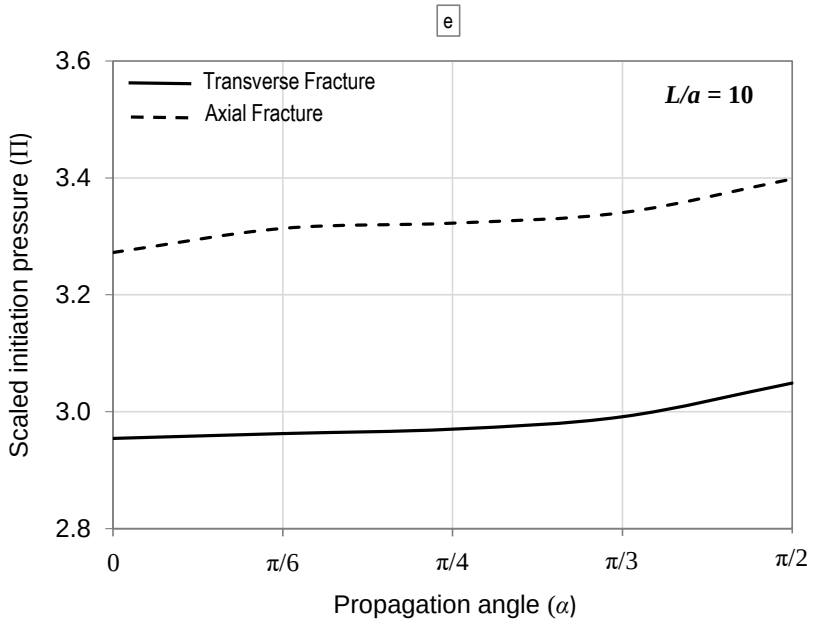

Figure 4.12: Scaled FIP (Π) of transverse versus axial fractures as function of the angle (α) for variable fracture length, with $K_{C,3}/K_{C,1}$ =2

In the following, we compared the FIP estimated from the isotropic approach to the FIP estimated using the method developed in this study for TIV toughness ratio $K_{C,3}/K_{C,1} = 2$. The FIP in case of TI fracture toughness is the pressure that fulfil the condition $K_I/K_C = 1$ for all local angles at the fracture tip. In this case we assume that it is the FIP that the fracture reaches to get initiated in all the local directions, which corresponds to the maximum fracture pressure at $= \pi/2$. The curves corresponding to the FIP of transverse and axial fractures for $K_{C,3}/K_{C,1} = 1$ and $K_{C,3}/K_{C,1} = 2$ are displayed in Figure 4.13. The results show that the FIP of both transverse and axial fracture is higher in the case of anisotropic fracture toughness ($K_{C,3}/K_{C,1} = 2$) compared to the isotropic case ($K_{C,3}/K_{C,1} = 1$).

The cross over point shown as black dots in Figure 4.13 represent the length of transition from the axial fracture domination to the transverse fracture domination. This means that for a fracture length larger than the transition length, transverse fractures becomes more favourable to initiation.

Such a transition length happens at a value of approximately $L/a = 0.15$ for the isotropic case. Alternatively, for the case of TIV fracture toughness with $K_{C,3}/K_{C,1} = 2$, the transition from axial dominated to transverse dominated fracture occurs at length $L/a = 0.35$.

Consequently, for normal stress regime condition, in the presence of fracture toughness anisotropy, larger fractures are needed to dominate the initiation of transverse cracks compared to the isotropic medium.

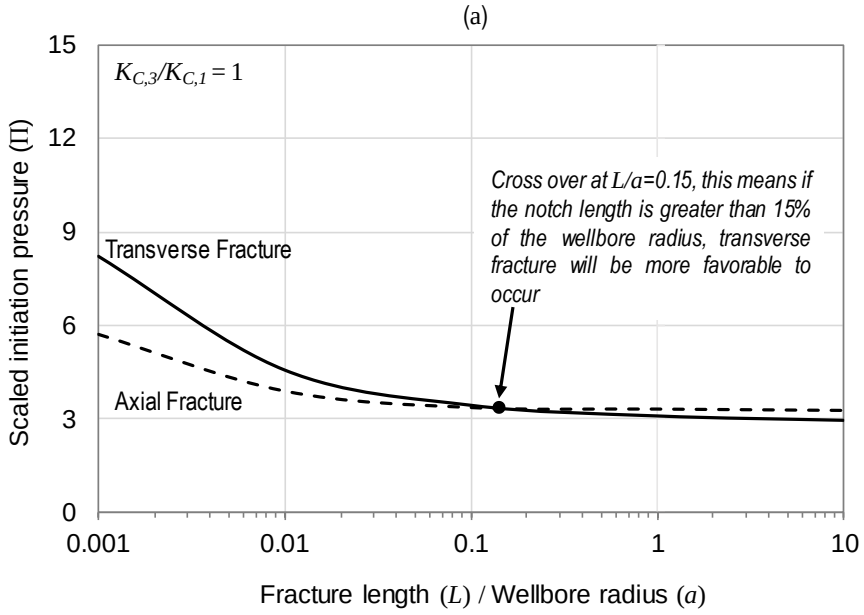

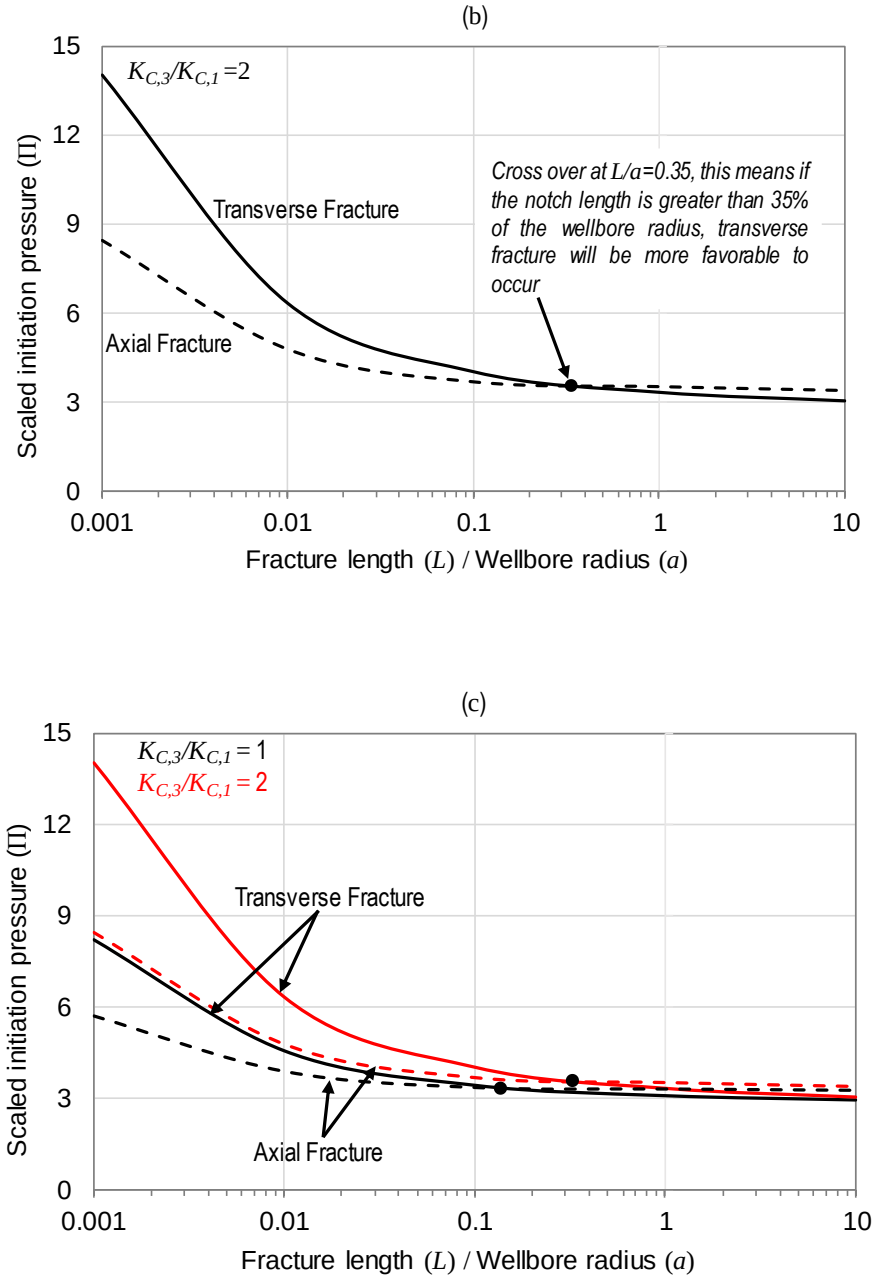

Figure 4.13: FIP for transverse and axial fracture in (a) isotropic fracture toughness ($K_{C,3}/K_{C,1}$ = 1), (b) anisotropic fracture toughness ($K_{C,3}/K_{C,1}$ = 2), (c) isotropic versus anisotropic

4.6 TIV due to Young's Modulus

Stress determination is an important part of geomechanical analysis. The Mechanical Earth Model (MEM) is the most common approach to identify the magnitude of the three principle stresses also known as in-situ far field stresses. The details of the MEM workflow can be found from several literatures (e.g. Rasouli et al 2011). In simple isotropic medium, the vertical stress (σ_v) is defined from equation (4.16) by integrating the density. However, the maximum (σ_H) and the minimum (σ_h) horizontal stresses are functions of the vertical stress and the rock elastic properties (Young's modulus and Poisson's ratio) as shown in equations (4.17) and (4.18):

$$\sigma_v = g\int_0^z \rho_b(z)dz \tag{4.16}$$

$$\sigma_h = K_0(\sigma_v - \alpha P_p) + \alpha P_p + \sigma_{Tectonic} \tag{4.17}$$

where

ρ_b : bulk density

g : acceleration due to gravity

z : vertical depth

α : Biot's poro-elastic coefficient

P_p : pore pressure

$$K_0 = \frac{\nu}{1-\nu} \tag{4.18}$$

In anisotropic medium, the material anisotropy does not affect the vertical stress. However, it can affect the horizontal stresses and the effect is expressed in the modified parameter K_0 proposed

by Amadei et al. (1987) and Pan and Amadei (1995), where K_0 for transversely isotropic material with horizontal plane of isotropy is:

$$(K_0)_{aniso} = \frac{E_h}{E_v}\frac{\nu_v}{1-\nu_h} \tag{4.19}$$

where ν is Poisson's ratio for isotropic material, E_h and E_v are the horizontal and vertical Young's modulus, and ν_h and ν_v are Poisson's ratio in the horizontal and vertical directions respectively.

The modified expressions for estimation of the maximum and minimum horizontal stresses are respectively:

$$\sigma_H = \frac{E_h}{E_v}\frac{\nu_v}{1-\nu_h}(\sigma_v - \alpha P_p) + \alpha P_p + \sigma_{H,Tectonic} \tag{4.20}$$

$$\sigma_h = \frac{E_h}{E_v}\frac{\nu_v}{1-\nu_h}(\sigma_v - \alpha P_p) + \alpha P_p + \sigma_{h,Tectonic} \tag{4.21}$$

These equations are used in the calculation of the hoop stresses in equation (4.1) to estimate the FIP in order to investigate the effect of the anisotropy in Young's modulus on the FIP.

In the following we assume that $E_h > E_v$, so we keep E_v stable and we vary E_h. Both fracture geometries under different E_h/E_v ratios are plotted in Figure 4.14. It is seen that the FIP for both transverse and axial fractures is affected by the anisotropy in Young's modulus. As shown in the curves, the FIP of both fracture geometries increases with increasing the ratio E_h/E_v.

This is because an increase of the ratio E_h/E_v leads to increasing the maximum and minimum horizontal stresses of TIV formations, which led to increasing the FIP.

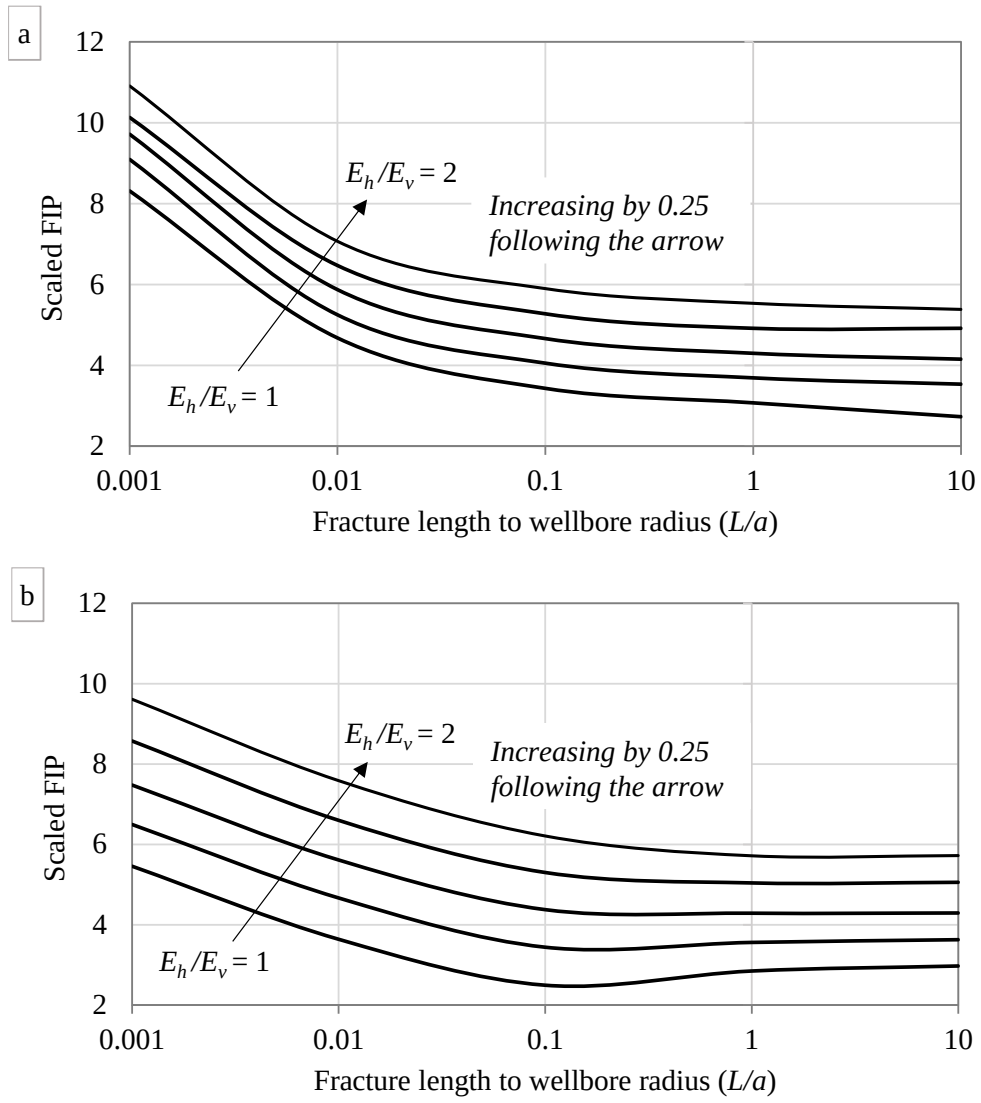

Figure 4.14: FIP of (a) transverse fracture and (b) axial fracture, as a function of the scaled fracture lengths for different E_h/E_v

4.7 Summary

The analysis performed in this Chapter highlighted the major impact of TIV in fracture toughness and rock stiffness on the FIP as well as the fracture shape. We presented models which consider the effect of TIV in fracture toughness and in Young's modulus, these models integrate the impact of stresses, pressurization rate and also consider two fracture geometries, the axial and transverse fractures. It was seen that these models are based on some simplified assumptions, so when one using these models, should carefully consider their limits and application ranges.

It was observed that in case of TI fracture toughness and stiffness, the FIP is higher compared to the isotropic case, which in turn affects the competition between transverse and axial fractures. In fact, in a medium with TIV fracture toughness such as unconventional shales, higher pressure is required to initiate a hydraulic fracture compared to isotropic medium. Therefore, modelling shales assuming isotropic approaches is a wrong practice and results in underestimated fracturing pressure.

In hydraulic fracturing design, a small transverse crack or fracture, which is known as notch, can be created along the open hole section as a point of interest or sometimes in order to favour transverse fractures. This Chapter concluded that in TIV toughness medium, to dominate these transverse notches among the other existing fractures and be the point of hydraulic fracture initiation; larger notches are needed compared to isotropic medium. Consequently, assuming shale as isotropic when designing the hydraulic fracture can lead to underestimation of the notch size, which results in suboptimal hydraulic fracture design.

While these models provide great knowledge about the effect of the anisotropy of different parameters on crack initiation from an existing notch, they cannot be conveniently used for simulation of real cases where multiple fractures with different geometry and properties are distributed around a wellbore. Therefore, we introduce the numerical modelling in the next Chapter, which will be used to conduct numerical simulations of different scenarios of single and multiple hydraulic fracture initiation and propagation in different propagation regimes. The results will be compared with the analytical solutions. We also expand this to more complex real cases example where analytical solutions do not exist and interpret the results. The results of numerical simulations will be presented in Chapter 5.

CHAPTER 5

Numerical Simulations

5.1 Introduction

In this Chapter, numerical simulations are conducted for several scenarios of hydraulic fracturing in a medium with vertical transversely isotropic (TIV) fracture toughness. To perform the numerical simulations, ResFrac a fully coupled numerical simulator, which is presented in Chapter 3, is used to model single and multiple hydraulic fracturing in formations with TIV fracture toughness. The impact of transversely isotropic fracture toughness on single and multiple hydraulic fractures will be presented and the results of pressure will be compared to the analytical models developed in the preceding Chapter. The effect of toughness anisotropy on the net pressure as well as fracture morphology will be modeled for single radial and constant height (PKN) hydraulic fracture. In addition, the combined effect of toughness anisotropy and stress shadow will be modelled for the case of simultaneous propagation of multiple radial and multiple constant height hydraulic fractures in two fundamentals propagation regimes (toughness-dominated and viscosity-dominated regimes). In particular, the focus is to evaluate the modification in fracture morphology resulting from changes in TIV fracture toughness, propagation regimes and stress shadow. The models are presented for different propagation regimes and cluster spacing, as the most important

parameters affecting the fracture morphology in case of multiple hydraulic fracture propagation, while the cases of single hydraulic fracture are presented for different ratios of TIV toughness in toughness dominated regime. Therefore, an overview of the different propagation regimes and the parametric analysis for radial, constant height and anisotropic fracture toughness cases will be presented in the first section of this Chapter. Next, the results of the numerical simulations will be discussed, and conclusions are made. Then, field case application using the data from the Bakken Formation in the Williston Basin will be presented as a field scale hydraulic fracturing model. Finally, a brief summary of the main results of this chapter will be presented.

5.2 Limiting Regimes of Propagation

A series of physical mechanisms such as elasticity, fluid flow, fracture mechanics, and leak-off, are the main parameters that control the initiation and propagation of a hydraulic fracture. Depending on which of this dissipative mechanism dominates over the other, the limiting regimes are defined as (Dontsov 2016):

1. Viscosity storage dominated regime: if the dissipative mechanism is associated with fluid viscosity and most of the fluid stay stored in the fracture.
2. Toughness storage dominated regime: if the dissipative mechanism is associated with rock toughness and most of the fluid stay stored in the fracture.
3. Leak-off viscosity regime: in which fluid viscosity dominates the fracture response and most of the injection fluid leak-off to the formation.
4. Leak-off toughness regime: in which the rock's fracture toughness dominates the response and most of the fluid leaks into the formation.

Scaling and dimensional analysis are of great importance to understand the response of the system to the limiting regimes of propagation. The complete governed equations and dimensional analysis

of the approximate solution for a penny-shaped hydraulic fracture is presented by Dontsov (2016). For the limiting solution of a hydraulic fracture propagating in homogeneous anisotropic rocks, the approximate expressions for the limiting solutions are obtained and presented in Dontsov (2019). In this case, the rock is represented by having two different fracture toughness in the vertical and horizontal directions. In addition, the approximate solution of the different propagation regimes for the problem of constant height (PKN) hydraulic fracture is constructed and investigated by (Dontsov 2021a).

In this study, we are interested on investigating the effect of TIV toughness on single and multiple propagation of two cases of fracture geometries separately (radial fracture and constant height fracture) in the storage toughness-dominated and storage viscosity-dominated regimes with no leak-off.

The limiting solutions for different propagation regimes and their locations in the two-dimensional parametric space for a single radial hydraulic fracture depends on two dimensionless parameters which are given by Dontsov (2021b) :

$$\tau = \left(\frac{K'^{18} t^2}{\mu'^5 E'^{13} Q^3} \right)^{1/2} \tag{5.1}$$

$$\phi = \frac{\mu'^3 E'^{11} C'^4 Q}{K'^{14}} \tag{5.2}$$

where

$K' = \sqrt{32/\pi}\, K_{IC}$, K_{IC} : fracture toughness,

$E' = E/\left(1-\nu^2\right)$, E : Young's modulus and ν : Poisson's ratio,

$\mu' = 12\mu$, μ: fluid viscosity,

$C' = 2C_l$, C_l: Carter's leak-off coefficient,

Q: injection rate.

In case of a medium with anisotropic fracture toughness, the effect of the ratio $R_K = K_{C,3}/K_{c,1}$ is implemented to the parametric analysis regimes by (Dontsov 2019b) and influence the zones of applicability of limiting regimes. Figure 5.1 shows the parametric space with the zones corresponding to different propagation regimes in case of isotropic ($R_K = 1$) and anisotropic fracture toughness ($R_K = 3.2$), where the dashed black lines correspond to the zones of the propagation regimes in isotropic formations. It is seen from the parametric space presented in Figure 5.1 that for anisotropic fracture toughness, the critical value of the parameter "τ" shifted to the right in case of toughness regime while it is moved to the left in case of viscosity regime leading to further separation of these two fundamental limits. Which means that in case of anisotropic toughness higher value of the parameter τ is needed to be in the toughness-dominated regime compared to the case of isotropic fracture toughness. However, lower value of the parameter τ is required in case of anisotropic fracture toughness to be in the viscosity-dominated regime. It is to be mentioned that these are approximate values. The parametric space is presented in terms of logarithmic values of the parameters.

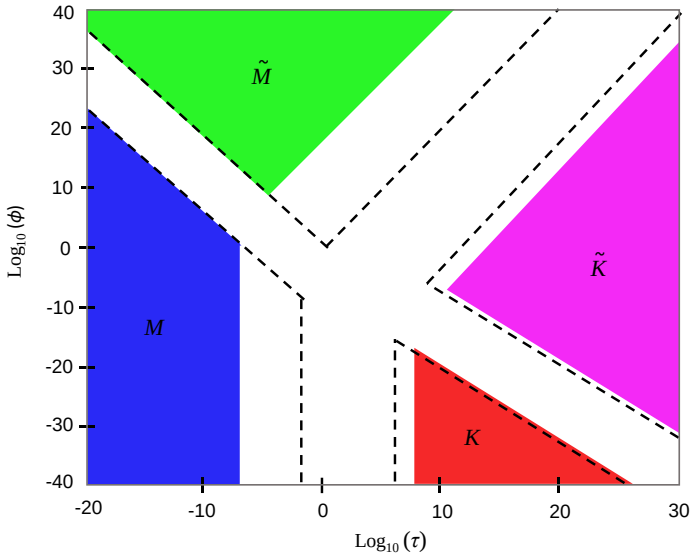

Figure 5.1: Parametric space of propagation regimes in case of isotropic (R_K=1) and anisotropic fracture toughness (R_K=3.2) (Modified after Dontsov (2019))

The problem of constant height hydraulic fracture or Perkins-Kern-Nordgren (PKN) fracture is similar to the radial fracture geometry; however, the effect of the barriers is added to the parametric analysis in this case. Therefore, the parameters that define the limiting regimes in case of constant height fracture geometry are defined as following (Dontsov 2021a):

$$\tau = \frac{2\pi^{1/2} E'^4 \mu Q^2 t}{H^{7/2} K_{IC}^5} \tag{5.3}$$

$$\phi = \left(\frac{H^5 K_{IC}^6 C'^4}{4\pi^3 E'^4 \mu^2 Q^4} \right)^{1/4} \tag{5.4}$$

where H is the target layer height.

The parametric space of the limiting regimes for PKN fracture is shown in Figure 5.2.

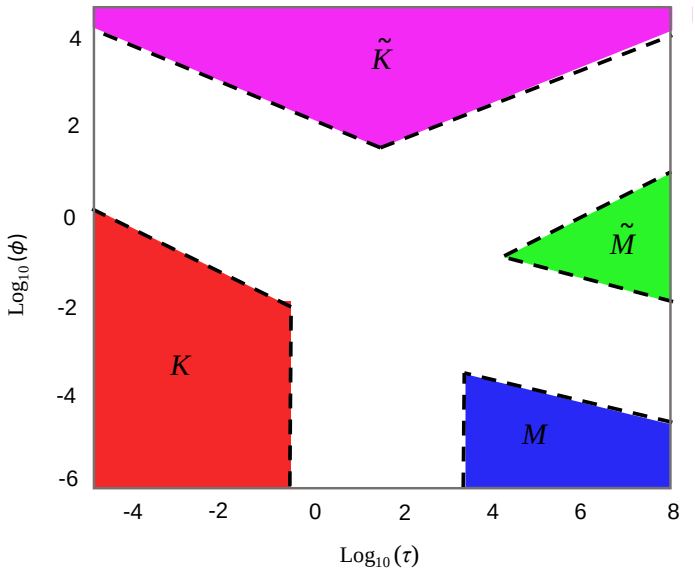

Figure 5.2: Parametric space of propagation regimes for PKN fracture (Modified after (Dontsov 2021a))

5.3 Radial Fracture

Due to its simplicity and for better understanding of its mathematical structure of the solution, the radial fracture is the first fracture geometry that is considered for analysis of the effect of TIV fracture toughness in this study. Simulations of the propagation of single and multiple radial hydraulic fractures in TIV fracture toughness are conducted. Toughness dominated regime is used to simulate single hydraulic fracture, while both toughness and viscosity dominated regimes are used to simulate the morphology of multiple hydraulic fractures propagating in TIV fracture toughness. The input parameters are presented in Table 5. 1.

Table 5. 1 Input parameters for the propagation of radial hydraulic fracture in toughness regime and viscosity regime

Property	*K*	*M*
Young's Modulus, *E* [GPa]	25	25
Toughness, K_{IC} [Mpa.m^0.5]	7	1
Poisson's Ratio, *v*	0.25	0.25
Fluid Viscosity, μ [Pa.s]	0.001	0.05
Flow Rate, *Q* [m^3/s]	0.1	0.2
Time *t* [hrs]	1	5

Carter'sleak-off coefficient C_l [m/s^1/2]	0	0
τ	5 X 10^5	4 X 10^{-4}
ϕ	0	0

Figure 5.3 shows the location of the problem parameters of Table 5. 1 inside the parametric space for the case of radial fracture. This parametric space corresponds to the dashed lines of the limiting regimes presented in Figure 5.1.

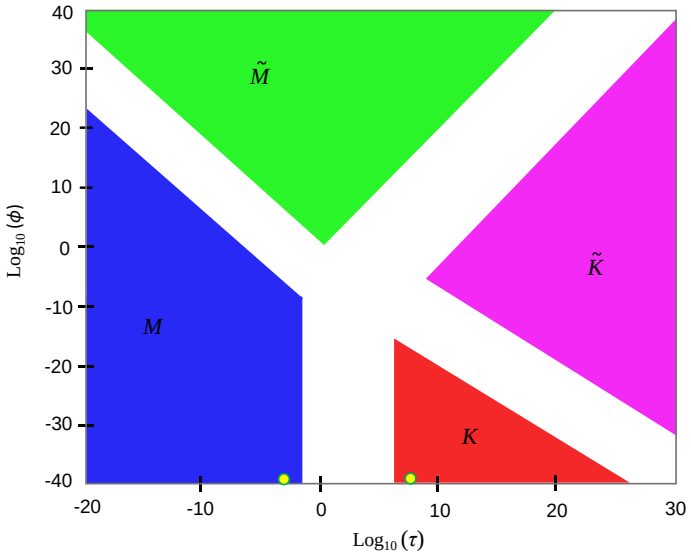

Figure 5.3: Parametric space of radial fracture propagation regimes. Circular marker correspond to the location of *K* and *M* parameters of Table 5. 1 (Modified after Dontsov (2019))

5.3.1 Single Hydraulic Fracture

In this part, the propagation of single radial fracture in TIV fracture toughness medium is investigated in toughness-dominated (*K*) regime using the parameters in Table 5. 1. The effect of the ratio of toughness anisotropy $K_{C,3}/K_{C,1}$ on the net pressure and the fracture morphology is presented. Then, a sensitivity analysis of the fracture parameters (width, radius, height, length, and aspect ratio) will be discussed and compared to existing analytical solutions for both isotropic and anisotropic cases.

5.3.1.1 Effect of $K_{C,3}/K_{C,1}$ on Net Pressure and Fracture Geometry

The fracture geometry and the corresponding net pressure of radial fracture propagation under variable $K_{C,3}/K_{C,1}$ after 1 hour of fluid injection are presented respectively in Figure 5.4 and Figure 5.5. In term of fracture morphology, it is seen that the TIV toughness has a significant effect on the fracture shape. In the isotropic case $K_{C,3}/K_{C,1} = 1$, the fracture is circular and symmetric. However, increasing the toughness anisotropic ratio $K_{C,3}/K_{C,1}$ led to a significant modification in the fracture morphology. The fracture propagation is fully contained by the high value of fracture toughness ($K_{C,3}$) in the vertical direction while it is getting easier and more elongated in the direction of minimum toughness $K_{C,1}$. Hence, the fracture is elliptical and the aperture is higher in this case. These results validate the analytical model results in the previous section where it was noticed that the fracture initiate and propagate in the direction of $K_{C,1}$ earlier than in other directions of the fracture front. Consequently, the fracture shape can be affected by the toughness anisotropy and make it more elongated in the direction of minimum toughness.

The net pressure versus time curves plotted in Figure 5.5, were exported from the simulation results. The FIP was defined from the net pressure curves at the time when the hydraulic fracture created. The results show that the net pressure increases with increasing the TIV fracture toughness ratio $K_{C,3}/K_{C,1}$ and accordingly, the FIP is increasing with increasing the ratio $K_{C,3}/K_{C,1}$.

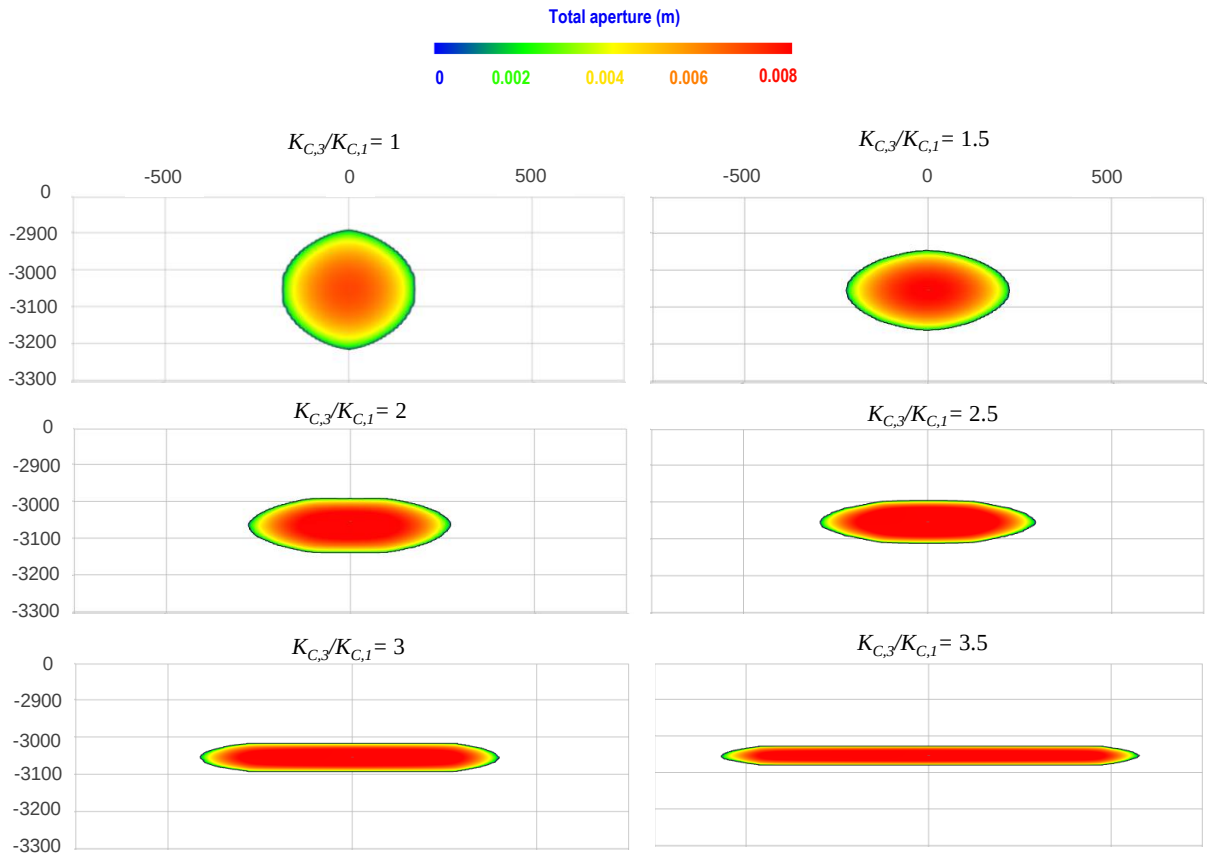

Figure 5.4: Fracture geometry for variable $K_{C,3}/K_{C,1}$ in case of radial fracture

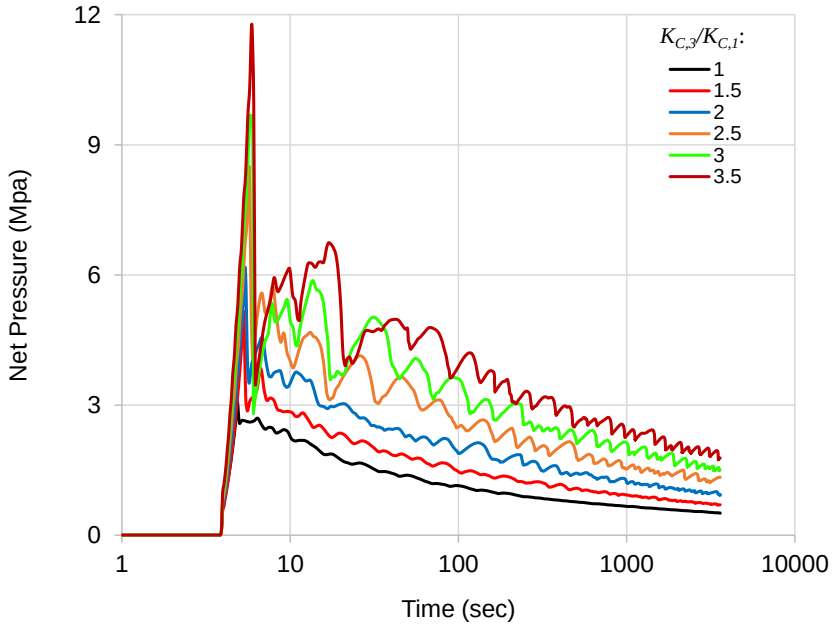

Figure 5.5: Net pressure of radial fracture for variable $K_{C,3}/K_{C,1}$

5.3.1.2 Effect of $K_{C,3}/K_{C,1}$ on Fracture Parameters

In this section, we consider a constant TIV fracture toughness ratio of $K_{C,3}/K_{C,1} = 2$ and we compare the fracture parameters exported from the results of the numerical simulations with the parameters estimated from the analytical solutions for both isotropic fracture toughness $K_{C,3}/K_{C,1} = 1$ and TIV fracture toughness $K_{C,3}/K_{C,1} = 2$.

For a radial hydraulic fracture propagating in toughness-dominated regime in isotropic medium $K_{C,3}/K_{C,1}$ = 1, the fracture width w and radius R can be calculated respectively as following (Dontsov 2016):

$$w = 0.6537\left(\frac{K'^4 Qt}{E'^4}\right)^{1/5}\left(1-\rho^2\right)^{1/2} \tag{5.5}$$

$$R = 0.8546\left(\frac{E'Qt}{K'}\right)^{2/5} \tag{5.6}$$

where ρ is the spatial coordinate of the fracture front.

The results of the fracture width w, and radius R estimated from the analytical solutions (Eq. (5.5) and (5.6) are plotted in Figure 5.6 along as with the fracture width and radius resulted from numerical simulations. It is seen that the results of the fracture radius from the analytical solution are in good agreement with the simulation. However, the fracture width is slightly over estimated from the analytical solutions, but still in the range.

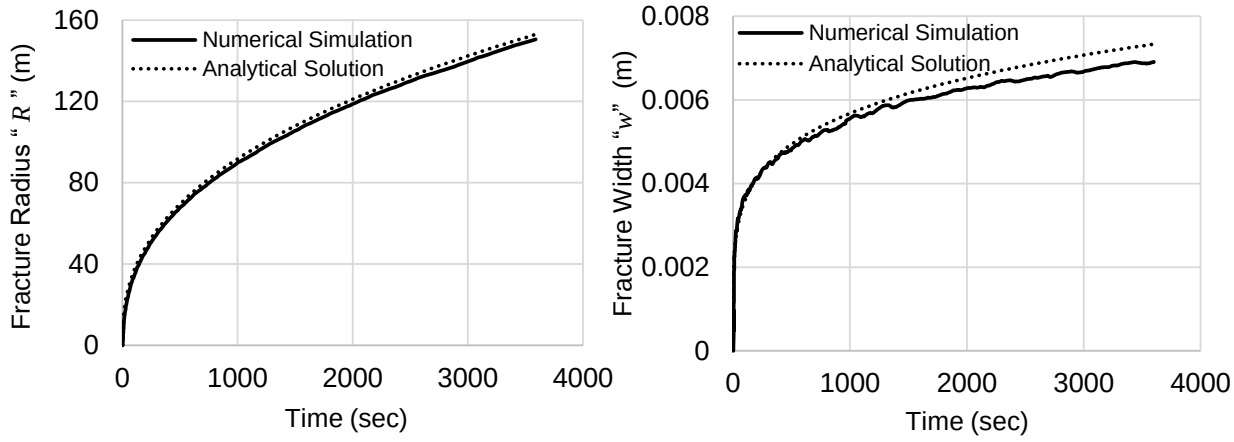

Figure 5.6: Numerical simulation versus analytical solution of radial fracture radius and fracture width for $K_{C,3}/K_{C,1}$ = 1

Similarly, for the case of TIV fracture toughness $K_{C,3}/K_{C,1}$= 2, the fracture parameters: horizontal half length "*c*" along the direction of $K_{C,1}$, vertical half length "*b*" along the direction of $K_{C,3}$, the aspect ratio "*c*/*b*", and the fracture width w_{aniso} are estimated using the analytical solutions presented by Dontsov (2019) for a radial fracture propagating in anisotropic rock. In this case, the following system of equations and dimensionless parameters are used to solve problem of radial fracture propagating in a medium with TIV fracture toughness and in toughness storage regime.

$$b = B \times L_K \tag{5.7}$$

$$c = C \times L_K \tag{5.8}$$

$$w_{aniso} = W \times \varepsilon L_K \tag{5.9}$$

where and L_K, ε and t_{mk} are parameters used to simplify the calculations:

$$L_K = \left(\frac{M' E_h'^{2n+1} Q^n}{K_{C,1}'^{2n+2}} \right)^{1/(2n-1)}, \qquad \varepsilon = \frac{K_{C,1}'}{E_h' L_K^{1/2}}, \qquad t_{mk} = \frac{K_{C,1}' L^{5/2}}{E_h' Q}, \qquad M' = \frac{2^{2n+1}(2n+1)^n}{n^n} k$$

and *B*, *C*, and *W* are the dimensionless form of the fracture parameters and can be obtained from:

$$B = c_K \left(R_K R_E\right)^{-6/5} \tau^{\alpha_K}, \qquad C = \left(R_K R_E\right)^2 B, \qquad W = \frac{R_K R_E}{\sqrt{2}} B^{1/2} = \frac{1}{\sqrt{2}} C^{1/2},$$

which depend on the following dimensionless parameters:

$$\tau = \frac{t}{t_{mk}}, \qquad R_K = \frac{K_{C,3}}{K_{c,1}} = 2 \quad , \qquad R_E = \frac{E_h}{E_v} = 1,$$

and the constants : $c_K = \left(\frac{3}{\sqrt{2}\pi}\right)^{2/5}$ and $\alpha_K = \frac{2}{5}$,

In the expression of the scaled consistency index $M', k = \mu$ refers to the consistency index and n=1 is the fluid behaviour index.

The results of the fracture parameters estimated from the analytical solutions along as with the parameters exported from the numerical simulation results are plotted in Figure 5.7 and Figure 5.8. As it can be noticed from Figure 5.7, the results of the analytical solutions of the vertical half-length "*b*", the horizontal half-length "*c*", and the aspect ratio "*c*/*b*" are in good agreement with the numerical simulation results. Figure 5.8 shows the results of fracture width in case of TIV fracture toughness $K_{C,3}/K_{C,1}$= 2. The analytical solutions of the fracture width are in alignment with the numerical simulation results.

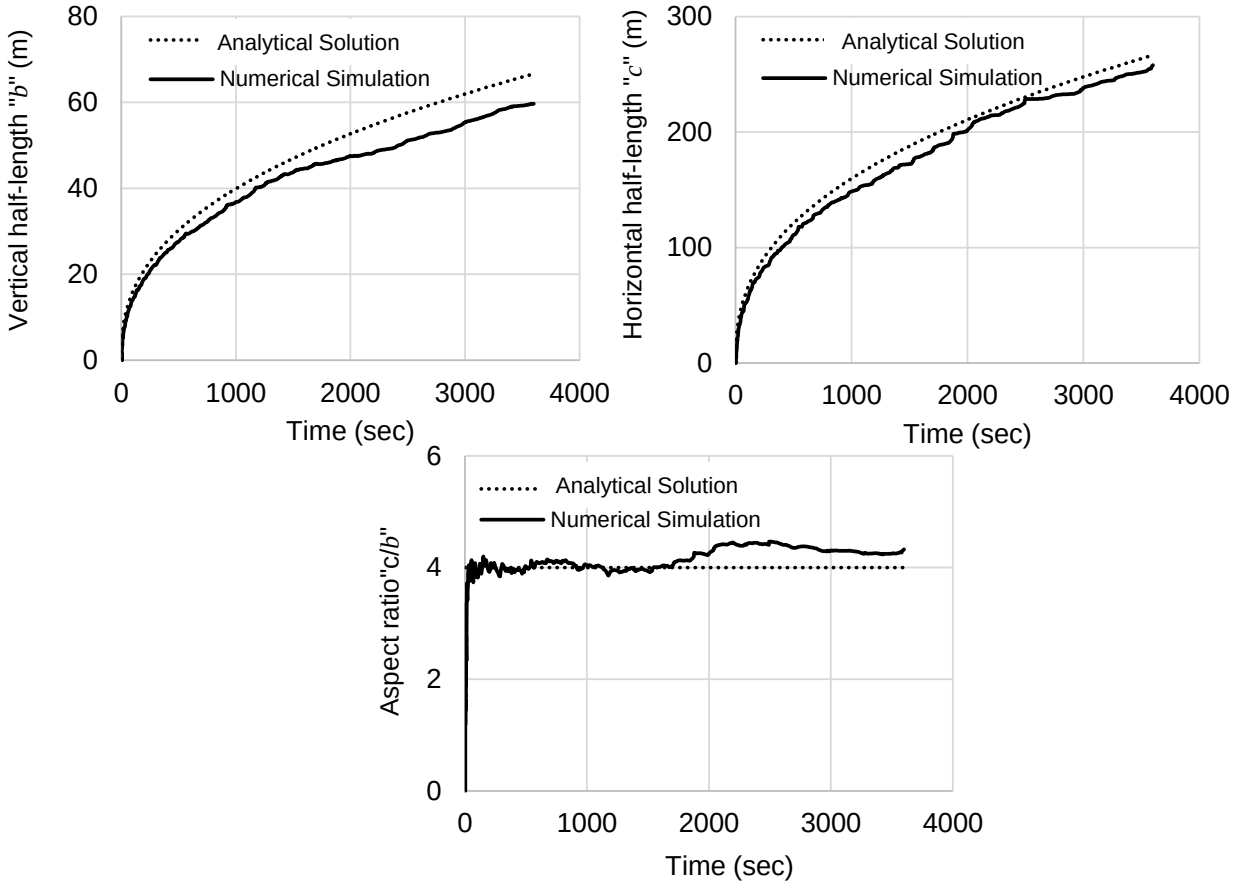

Figure 5.7: Numerical simulation versus analytical solution of radial fracture parameters for $K_{C,3}/K_{C,1}$ = 2

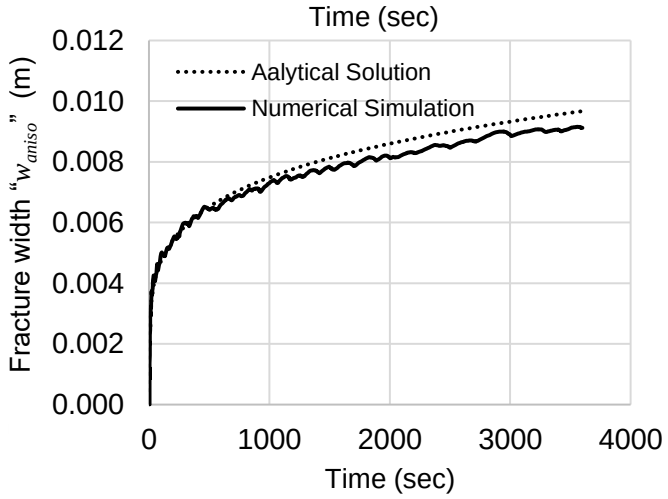

Figure 5.8: Numerical simulation versus analytical solution of radial fracture width for $K_{C,3}/K_{C,1}$ = 2

As it was noticed from the results of the simulations presented above in the previous part, increasing the ratio $K_{C,3}/K_{C,1}$ has a strong influence on the fracture aperture. This influence led

to increasing the aperture inside the fracture. The fracture width (aperture) of both analytical solutions and numerical simulations are plotted in Figure 5.9 for the case of isotropic $K_{C,3}/K_{C,1}$ = 1 and anisotropic fracture toughness $K_{C,3}/K_{C,1} = 2$. The solid lines show numerical simulation results, while the dashed lines show the analytical solution results. The black color is used for $K_{C,3}/K_{C,1}$ = 1, while the red color is used for the case of $K_{C,3}/K_{C,1} = 2$. It is shown that both analytical solutions and numerical simulations present higher fracture width (aperture) for case of TIV fracture toughness (in red) compared to the isotropic case, which confirm the previous observations.

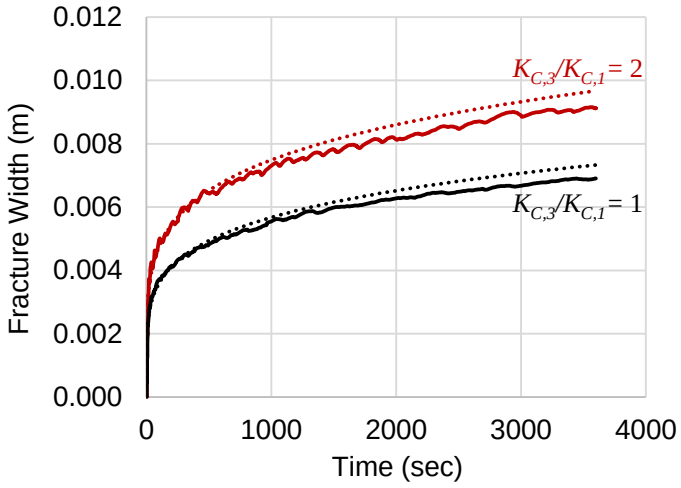

Figure 5.9: Numerical simulation versus analytical solution of radial fracture width for $K_{C,3}/K_{C,1}$ =1 versus $K_{C,3}/K_{C,1}$ =2

5.3.2 Multiple Hydraulic Fractures

In order to study the morphology of simultaneous multiple radial fracture propagating in a medium with TIV fracture toughness, 5 hydraulic fractures are initiated simultaneously from a horizontal wellbore with limited entry conditions (i.e. the fluid flux evenly distributed between the fractures). One important consideration during HF of multiple fractures in horizontal wells is the stress shadow effect. In this case, the effect of stress shadow combined with the TIV fracture toughness

will be investigated for the toughness and viscosity regimes. Due to the similarity between single and multiple radial fractures, the dimensionless parameters presented previously in Table 5. 1 for the problem of single radial fracture are used for the analysis of multiple fractures propagating in toughness (*K*) and viscosity (*M*) regimes.

5.3.2.1 Toughness Storage Regime (*K*)

Sensitivity of the results to fracture spacing and TIV fracture toughness for simultaneous propagation of multiple radial fractures in toughness regime are shown in Figure 5.10. It is clearly seen that toughness anisotropy combined with the stress shadow effect have a significant impact on the fracture morphology. For small spacing (10 m , 20m, and 40 m), the effect of stress shadow is significant and the hydraulic fractures intend to avoid each other, with minimum overlap between the fractures, leading to a petal-like fracture shape (Dontsov 2021b). These petals all together form a radial shape in the case of isotropic fracture toughness $K_{C,3}/K_{C,1} = 1$; however, in case of TIV fracture toughness $K_{C,3}/K_{C,1} = 2$, the system of fractures form elliptical shape. In case of $K_{C,3}/K_{C,1} = 1$, for large spacing (80m and 160 m), the stress shadow effect is less, and egg shape fractures are observed for spacing 80 m, while radial and more uniform hydraulic fractures developed for spacing of 160 m. However, in case of TIV fracture toughness $K_{C,3}/K_{C,1} = 2$, the hydraulic fractures are elliptical and we still can see the stress shadow effect leading the fractures to avoid each others (one move to the right and other to the left) even for large spacing (160 m). This is because by increasing the toughness in the vertical direction, the overall fracture toughness of the system is increased, so in this case we are moving more toward the toughness dominated regimes limit in which this type of behavior is more pronounced. This means that in case of TIV fracture toughness there is more stress shadow effect and more interaction between the fractures compared to the case of isotropic fracture toughness.

One can see that the fracture aperture (width) is higher in case of TIV fracture toughness compared to isotropic case. This phenomenon was observed for single radial fracture and was discussed and proven analytically and numerically in the previous section.

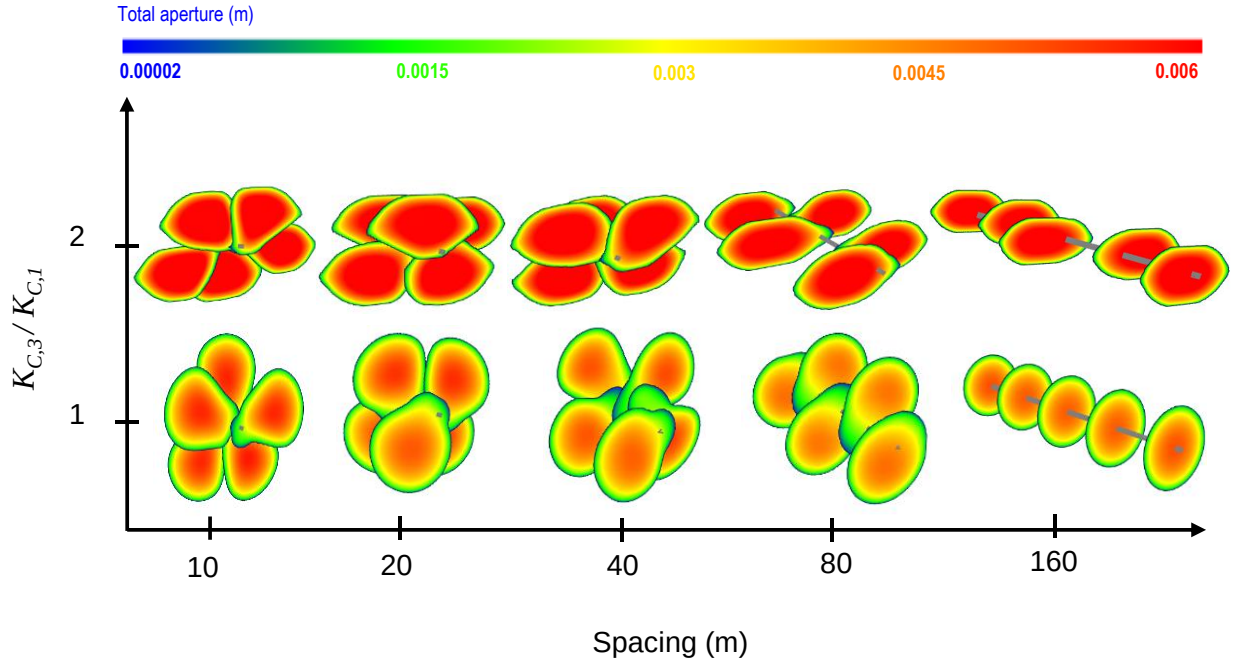

Figure 5.10: Simultaneous propagation of 5 radial fractures in toughness dominated regime with different spacing for cases of $K_{C,3}/K_{C,1}$ =1 versus $K_{C,3}/K_{C,1}$ =2

5.3.2.2 Viscosity Storage Regime (M)

To demonstrate how multiple radial hydraulic fractures behave in viscosity-dominated regime with the presence of fracture toughness anisotropy, the simulation of multiple radial fractures with different spacing are performed in isotropic and TIV fracture toughness using the parameters presented in Table 5. 1 for viscosity dominated regime (*M*).

Figure 5.11 shows the results of the simultaneous propagation of 5 hydraulic fractures in viscosity dominated regime for the case of isotropic $K_{C,3}/K_{C,1}$ = 1 and TIV fracture toughness $K_{C,3}/K_{C,1}$ = 4.

First, it is to be mentioned that there is a clear variation in the fracture geometry with respect to the results of the toughness-dominated regimes (*K*) presented in the previous section in Figure 5.10. While in toughness dominated regime (*K*) the fractures are segmented and avoiding each other's, fractures in viscosity dominated regime (*M*) are more symmetric and overlapped. Comparison between fracture morphology in isotropic and TIV fracture toughness demonstrate that there is no change in behavior for $K_{C,3}/K_{C,1}$ = 2 (the results are similar to $K_{C,3}/K_{C,1}$ = 1). This is in good agreement with the definition of limiting viscosity dominated regime (*M*), which is associated with the dominance of fluid viscosity where the effect of fracture toughness is negligible. At the same time, a small change is seen when increasing the ratio of toughness anisotropy to $K_{C,3}/K_{C,1}$ = 4. Fractures for large spacing (80 m and 160 m) still overlapped and nearly circular with a small effect of the high value of the vertical fracture toughness that slightly restrict the propagation in the vertical direction and elongated along the horizontal direction. However, for small spacing (10, 20, and 40), the interaction between the fractures is more pronounced and the overlap is minimized compared to the isotropic case (spacing of 40 m). This asymmetry is caused by the fact that the stress shadow effect is higher in the presence of TIV fracture toughness. In addition, the aperture is slightly higher in case of TIV fracture toughness compared to the isotropic case. These results of the combined effect of TIV fracture toughness and stress shadow are qualitatively similar to the results of the toughness-dominated (*K*) regime.

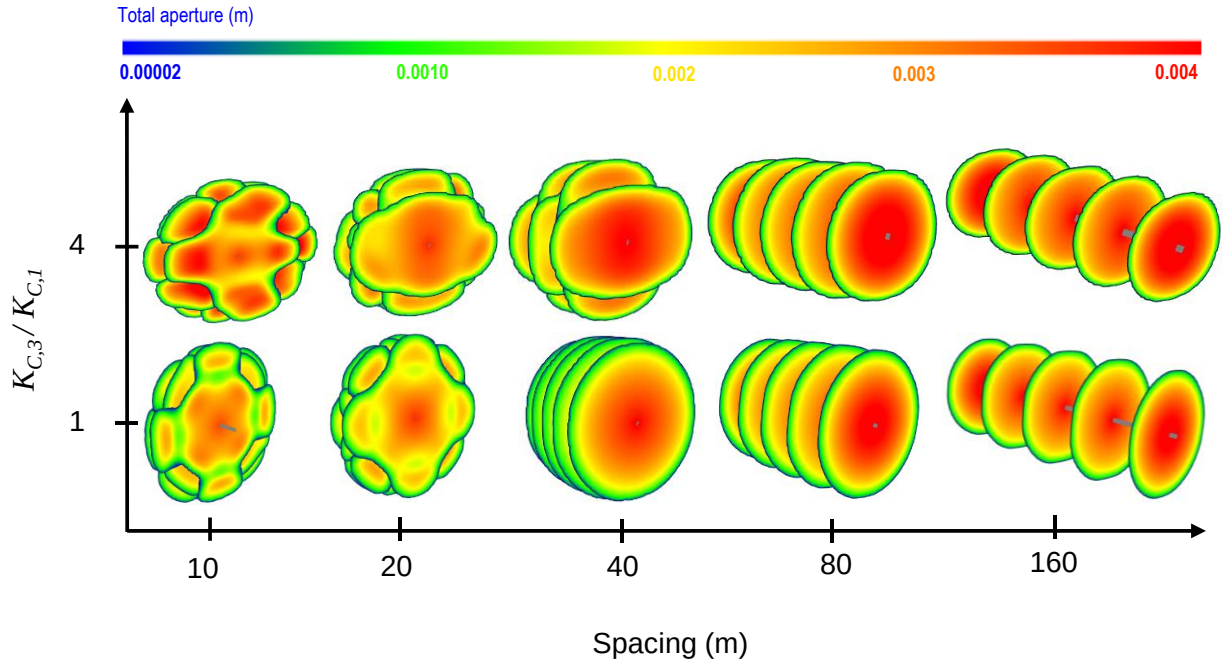

Figure 5.11: Isotropic versus anisotropic simultaneous propagation of 5 radial fractures in viscosity dominated regime with different spacing.

In summary, it is important to note that the TIV fracture toughness has a relatively strong effect on the fracture pressure, fracture parameters as well as fracture morphology. The overall shape of the system of fractures becomes somehow elliptical in case of the TIV fracture toughness for all scenarios of single and multiple hydraulic fractures in toughness and viscosity dominated regimes. The fracture pressure and aperture are higher and the stress shadow effect is more pronounced when the rock exhibit TIV fracture toughness. Since the effect of the TIV fracture toughness on the morphology of multiple hydraulic fractures is qualitatively the same for toughness and viscosity regimes, it is assumed that the rest of the propagation regimes obey similar behaviour.

5.4 Constant Height Fracture

While there is a variety of relatively simple fracture geometries such as the case of radial fracture presented in the previous section, the geometry of a constant height (PKN) hydraulic fracture is another simple geometry that can be considered (Figure 5.13). This is the case of this section, in

which the propagation of single and multiple constant height (PKN) hydraulic fractures in the presence of fracture barriers is investigated in TIV fracture toughness and compared to the isotropic case.

The input parameters for toughness regime (*K*) and viscosity regime (*M*) in case of PKN fracture are presented in Table 5. 2.

Table 5. 2 Input parameters for the propagation of constant height hydraulic fracture

Property	*K*	*M*
Young's Modulus, *E* [GPa]	10	25
Toughness, K_{IC} [Mpa.m^0.5]	5	3
Target Layer Height, H[m]	80	80
Poisson's Ratio, ν	0.25	0.25
Fluid Viscosity, μ [Pa.s]	0.003	0.05
Flow Rate, Q [m^3/s]	0.1	0.2
Time t [hrs]	1	1
Carter'sleak-off coefficient C_l [$m/s^1/2$]	0	0
τ	0.35	1.2×10^4
ϕ	0	0

Figure 5.12 shows the location of the problem parameters of Table 5. 2 inside the parametric space for the case of constant height fracture.

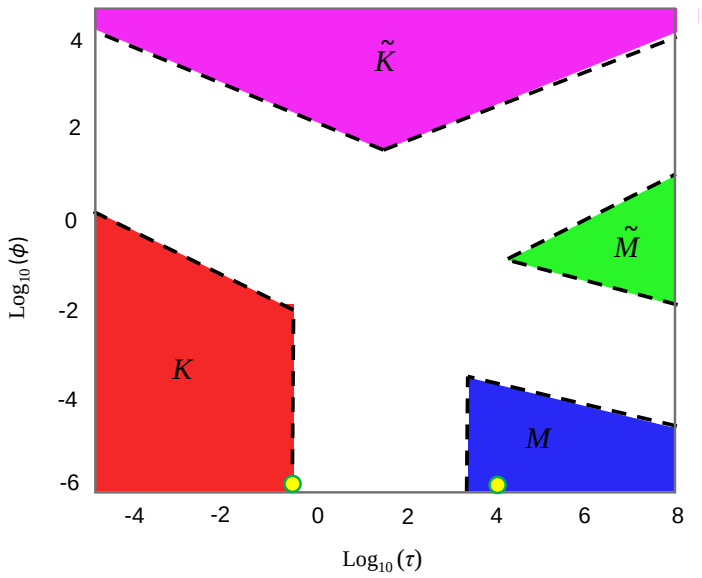

Figure 5.12: Parametric space of propagation regimes for PKN fracture. Circular markers correspond to the location of *K* and *M* parameters of Table 5. 2 (Modified after (Dontsov 2021a))

5.4.1 Constant Height Fracture with Toughness Barriers

In this section, the propagation of single and multiple constant height (PKN) hydraulic fractures in the presence of fracture toughness barriers is investigated in toughness-dominated regime (*K*). The toughness value at the bounding layers (upper and lower layer) corresponds to $K_{C,3}$ whereas the fracture toughness in the target layer corresponds to $K_{C,1}$ as shown in Figure 5.13.

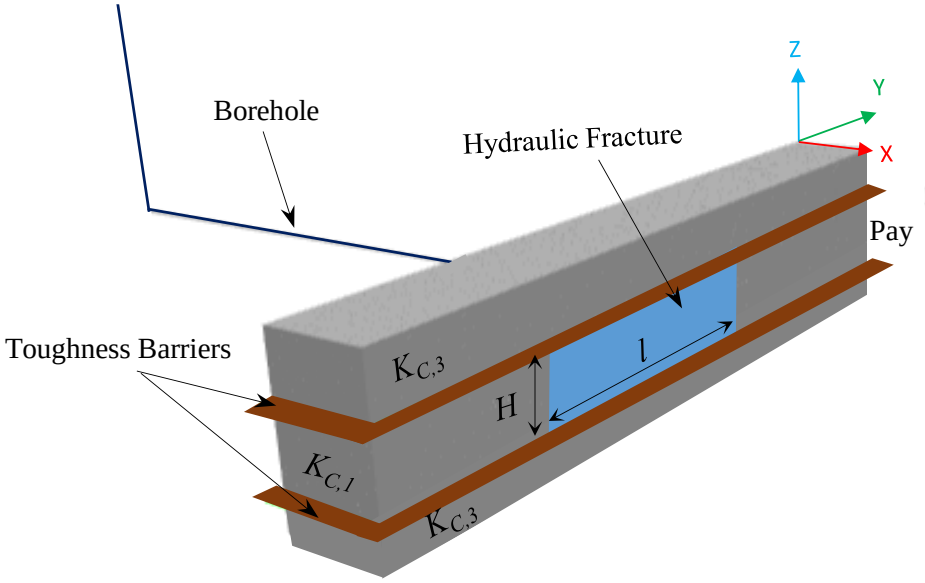

Figure 5.13: Schematics of PKN constant height fracture

5.4.1.1 Single PKN Fracture

To better understand the effect of toughness contrast on the fracture net pressure and fracture parameters, simulations of single constant height hydraulic fracture in different toughness contrast $K_{C,3}/K_{C,1}$ and variable layer size H were conducted in toughness-dominated regime. Here, we keep the value of $K_{C,1}$ in the target layer constant, and we increase the value of $K_{C,3}$ in the upper and lower bounding layers.

a. Effect of $K_{C,3}/K_{C,1}$ on Net Pressure and Fracture Geometry

The sensitivity analysis for the propagation of constant height fracture in a layer of thickness $H = 80\,\text{m}$ under variable $K_{C,3}/K_{C,1}$ is presented in Figure 5.14. In this case, we increase the toughness $K_{C,3}$ in the upper and lower bounding layers.

In term of fracture morphology, it is seen that when there is no fracture barriers $K_{C,3}/K_{C,1} = 1$, the fracture propagate in circular and symmetric shape. This case corresponds to the radial fracture. However, in the presence of the toughness barrier ($K_{C,3}/K_{C,1} > 1$) the fracture is getting contained in the vertical direction (height "H") while it is getting longer in the horizontal direction (length "l"). Nevertheless, it is clear from the figure that the effect of the toughness contrast for $K_{C,3}/K_{C,1} = 1.5$ is less compared to $K_{C,3}/K_{C,1} = 2,\ 2.5,\ 3, \text{and}\ 3.5$. After a certain toughness contrast, approximately $K_{C,3}/K_{C,1} = 2$, the fractures are qualitatively identical for all cases ($K_{C,3}/K_{C,1} = 2,\ 2.5,\ 3, \text{and}\ 3.5$). It is to be mentioned that this critical magnitude of TIV fracture toughness from which the fractures are identical, depends on the target layer thickness "H". Therefore, a sensitivity analysis to the target layer thickness "H" is conducted and the results are presented in the following.

The net pressure corresponding to the fracture geometries presented in Figure 5.14 were exported from the numerical simulation results and plotted in Figure 5.15. The net pressure increases as the toughness contrast increases from $K_{C,3}/K_{C,1}$= 1 to $K_{C,3}/K_{C,1} = 2$, then the net pressure stabilize and become identical for all cases $K_{C,3}/K_{C,1} = 2,\ 2.5,\ 3, \text{and}\ 3.5$. This limit is exactly the same magnitude ($K_{C,3}/K_{C,1} = 2$), after which the fractures geometry became more regular and similar. In other words, one can say that for a particular properties (presented in Table 5. 2) the fractures becomes qualitatively and quantitatively similar when exceeding a certain value of toughness contrast which corresponds to $K_{C,3}/K_{C,1} = 2$.

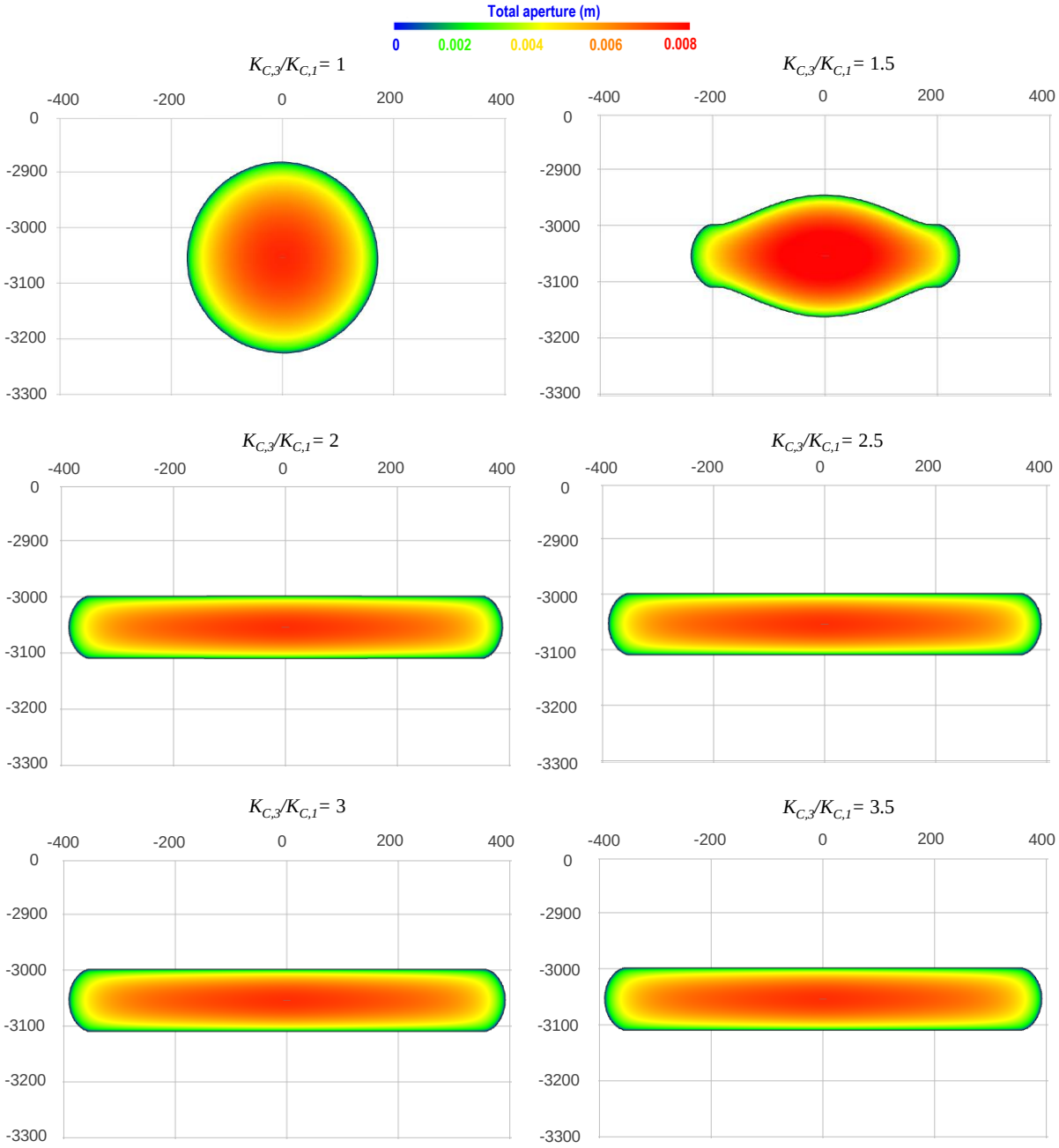

Figure 5.14: Fracture geometry for variable for cases of $K_{C,3}/K_{C,1}$ in case of constant height fracture

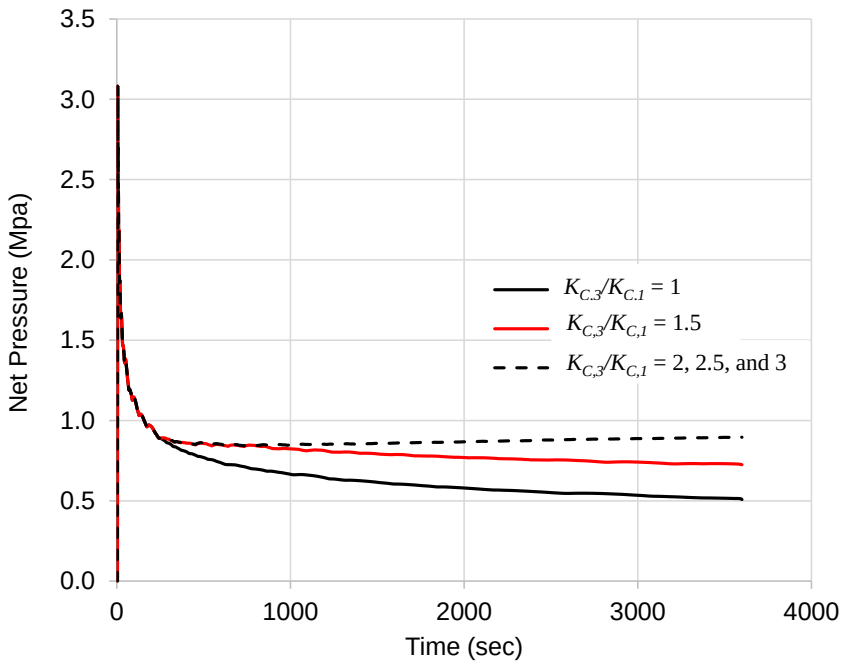

Figure 5.15: Net pressure of constant height fracture for variable $K_{C,3}/K_{C,1}$

The results of the sensitivity analysis to the layer size "H" of the constant height fracture for variable $K_{C,3}/K_{C,1}$ are presented in Figure 5.16. The results indicates that for small layer thickness H = 60 m, higher toughness contrast is needed to fully contain the fracture height in the vertical direction. In this case, the magnitude of fracture contrast corresponds to $K_{C,3}/K_{C,1} = 3$. However, with increasing the layer size H, the effect of toughness contrast increases, hence lower toughness contrast is needed to fully contain the fracture height. In other words, for a particular value of H, the toughness contrast reaches a certain magnitude where the effect of increasing the toughness contrast $K_{C,3}/K_{C,1}$ is not seen and the fractures become qualitatively similar. The magnitude of the fracture contrast, for which this transition happens is $K_{C,3}/K_{C,1} = 2$ in case of H = 80 m and H = 140 m, while for H =180 m the transition happens at the value corresponding to $K_{C,3}/K_{C,1} = 1.5$, in which the fractures become more regular. The fracture length evolution indicates that the fracture is getting more elongated in the horizontal direction with decreasing the layer size. Results

also demonstrate that for a particular H, the fracture length increases with increasing the toughness contrast $K_{C,3}/K_{C,1}$ until it reaches a certain limit of $K_{C,3}/K_{C,1}$ where the fractures are fully contained and similar. One can clearly see that fractures become more regular after this limit of $K_{C,3}/K_{C,1}$.

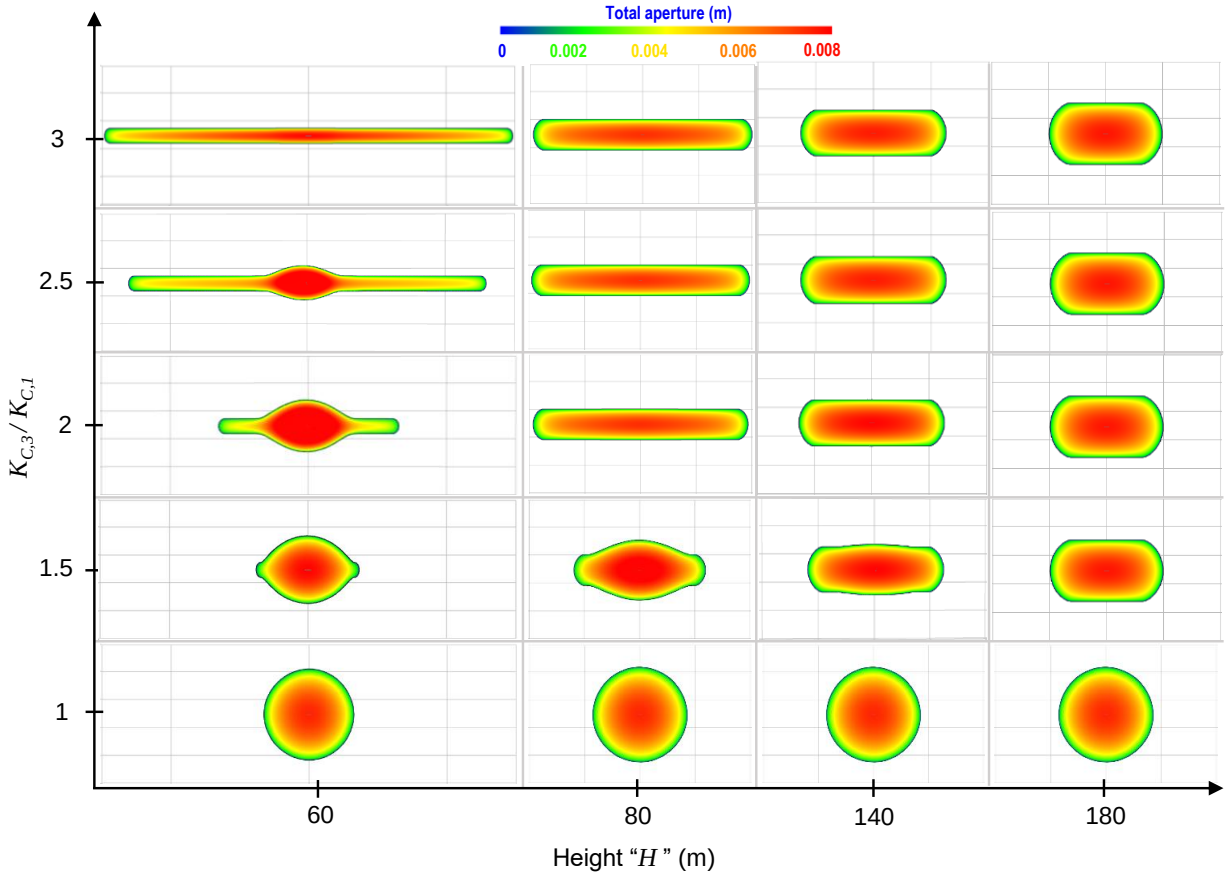

Figure 5.16: Fracture morphology of constant height case for variable $K_{C,3}/K_{C,1}$ and target layer thickness "H"

5.4.1.2 Effect of $K_{C,3}/K_{C,1}$ on Fracture Parameters

In this section, we compare the fracture parameters exported from the results of the numerical simulations with the parameters estimated from the analytical solutions for fracture toughness contrast $K_{C,3}/K_{C,1} = 2$. In the limit of toughness storage dominated regime, the pressure and fracture width are constant throughout the fracture. The form of the solutions for fracture length l

, and fracture width w_{PKN} in the limit of toughness dominated regime are respectively as following (Dontsov 2021a):

$$l = \frac{E'Qt}{\sqrt{4\pi}K_{IC}H^{3/2}} \tag{5.10}$$

$$w_{PKN} = \frac{K_{IC}\sqrt{\pi H}}{E'} \tag{5.11}$$

Figure 5.17 plots the results of the constant height fracture parameters (fracture length l, fracture height H, and fracture width w_{PKN}) estimated from the analytical solutions along as with the parameters exported from the numerical simulation results. As can be seen from the figure, the results of the analytical solution for the fracture parameters l, H and w_{PKN} are in good agreement with the simulation results.

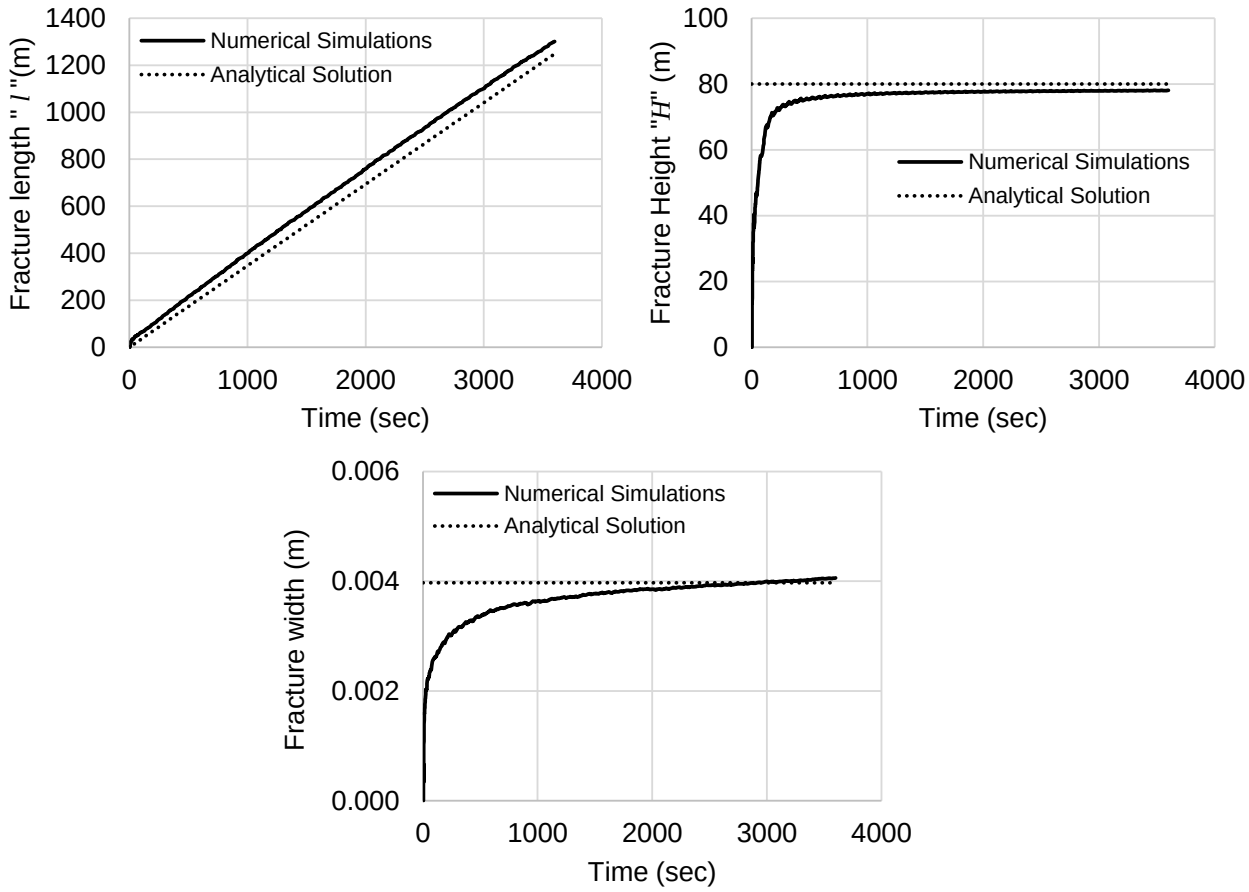

Figure 5.17: Numerical simulation versus analytical solution of PKN fracture parameters for $K_{C,3}/K_{C,1}$ = 2

Figure 5.18 shows the numerical simulation results of the fracture width for the case of $K_{C,3}/K_{C,1} = 1$ and $K_{C,3}/K_{C,1} = 2$ corresponding to the fracture geometries shown in Figure 5.14. The observed results demonstrate that the fracture width (aperture) in case of $K_{C,3}/K_{C,1} = 2$ is slightly higher compared to the case $K_{C,3}/K_{C,1} = 1$ (radial fracture).

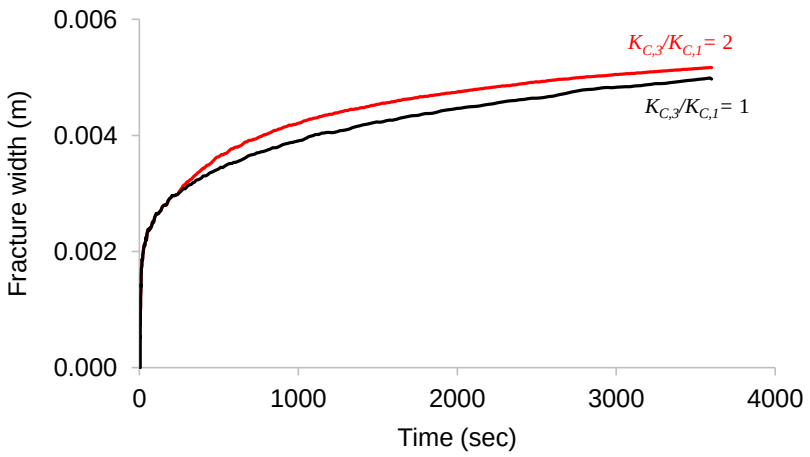

Figure 5.18: Numerical simulation results of PKN fracture width for $K_{C,3}/K_{C,1}$ = 1 versus $K_{C,3}/K_{C,1}$ = 2

5.4.1.3 Multiple PKN Fractures

This section investigates the simultaneous propagation of multiple constant height fractures in the presence of toughness contrast. Five hydraulic fractures are initiated simultaneously from a horizontal wellbore under limited entry conditions (i.e., the fluid flux evenly distributed between the fractures). In particular, the focus is to identify the effect of toughness contrast combined with stress shadow effect on the fracture morphology of multiple fractures. One important consideration in studying constant height fracture geometry is the layer size as discussed in the previous section of the single constant height problem, therefore, variable layer size will be considered. Due to the similarity between single and multiple fractures, the dimensionless parameters presented previously in Table 5. 2 for the problem of single constant height fracture are used for the analysis of multiple constant height fractures propagating in toughness-dominated regime (*K*).

Figure 5.19 shows results of multiple fractures propagating under the toughness dominated regime condition with variable spacing and layer size "*H*", for the cases of toughness contrast $K_{C,3}/K_{C,1} = 1.5$, $K_{C,3}/K_{C,1} = 2$, and $K_{C,3}/K_{C,1} = 3$ respectively. First, it is to be mentioned that the results are similar to the propagation of multiple radial fractures in toughness-dominated regime, where the

fracture geometries are more complex especially for small spacing. There is a clear variation in the fracture geometry with respect to the layer size "*H*" and the spacing between the fractures for all the cases of toughness contrast ($K_{C,3}/K_{C,1} = 1.5$, $K_{C,3}/K_{C,1} = 2$, and $K_{C,3}/K_{C,1} = 3$). However, the fractures in the case of toughness contrast: $K_{C,3}/K_{C,1} = 2$ are nearly identical to the fractures in case of $K_{C,3}/K_{C,1} = 3$, while they are both different from the case of $K_{C,3}/K_{C,1} = 1.5$. This was observed in the case of single fracture where at a certain value of the toughness contrast from which the fractures become identical with increasing the toughness contrast.

For the case of *H* = 140 m and large spacing (80 m and 160 m), the fractures exhibit a nearly radial fracture geometry for all cases of toughness contrast. This is because the layer size is not enough to fully contain the fracture in these conditions, even with high toughness contrast. However, for small spacing (10 m 20 m and 40m), the fractures are more contained and nearly identical for both cases ($K_{C,3}/K_{C,1} = 2$ and $K_{C,3}/K_{C,1} = 3$), while they are less contained in case of $K_{C,3}/K_{C,1} = 1.5$.

For the case of *H* = 80 m, the fractures are similar and fully contained for all cases of toughness contrast ($K_{C,3}/K_{C,1} = 1.5$, $K_{C,3}/K_{C,1} = 2$, and $K_{C,3}/K_{C,1} = 3$) with all spacing scenarios; except for the case $K_{C,3}/K_{C,1} = 1.5$ with small spacing (10 m, 20 m and 40 m), where we can see a slight change with respect to the other two cases. This is due to the fact that this magnitude of toughness contrast ($K_{C,3}/K_{C,1} = 1.5$) is not enough to fully contain the fractures in these conditions.

For the case of *H* = 60 m, there is an evident variation in the fracture geometry for the case of $K_{C,3}/K_{C,1} = 1.5$ with respect to the other cases ($K_{C,3}/K_{C,1} = 2$ and $K_{C,3}/K_{C,1} = 3$), which are more similar and the fractures are getting more contained in height. In case of $K_{C,3}/K_{C,1} = 1.5$, the fractures are partially contained and show similar behaviour to the multiple radial fractures propagating in TIV fracture toughness.

The fractures are getting longer in the horizontal direction with decreasing the layer size. However, the fractures are less contained in height for higher layer size and large spacing. In case of small toughness contrast $K_{C,3}/K_{C,1} = 1.5$ and small spacing, the fractures are also less contained in height. This is important especially for cases of hydraulic fracturing in multiple laterals, where the frac hits can happen.

The toughness contrast magnitude $K_{C,3}/K_{C,1} = 1.5$, is less efficient for case of H = 60 m where the fractures are not fully contained especially for small spacing. However, with increasing the spacing, the effect of the toughness contrast is more pronounced and the fractures are more contained especially for the case of H = 80 m, which represent a better layer size to fully contain the hydraulic fractures compared to the other layer sizes.

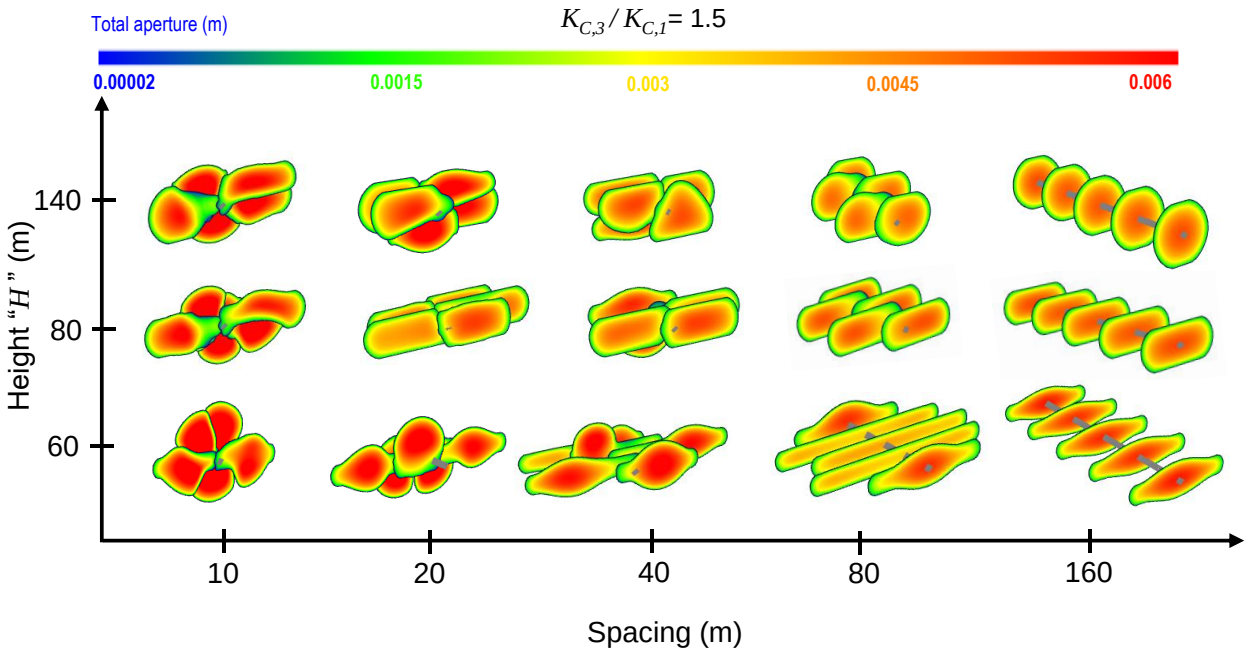

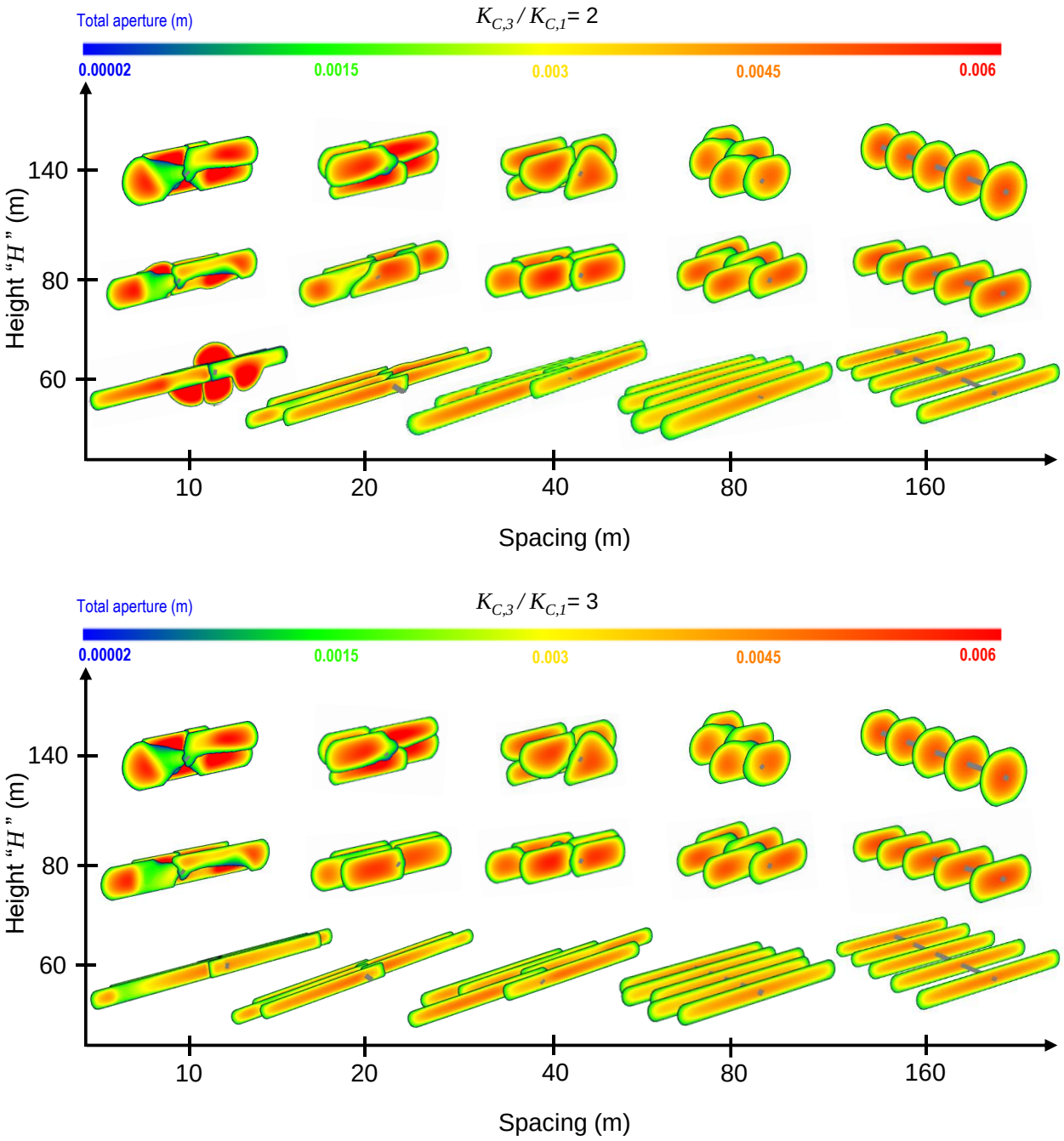

Figure 5.19: Simultaneous propagation of 5 constant height fractures in toughness dominated regime with different spacing and variable layer sizes H for the cases of $K_{C,3}/K_{C,1}$ 1.5, $K_{C,3}/K_{C,1}$ = 2, and $K_{C,3}/K_{C,1}$ = 3

5.4.2 Morphology of Multiple PKN Fractures in TIV Toughness

To illustrate the effect of TIV toughness in the target layer, we applied a stress barriers in the bounding layers and we set the fracture toughness in vertical direction $K_{C,3}$ and horizontal direction $K_{C,1}$ to get the ratio $K_{C,3}/K_{C,1}$= 2 as shown in Figure 5.20.

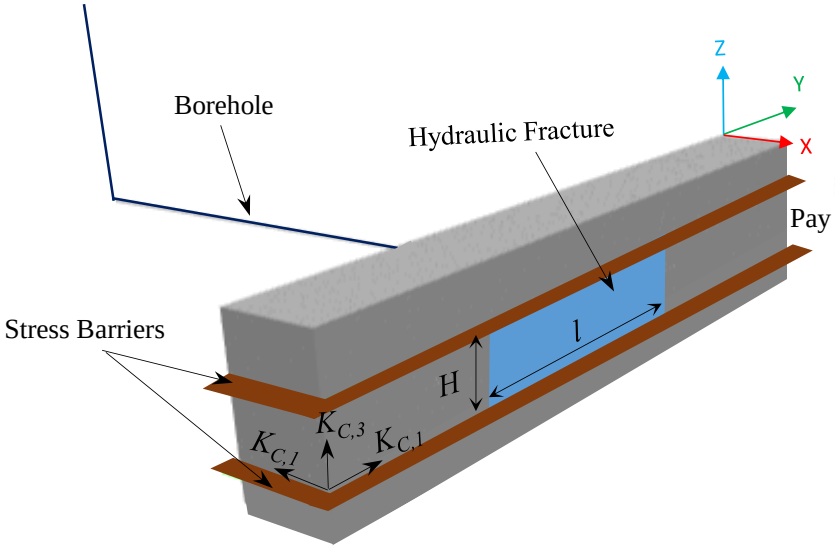

Figure 5.20: Schematics of PKN constant height fracture with TIV toughness in the target layer (pay zone)

5.4.2.1 Toughness Storage Regime (K)

Simulations of simultaneous propagation of multiple constant height fractures for isotropic and TIV fracture toughness ($K_{C,3}/K_{C,1}$= 2) cases with variable spacing were conducted in toughness dominated regime. The results are presented in Figure 5.21. One can see that the TIV fracture toughness greatly affects the interaction between the fractures compared to the isotropic case. It is to be noted that for small spacing, the fractures are more asymmetric with high fracture length contrast. Once the spacing get larger, more symmetric and nearly identical fractures are observed for both isotropic and anisotropic toughness cases. It is important to note that for large spacing in case of TIV toughness, the overall shape of the fracture system becomes elliptical and qualitatively

similar to the radial case in TIV fracture toughness. In addition, the aperture is higher compared to the isotropic case, which is also observed for multiple radial fractures.

The interaction between the fractures is higher in TIV fracture toughness compared to the isotropic case where even for high spacing 160 m we still can observe stress shadow effect.

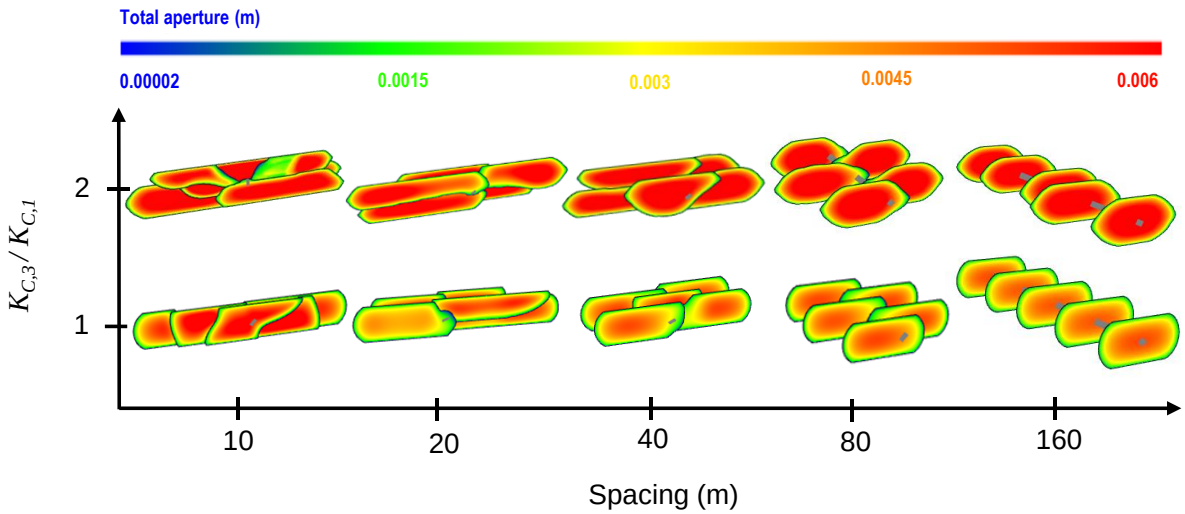

Figure 5.21: Simultaneous propagation of 5 PKN fractures in toughness dominated regime with variable spacing for cases of $K_{C,3}/K_{C,1}$ =1 versus $K_{C,3}/K_{C,1}$ =2

5.4.2.2 Viscosity Storage Regime (M)

A series of numerical simulations are conducted in viscosity-dominated regime based on the parameters presented in Table 5. 2 for variable TIV fracture toughness cases ($K_{C,3}/K_{C,1}$= 1, 2, and 4) and spacing. The results of simultaneous propagation of 5 PKN hydraulic fractures are presented in Figure 5.22. In term of fracture behavior, the results for the case of $K_{C,3}/K_{C,1}$= 1 are qualitatively similar to the case of radial fracture, where the fractures are overlapped and have more identical morphology. However, with increasing the TIV toughness, the fractures are getting more complex especially in cases of small spacing (10m, 20m, and 40m) and the overlap is minimized.

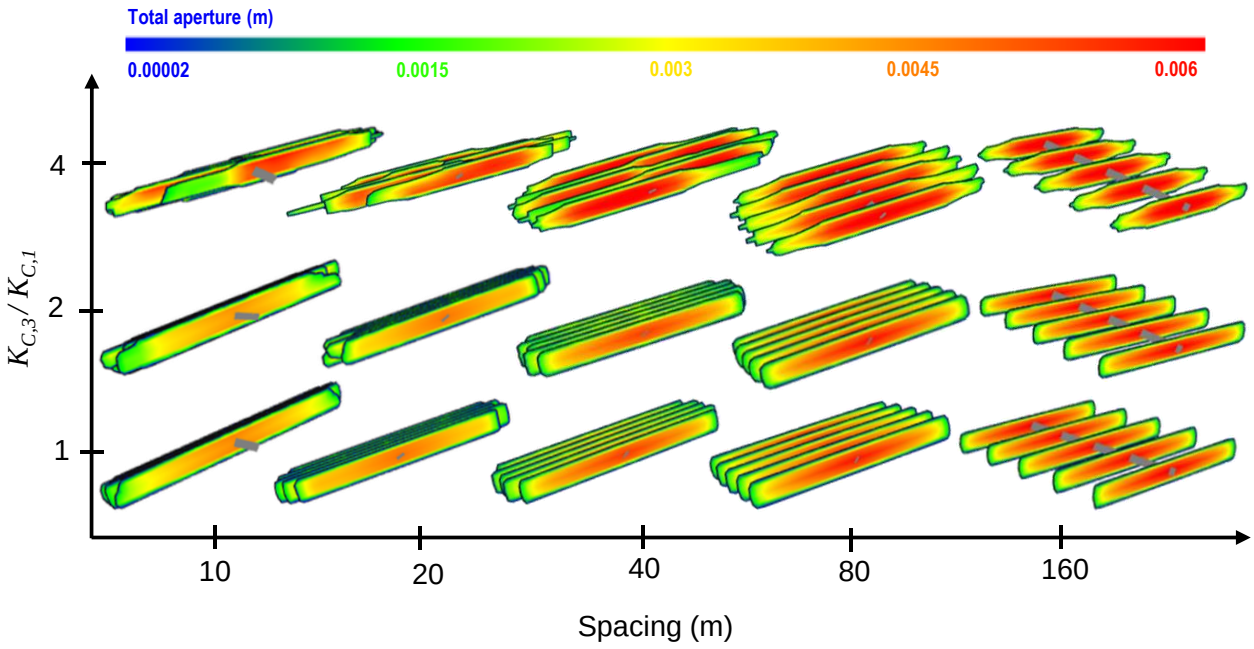

Figure 5.22: Simultaneous propagation of 5 PKN fractures in viscosity-dominated regime (*M*) with variable spacing for cases of $K_{C,3}/K_{C,1}$ =1, $K_{C,3}/K_{C,1}$ =2, and $K_{C,3}/K_{C,1}$ =4

5.5 Field Example (Bakken)

In real field applications, the propagation and geometry of hydraulic fracture is more complex. However, the simplified models presented in the previous sections can provide a good initial insight into the propagation mechanism. The field example presented in this section corresponds to the data from the Bakken Formation. The input parameters are shown in Table 5. 3. In this example, we considered three stages.

Table 5. 3 The Bakken Formation elastic and mechanical properties and in-situ stresses (Schmidt et al. 2011)

Property	Unit	Value
Density, ρ	lb/ft^3	165
Young's Modulus, E	Mpsi	4.351
Uniaxial Compressive Strength, *UCS*	psi	7251.89
Tensile Strength, T_o	psi	725.189
Toughness, $K_{IC\text{-}isotropic}$ $K_{C,1}$, $K_{C,2}$	Mpsi.in$^{1/2}$	1820.1
Toughness, $K_{C,3}$	Mpsi. in$^{1/2}$	4000
Friction Angle, ϕ	degree	30
Poisson's Ratio, ν	-	0.25
Porosity,$\emptyset$	%	2

Permeability, K	Darcy	1e-5
Minimum Horizontal Stress, σ_h	psi	7950
Maximum Horizontal Stress, σ_H	psi	8930
Vertical Stress, σ_v	psi	9930
Fluid Viscosity, μ	cP	2

The value of fracture toughness in the vertical direction is set to $K_{C,3}$= 4000 Mpsi.in$^{1/2}$. In this case, the corresponding values of the toughness anisotropy ratio is $K_{C,3}/K_{C,1} = 1$ for the isotropic scenario (*a*), and $K_{C,3}/K_{C,1} = 2.19$ for the anisotropic scenario (*b*). The results of the simulations are presented in Figure 5.23. The fractures behavior in real field cases are more complex due to the existence of different layers, different stages and injection schedule, proppant, non-Newtonian fluids, and many other elements. In the isotropic case (*a*), the fractures are asymmetric with limited overlap. The fracture height and length vary between fractures along the stage, and from stage to stage. However, in case of anisotropic toughness (*b*), the fracture height is fully contained and longer fractures are observed. The aperture seems to be higher in the case of anisotropic toughness (*b*) compared to the isotropic case (*a*). These observations are in agreement with the results of the simple fracture geometries presented previously with more complexity for the field case. This field example demonstrates how the presence of toughness anisotropy affects the hydraulic fractures propagation and morphology in a field scale model. Such analysis can help to get an idea on how to adjust the hydraulic fracturing design in anisotropic shale formations, especially in the case of multilaterals where the frac hits is a potential scenario.

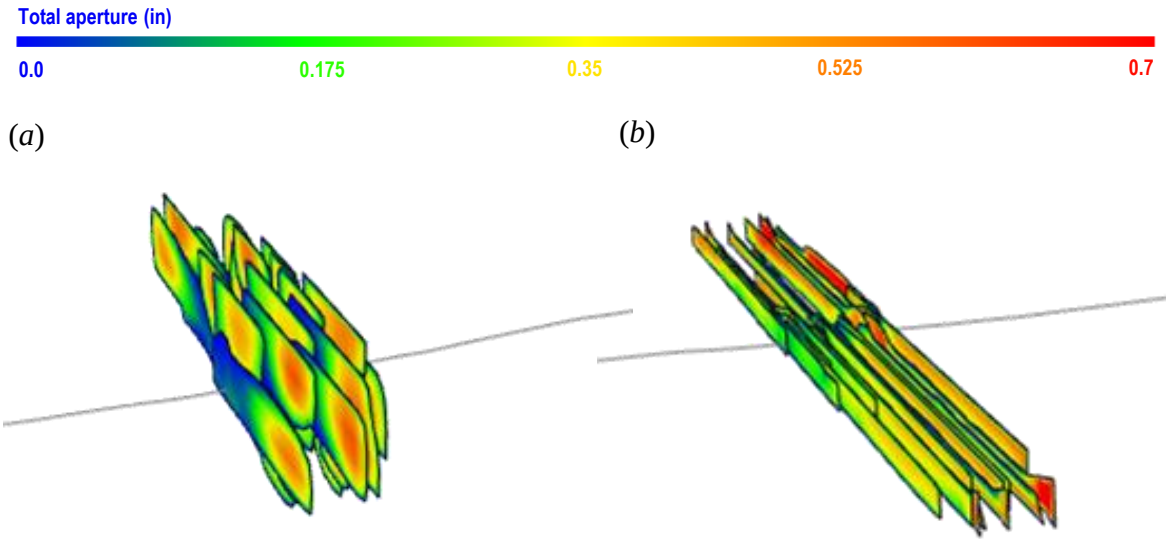

Figure 5.23: Field case hydraulic fracture geometries for isotropic toughness: (*a*) $K_{C,3}/K_{C,1}$ =1 and anisotropic toughness: (*b*) $K_{C,3}/K_{C,1}$ =2.1

5.6 Summary

In this Chapter, more than 120 different simulations of hydraulic fracturing models in anisotropic toughness with varied fracture geometries and different scenarios of propagation regimes were conducted to evaluate the effect of transverse isotropic toughness on the propagation of single and multiple hydraulic fractures. In addition, an example from the Bakken Formation in the Williston Basin was modeled as a field case study. The main conclusions drawn from the results of these simulations are summarized as below:

- ResFrac software, which is a fully coupled physics-based numerical simulator, showed great capabilities to simulate single and multiple hydraulic fractures in anisotropic toughness in different propagation regimes.

- Radial and constant height (PKN) are of great interest, in term of mathematical simplicity, to obtain preliminary information about the fracture behavior in anisotropic fracture toughness.

- The dimensionless parameters for the limiting propagation regimes for single fracture can be applied to define the propagation regimes for the simultaneous propagation of multiple fractures.

- In term of fracture morphology, the simulations showed that the TIV fracture toughness has a significant effect on the fracture shape of single radial fracture and multiple fractures. Increasing the toughness anisotropic ratio led to a significant modification in the fracture morphology. The fracture propagation is fully contained by the high value of fracture toughness in the vertical direction while it is getting easier and more elongated in the direction of minimum toughness. Which is in agreement with the results of the analytical models presented in the previous Chapter.

- Both analytical solutions and numerical simulations of single radial fracture show that toughness anisotropy has a strong influence on the fracture aperture and net pressure. This influence led to increasing both fracture aperture and net pressure.

- Fractures in toughness-dominated regime, are segmented and avoiding each other's in case of simultaneous propagation of multiple radial fractures. However, in viscosity-dominated regime, fractures are more symmetric and overlapped. This is observed for both cases of isotropic and anisotropic toughness.

- The stress shadow effect is more pronounced when the rock exhibit TIV fracture toughness.

- The overall shape of the system of fractures is circular in case of isotropic fracture toughness and becomes somehow elliptical in case of the TIV fracture toughness for all scenarios of

single and multiple hydraulic fractures, more pronounced in toughness compared to viscosity dominated regimes.

- The presence of toughness barriers in the bounding upper and lower layers greatly affect the fracture propagation.
- The fracture containment of a single fracture is affected by the toughness contrast between the bounding layers and the target layer, and affected by the target layer size. The fracture is getting more contained in height with increasing the toughness contrast magnitude. Similarly, the net pressure increases with increasing the toughness contrast.
- Morphology of the simultaneous propagation of constant height fractures in toughness-dominated regime is similar to the multiple radial fractures in toughness-dominated regime where the fracture geometries are more complex especially for small spacing.
- Higher toughness contrast is needed to fully contain the fracture in case of small target layer thickness and small spacing between multiple constant height fractures.
- In general, fractures propagating in anisotropic toughness result in higher aperture and pressure than fractures propagating in a medium with isotropic toughness.
- Field example analysis can help to get an idea on how to adjust the hydraulic fracturing design in shale anisotropic formations especially in case of multilaterals where the frac hits is a potential scenario.

It is important to note that more field tests and experiments are needed to study the effect of toughness anisotropy on the hydraulic fracture behavior in shale formations.

CHAPTER 6

Conclusions and Recommendations

The effect of vertical transversely isotropic fracture toughness on fracture initiation and propagation was studies in details as part of this research project. In particular, the focus of the analytical models is to identify the impact of the toughness anisotropy and Young's modulus anisotropy on the fracture initiation pressure and the competition between transverse versus axial fractures. However, the numerical simulations focus more on investigating the change in fracture morphology resulting from the presence of toughness anisotropy. The first Section of this Chapter lists the main conclusions made from this work and the second Section presents some of the future work that is recommended as continuation of this study.

6.1 Conclusions

From this study the following major conclusions can be drawn:

- Analytical models are of great use to obtain preliminary information about the impact of the TIV due to fracture toughness and due to Young's modulus on fracture initiation pressure; and how different parameters may influence it. However, each of them has simplified assumptions, which make their results to deviate from the real cases. Therefore, conducting numerical simulations, before field trial, is necessary.

- The results of analytical models indicated that the pressure to initiate a crack decreases with increasing the crack length, or in other word, the pressure to propagate crack is reducing as crack length becomes larger.

- Among other parameters, it is evident that stress anisotropy has a dominant effect on whether transverse or axial fracture will initiate from an OH lateral. However, this study shows that toughness anisotropy and rock stiffness anisotropy has a strong effect on the competition between transverse and axial fractures.

- Theoretically, axial fractures dominate and initiate from multiple section of the wellbore especially in the absence of any pre-existing fracture, or effective notches (e.g. inadequate length). In this case, the fracture initiation pressure is very large.

- The analytical results showed that the transversely isotropic fracture toughness and transversely isotropic Young's modulus greatly affect the fracture initiation pressure (FIP) of both transverse and axial fractures. An increase in the anisotropic ratio of the fracture toughness led to increasing the initiation pressure of both fracture geometries.

- Results of analytical models showed that minimum pressure to initiate a transverse or axial fracture reduces as the crack size increases. However, the fracture with the lowest initiation pressure is the most favourable one for initiation.

- Assuming a horizontal wellbore drilled along the minimum horizontal stress direction, the initiation pressure of axial fracture size less than a certain length is lower than the initiation pressure of transverse fracture of the same length; therefor, axial crack is favorable to initiate. Whereas, exceeding this limit, the transverse fracture is more favorable to open. This transition length from axial domination to transverse domination is proven that it is mostly affected by the stress anisotropy.

- The analytical models proves that the transition length from axial dominated fracture to transverse dominated fracture is also affected by the toughness anisotropy and Young's modulus anisotropy. As the anisotropic ratio of toughness and Young's modulus increases, this transition length increases, i.e. larger fractures needed to favor transverse fractures compared to the isotropic case.

- The fracture initiation in case of direction dependent fracture toughness is variable with direction and is controlled by the local initiation direction angle at the fracture front. The fracture initiation is easier in the direction of minimum fracture toughness (horizontal direction) and getting gradually harder moving toward the direction of maximum fracture toughness (vertical direction). Therefore, the fracture initiation in one direction earlier than in the other directions and hence the elliptical fracture shape is expected.

- The impact of toughness anisotropy is more pronounced in case of small fractures compared to the large fractures and for transverse fractures compared to axial fractures. This can be

explained by the fact that with moving far away from the wellbore, far field stress effect is more dominant.

- ResFrac software, which is a fully coupled physics-based numerical simulator, showed great capabilities to simulate single and multiple hydraulic fractures in anisotropic toughness in different propagation regimes.

- Realistic field cases of hydraulic fracturing in shale formations are more complex of course, therefore, we always need to run a fully coupled numerical simulations to get a more precise idea on the problem. However, some estimates can be done with simple models.

- Radial and constant height (PKN) are of great interest, in term of mathematical simplicity, to obtain preliminary information about the fracture behavior in anisotropic fracture toughness.

- In term of fracture morphology, it is seen that the TIV fracture toughness has a significant effect on the fracture shape of single radial fracture. Increasing the toughness anisotropic ratio led to a significant modification in the fracture morphology. The fracture propagation is fully contained by the high value of fracture toughness in the vertical direction while it is getting easier and more elongated in the direction of minimum toughness. This is in good agreement with the analytical models.

- The results show that the net pressure increased with increasing the TIV fracture toughness ratio and accordingly, the fracture initiation pressure increases with increasing the toughness anisotropy. This is in good agreement with the analytical models.

- Both analytical solutions and numerical simulations of single radial fracture show that toughness anisotropy has a strong influence on the fracture aperture. This influence led to increasing the aperture inside the fracture.

- Fractures in toughness-dominated regime, are segmented and avoiding each other's in case of simultaneous propagation of multiple radial fractures. However, in viscosity-dominated regime, fractures are more symmetric and overlapped. This is observed for both cases of isotropic and anisotropic toughness.

- The stress shadow effect is more pronounced when the rock exhibit TIV fracture toughness. There is more interaction between the fractures, in case of anisotropic toughness, even with high spacing between the clusters compared to isotropic toughness.

- The overall shape of the system of fractures is circular in case of isotropic fracture toughness and becomes somehow elliptical in case of the TIV fracture toughness for all scenarios of single and multiple hydraulic fractures, more pronounced in toughness compared to viscosity dominated regimes.

- The presence of toughness barriers in the upper and lower bounding layers greatly affect the fracture propagation. In this case, the fracture corresponds to the PKN or constant height fracture, where the fracture is contained in the vertical direction (height "H") while it is longer in the horizontal direction (length "l").

- The fracture containment of a single fracture is affected by the toughness contrast between the bounding layers and the target layer, and affected by the target layer size. The fracture is getting

more contained in height with increasing the toughness contrast magnitude. Similarly, the net pressure increases with increasing the toughness contrast.

- For a particular layer thickness, the fracture becomes fully contained at a specific toughness contrast magnitude, from which the effect of increasing the toughness contrast is not seen on the fracture containment and on the net pressure change. At this limit, the fractures become qualitatively similar.

- Higher toughness contrast is needed to fully contain the fracture in case of small target layer thickness. However, with increasing the layer size, the effect of toughness contrast increases, hence lower toughness contrast magnitude is needed to fully contain the fracture height compared to small layer size.

- The fracture length evolution indicates that the fracture is getting more elongated in the horizontal direction with decreasing the layer size. Results also demonstrate that for a particular layer size, the fracture length increases with increasing the toughness contrast, until it reaches a certain magnitude where the fractures become fully contained and identical.

- Morphology of the simultaneous propagation of constant height fractures in toughness-dominated regime is similar to the multiple radial fractures in toughness-dominated regime where the fracture geometries are more complex especially for small spacing between the fractures. Once the spacing get larger, more symmetric and nearly identical fractures are observed for both isotropic and anisotropic toughness cases with more interaction in the later.

- In general, fractures propagating in anisotropic toughness result in higher aperture and pressure than fractures propagating in a medium with isotropic toughness.

- Field example analysis can help to get an idea on how to adjust the hydraulic fracturing design in shale anisotropic formations especially in case of multilaterals where the frac hits is a potential scenario.

- The models presented in this study allow engineers to optimize their hydraulic fracturing design in anisotropic shale formations by having idea on the treatment pressure, notch design, cluster spacing, and multilateral spacing.

6.2 Recommendations

Several ideas and potential ameliorations of hydraulic fracturing in shale formations with anisotropic toughness were mentioned throughout this study, which require further investigations. Here, some of these ideas are recommended as continuation of this study:

- Expanding the analytical models in 3D will be a great expansion of this work to compare their results with the simulations.
- While the FMI and other image logs can be used to determine the type of natural fractures (e.g. open, close, conductive) and their aperture and length marked on the wellbore wall, determining the length of these fractures penetrating into the formation (i.e. depth) is not straight forward. Investigation of the use of the image logs in combination with sonic scanner or the use of any other methods to estimate the depth of natural fractures will be important in order to provide a better guidance to design proper notch geometry in anisotropic formations.
- A few field scale notch makers have been proposed in open hole hydraulic fracturing. The operation of these tools are mechanical or hydraulic. There is a big demand of studies in this area to propose a deployable tool in order to make the required notch geometry and in specific

orientation as fast as possible with less inconvenience especially in shale formations that exhibit anisotropic properties.

- Developing new analytical solutions for the limiting regimes of propagation in case of the presence of toughness barriers is another future work to consider.
- Further investigation on the anisotropic toughness in case of multilaterals is important to better model the parent-child cases and prevent the frac-hits, especially, we saw that the presence of anisotropic toughness led to more elongation of the fracture in the horizontal direction.
- Quantitative investigation of simultaneous propagation of multiple hydraulic fractures propagation in anisotropic shale formations is needed to provide better selection of efficient hydraulic fracturing operation in these type of formations.

REFERENCES

Abbas, Safdar, Brice Lecampion, and Romain Prioul. 2013. “Competition Between Transverse And Axial Hydraulic Fractures In Horizontal Wells.” SPE Hydraulic Fracturing Technology Conference 13.

Aidagulov, Gallyam, Olga Alekseenko, Frank F. Chang, Kirk Bartko, Sergey Cherny, Denis Esipov, Dmitry Kuranakov, and Vasily Lapin. 2015. “Model of Hydraulic Fracture Initiation from the Notched Open Hole.” SPE Saudi Arabia Section Annual Technical Symposium and Exhibition 13.

Amadei, B., W. Z. Savage, and H. S. Swolfs. 1987. “Gravitational Stresses in Anisotropic Rock Masses.” International Journal of Rock Mechanics and Mining Sciences & Geomechanics Abstracts 24(1):5–14.

Amadei, Bernard. 1983. Rock Anisotropy and the Theory of Stress Measurements. Vol. 2. Berlin, Heidelberg: Springer Berlin Heidelberg.

Aziz, K., and Antonin Settari. 1979. Petroleum Reservoir Simulation. London: Elsevier Applied Science.

Barton, N., S. Bandis, and K. Bakhtar. 1985. “Strength, Deformation and Conductivity Coupling of Rock Joints.” International Journal of Rock Mechanics and Mining Sciences & Geomechanics Abstracts 22(3):121–40.

Benouadah, N., N. Djabelkhir, X. Song, V. Rasouli, and B. Damjanac. 2021. “Simulation of Competition Between Transverse Notches Versus Axial Fractures in Open Hole Completion Hydraulic Fracturing.” Rock Mechanics and Rock Engineering.

Berry, D. S. 1968. “THE THEORY OF STRESS DETERMINATION BY MEANS OF STRESS RELIEF TECHNIQUES IN A TRANSVERSELY ISOTROPIC MEDIUM.”

Berry, D. S., and C. Fairhurst. 1966. “Influence of Rock Anisotropy and Time-Dependent Deformation on the Stress-Relief and High-Modulus Inclusion Techniques Of.” Pp. 190-190–17 in Fifth Pacific Area National Meeting of the Society. 100 Barr Harbor Drive, PO Box C700, West Conshohocken, PA 19428-2959: ASTM International.

Bessmertnykh, Alena, and Egor Dontsov. 2018. Aspect Ratio of Hydraulic Fracture in Homogeneous Transversely Isotropic Material.

Britt, Larry Kevin, and Jerry Schoeffler. 2009. "The Geomechanics Of A Shale Play: What Makes A Shale Prospective."

Chandler, Michael R., Philip G. Meredith, Nicolas Brantut, and Brian R. Crawford. 2016. "Fracture Toughness Anisotropy in Shale." Journal of Geophysical Research: Solid Earth 121(3):1706–29.

Cramer, D. D. 1987. "Limited Entry Extended to Massive Hydraulic Fracturing." Oil Gas J.;(United States) 85(50).

Daneshy, Ali. 2011. "Hydraulic Fracturing of Horizontal Wells: Issues and Insights."

Delaney, Paul T., David D. Pollard, Joseph I. Ziony, and Edwin H. McKee. 1986. "Field Relations between Dikes and Joints: Emplacement Processes and Paleostress Analysis." Journal of Geophysical Research: Solid Earth 91(B5):4920–38.

Detournay, Emmanuel, and Roberto Carbonell. 1997. "Fracture-Mechanics Analysis of the Breakdown Process in Minifracture or Leakoff Test." SPE Production & Facilities 12(03):195–99.

Djabelkhir, Nejma. 2020. "Simulation of Notch Driven Hydraulic Fracture in Open." University of North Dakota.

Djabelkhir, Nejma, Xueling Song, Xincheng Wan, Omar Akash, Vamegh Rasouli, and Branko Damjanac. 2019. "Notch Driven Hydraulic Fracturing in Open Hole Completions: Numerical Simulations of Lab Experiments." 53rd U.S. Rock Mechanics/Geomechanics Symposium 6.

Dontsov, E. V. 2016. "An Approximate Solution for a Penny-Shaped Hydraulic Fracture That Accounts for Fracture Toughness, Fluid Viscosity and Leak-Off." Royal Society Open Science 3(12):160737.

Dontsov, E. V, and R. Suarez-Rivera. 2020. "Propagation of Multiple Hydraulic Fractures in Different Regimes." International Journal of Rock Mechanics and Mining Sciences 128:104270.

Dontsov, Egor. 2021a. Analysis of a Constant Height Hydraulic Fracture.

Dontsov, Egor. 2021b. “Understanding Fracture Morphology - Resfrac.” Retrieved March 25, 2022 (https://www.resfrac.com/blog/understanding-fracture-morphology).

Dontsov, Egor V. 2019a. “Scaling Laws for Hydraulic Fractures Driven by a Power-Law Fluid in Homogeneous Anisotropic Rocks.” International Journal for Numerical and Analytical Methods in Geomechanics 43(2):519–29.

Dontsov, Egor V. 2019b. “Scaling Laws for Hydraulic Fractures Driven by a Power-Law Fluid in Homogeneous Anisotropic Rocks.” International Journal for Numerical and Analytical Methods in Geomechanics 43(2):519–29.

Dundar, Emre Can. 2019. “Impact of Natural Fracture Induced Elastic Anisotropy on Completion and Hydraulic Fracturing Designs.” West Virginia University Libraries.

Hasan, A. .., and C. S. Kabir. 2002. Fluid Flow and Heat Transfer in Wellbores. Richardson, Tex.: Society of Petroleum Engineers.

Hattori, Gabriel, Jon Trevelyan, Charles E. Augarde, William M. Coombs, and Andrew C. Aplin. 2017. “Numerical Simulation of Fracking in Shale Rocks: Current State and Future Approaches.” Archives of Computational Methods in Engineering 24(2):281–317.

Jaeger, C. 1979. Rock Mechanics and Engineering. Cambridge University Press.

Karimi-Fard, M., L. Durlofsky, and Khalid Aziz. 2004. “An Efficient Discrete-Fracture Model Applicable for General-Purpose Reservoir Simulators.” SPE Journal - SPE J 9:227–36.

Ketter, Aaron A., John L. Daniels, James R. Heinze, and George Waters. 2008. “A Field Study in Optimizing Completion Strategies for Fracture Initiation in Barnett Shale Horizontal Wells.” SPE Production & Operations 23(03):373–78.

Khan, Safdar, Richard Elliot Williams, Sajjad Ansari, and Nader Khosravi. 2012. “Impact of Mechanical Anisotropy on Design of Hydraulic Fracturing in Shales.” Abu Dhabi International Petroleum Conference and Exhibition 7.

Kirsch, C. 1898. “Die Theorie Der Elastizitat Und Die Bedurfnisse Der Festigkeitslehre.” Zeitschrift Des Vereines Deutscher Ingenieure 42:797–807.

Li, H., Y. S. Zou, S. Liu, G. Q. Liu, Y. Z. Jing, and C. A. Ehlig-Economides. 2017. “Prediction of Fracture Initiation Pressure and Fracture Geometries in Elastic Isotropic and Anisotropic Formations.” Rock Mechanics and Rock Engineering 50(3):705–17.

Li, Quanshu, Huilin Xing, Jianjun Liu, and Xiangchon Liu. 2015. “A Review on Hydraulic Fracturing of Unconventional Reservoir.” Petroleum 1(1):8–15.

Ma, Tianshou, Yang Liu, Ping Chen, Bisheng Wu, Jianhong Fu, and Zhaoxue Guo. 2019. “Fracture-Initiation Pressure Prediction for Transversely Isotropic Formations.” Journal of Petroleum Science and Engineering 176(February):821–35.

Mánica, Miguel A., Daniel F. Ruiz, Jean Vaunat, and Antonio Gens. 2019. “Geomechanics of Shale Repositories.” Pp. 99–123 in Shale: Subsurface Science and Engineering. Vol. 7, Geophysical Monograph Series, edited by T. Dewers, J. Heath, and M. Sánchez. Wiley.

Martemyanov, A., S. Lukin, Yu Ovcharenko, V. Zhukov, Yu Andrianov, S. Vereshchagin, A. Eremeev, A. Konchenko, O. Tatur, and A. Yuferova. 2017. “Analytic Modelling for Wellbore Stability Analysis.” Procedia Structural Integrity 6:292–300.

McClure, Mark, Charles Kang, Soma Medam, and Chris Hewson. 2018. “ResFrac Technical Writeup.” ArXiv Preprint ArXiv:1804.02092.

McClure, Mark, Matteo Picone, Garrett Fowler, Dave Ratcliff, Charles Kang, Soma Medam, and Joe Frantz. 2020. “Nuances and Frequently Asked Questions in Field-Scale Hydraulic Fracture Modeling.” SPE Hydraulic Fracturing Technology Conference and Exhibition D021S003R007.

Milliken, Kitty L., and Nicholas W. Hayman. 2019. “Mudrock Components and the Genesis of Bulk Rock Properties.” Shale 1–25.

Moukhtari, Fatima-Ezzahra, Brice Lecampion, and Haseeb Zia. 2020a. “Planar Hydraulic Fracture Growth Perpendicular to the Isotropy Plane in a Transversely Isotropic Material.” Journal of the Mechanics and Physics of Solids 137:103878.

Moukhtari, Fatima-Ezzahra, Brice Lecampion, and Haseeb Zia. 2020b. “Planar Hydraulic Fracture Growth Perpendicular to the Isotropy Plane in a Transversely Isotropic Material.” Journal of the Mechanics and Physics of Solids 137:103878.

Nadri, Dariush, Joel Sarout, Andrej Bóna, and David Dewhurst. 2012. “Estimation of Anisotropy Parameters of Transversely Isotropic Shales with a Tilted Symmetry Axis.” Geophysical Journal International 190:1197–1203.

Nilson, R. H., and W. J. Proffer. 1984. “Engineering Formulas for Fractures Emanating From Cylindrical and Spherical Holes.” Journal of Applied Mechanics 51(4):929–33.

Pan, E., and B. Amadei. 1995. “Stress Concentration at Irregular Surfaces of Anisotropic Half-Spaces.” Acta Mechanica 113(1):119–35.

Rasouli, Vamegh, Zachariah John Pallikathekathil, and Elike Mawuli. 2011. “The Influence of Perturbed Stresses near Faults on Drilling Strategy: A Case Study in Blacktip Field, North Australia.” Journal of Petroleum Science and Engineering 76(1–2):37–50.

Savitski, Alexei, M. Lin, Azadeh Riahi, Branko Damjanac, and Neal Nagel. 2013. “Explicit Modeling of Hydraulic Fracture Propagation in Fractured Shales.”

Schmidt, Darren D., Steven A. Smith, James A. Sorensen, Damion J. Knudsen, John A. Harju, and Edward N. Steadman. 2011. EVALUATION OF KEY FACTORS AFFECTING SUCCESSFUL OIL PRODUCTION IN THE BAKKEN FORMATION, NORTH DAKOTA – PHASE II. 15 North 23rd Street, Stop 9018 Grand Forks, ND 58202-9018.

Scholz, Christopher H. 2010. “A Note on the Scaling Relations for Opening Mode Fractures in Rock.” Journal of Structural Geology 32(10):1485–87.

Serajian, Vahid, and Ahmad Ghassemi. 2011. “Hydraulic Fracture Initiation from a Wellbore in Transversely Isotropic Rock.” 45th US Rock Mechanics / Geomechanics Symposium.

Suarez-Rivera, Roberto, Jeff Burghardt, Sergei Stanchits, Eric Edelman, and Aniket Surdi. 2013. “Understanding the Effect of Rock Fabric on Fracture Complexity for Improving Completion Design and Well Performance.”

Suarez-Rivera, Roberto, Sidney Green, John Mclennan, and Mr Bai. 2006. “Effect of Layered Heterogeneity on Fracture Initiation in Tight Gas Shales.” 7.

Tan, Peng, Yan Jin, Ke Han, Bing Hou, Mian Chen, Xiaofeng Guo, and Jie Gao. 2017. “Analysis of Hydraulic Fracture Initiation and Vertical Propagation Behavior in Laminated Shale Formation.” Fuel 206:482–93.

Thomsen, Leon. 1986. “Weak Elastic Anisotropy.” GEOPHYSICS 51(10):1954–66.

Ugueto, Gustavo, Paul Huckabee, Magdalena Wojtaszek, Talib Daredia, and Alan Reynolds. 2019. “New Near-Wellbore Insights from Fiber Optics and Downhole Pressure Gauge Data.” SPE Hydraulic Fracturing Technology Conference and Exhibition D031S007R002.

Valliappan, V., J. J. C. Remmers, A. Barnhoorn, and D. M. J. Smeulders. 2019. “A Numerical Study on the Effect of Anisotropy on Hydraulic Fractures.” Rock Mechanics and Rock Engineering 52(2):591–609.

Warpinski, N. R., and L. W. Teufel. 1987. “Influence of Geologic Discontinuities on Hydraulic Fracture Propagation (Includes Associated Papers 17011 and 17074).” Journal of Petroleum Technology 39(02):209–20.

Willis-Richards, J., K. Watanabe, and H. Takahashi. 1996. “Progress toward a Stochastic Rock Mechanics Model of Engineered Geothermal Systems.” Journal of Geophysical Research: Solid Earth 101(B8):17481–96.

Xia, Lei, and Yawu Zeng. 2019. “Numerical Simulation of Hydraulic Fracturing in Transversely Isotropic Rock Masses Based on PFC-2D.” Journal of Vibro engineering 21(4):833–47.

Zia, Haseeb, Brice Lecampion, and Weihan Zhang. 2018. “Impact of the Anisotropy of Fracture Toughness on the Propagation of Planar 3D Hydraulic Fracture.” International Journal of Fracture 211(1):103–23.

Zimmerman, Robert W., Gang Chen, Teklu Hadgu, and Gudmundur S. Bodvarsson. 1993. “A Numerical Dual-porosity Model with Semianalytical Treatment of Fracture/Matrix Flow.” Water Resources Research 29(7):2127–37.